Souvik Nandi, Abinash Ojha, Ashirbad Nanda,
Rudra Narayan Sahoo, Rakesh Swain, Krushna Prasad Pattnaik
and Subrata Mallick*

Vildagliptin plasticized hydrogel film in the control of ocular inflammation after topical application: study of hydration and erosion behaviour

https://doi.org/10.1515/zpch-2021-3081
Received June 25, 2021; accepted July 25, 2021; published online August 6, 2021

Abstract: Vildagliptin (VID) is a dipeptidyl peptidase-4 (DPP-4) inhibitor used in controlling blood glucose level in type 2 diabetes. Vildagliptin improves beta cells function and is also suggested to effectively control the inflammation. The possible ocular anti-inflammatory property of vildagliptin has been explored using topically applied plasticized ocular film formulation. Film formulation was prepared by solvent cast and evaporation method using triethanolamine (TEA), dimethyl sulphoxide (DMSO), and polyethylene glycol 400 (PEG 400) as the plasticizer in HPMC hydrogel matrix base. Anti-inflammatory study was carried out in the carrageenan induced ocular rabbit model. Analytical methods confirmed that the drug was present almost in completely amorphized form in the film formulation. Level of hydration, swelling and erosion rate of the film played the controlling factor in the process of drug release, ocular residence and permeation. Maximum swelling rate of 363 h^{-1} has been shown by VHT compared to other formulation of VHD and VHP (174 and 242 h^{-1} respectively). Film containing DMSO exhibited highest *in vitro* release as well as *ex vivo* ocular permeation. Film formulation has shown a fast recovery of ocular inflammation in contrast to the untreated eye after inducing inflammation. Plasticized vildagliptin hydrogel film formulation could be utilized in the management and control of ocular inflammation particularly

***Corresponding author: Subrata Mallick**, School of Pharmaceutical Sciences, Siksha 'O' Anusandhan (Deemed to be University), Bhubaneswar 751003, India,
E-mail: profsmallick@gmail.com
Souvik Nandi, Abinash Ojha, Ashirbad Nanda, Rakesh Swain and Krushna Prasad Pattnaik, School of Pharmaceutical Sciences, Siksha 'O' Anusandhan (Deemed to be University), Bhubaneswar 751003, India
Rudra Narayan Sahoo, School of Pharmaceutical Sciences, Siksha 'O' Anusandhan (Deemed to be University), Bhubaneswar 751003, India; and School of Pharmacy and Life Sciences, Centurion University of Technology and Management, Odisha, India

with diabetic retinopathy after proper clinical studies in higher animal and human individuals.

Keywords: diabetes; DPP-4 inhibitor; film plasticizer; hydrogel; ocular anti-inflammation; vildagliptin.

1 Introduction

Vildagliptin (VID), a potent orally active dipeptidyl peptidase-4 (DPP-4) inhibitor is used for the treatment of type 2 diabetes mellitus [1–3]. Increased risk of cardiovascular disease, hepatitis-C infection and pancreatitis is reported in the people with diabetes [4]. Despite of an oral bioavailability of 85% it has shorter elimination half-life of 1.5 h. Being DPP-4 inhibitor vildagliptin is known to effectively control the inflammation besides improving beta cells function [5, 6]. The possible anti-inflammatory property of vildagliptin may add the additional value in the patients particularly with diabetic retinopathy [7].

Diabetes Mellitus (Type-2) is one of the most common health problems worldwide which is expected to reach 592 million patients by 2035 [8]. Cho et al. 2018 reported that more than 250 million people already affected by Type 2 Diabetes Mellitus [9]. The main cause of Type 2 Diabetes is a result of insulin resistance and impairment of insulin secretion from β cells [10]. Gliptin class of dipeptidyl peptidase-4 (DPP-4) inhibitors can effectively control the inflammation which occurs simultaneously with type-2 diabetes mellitus inflammation in the pancreatic beta cell [11–14].

Topical medication exerts low risk of systemic adverse effects and drug interactions. Topical delivery systems promote localized action and avoid systemic toxicity bypassing the first-pass metabolism [15]. Ocular hydrogel films are very much suitable for controlled ophthalmic drug delivery [16–18]. Polymeric hydrogel films have the capability of swelling after hydration in the tear fluid and form bond with the mucin protein chains, and increase the contact time in the site of action. Hydrogel formulations also overcome the nasolacrimal drainage problem associated with liquid ophthalmic drops exhibiting significantly low bioavailability [19]. Eye ointment is viscous and can increase the residence time but patient acceptability is less due to blurred vision, sticky eyes and uncomfortable feelings [20]. Hydroxypropyl methylcellulose (HPMC), a hydrogel forming polymer is very much suitable for ocular drug delivery formulation [21]. It is non-irritant to the eye and maintains inertness when used with a wide range of drugs in the ocular delivery systems. According to recent reports HPMC is also being used in the case of ophthalmic delivery.

Triethanolamine (TEA), Dimethyl sulphoxide (DMSO), and Polyethylene glycol 400 (PEG 400) have been used as plasticizer in the ocular film formulation [22–24]. The effect of plasticizer on the *in vitro* drug release and *ex vivo* corneal permeation has been studied. The possible ocular antiinflammatory study was examined on carrageenan induced rabbit eye model.

2 Materials and methods

2.1 Material

Vildagliptin (MW: 303.399 g/mol) was a gift sample provided by Glenmark Pharmaceutical Ltd (Mumbai). Hydroxypropyl methylcellulose HPMC K15M: Qualikems (Vadodara), TEA: Burgoyne Urbidges & Co. (Mumbai), DMSO and PEG 400: MERCK. Carrageenan was purchased from Himedia Laboratories Pvt. Ltd.

2.2 Vildagliptin film formulation

HPMC was soaked with distilled water and refrigerated for 24 h for complete hydration and swelling. Vildagliptin and plasticizer (triethanolamine, dimethyl sulphoxide or PEG 400) were added to the swelled mass and stirring was continued for 12 h using magnetic stirrer [25, 26]. The gel-like mass was then poured in a petridish and placed in an incubator at 45 °C for 24 h for drying upto constant weight [27].

2.3 Thickness and folding endurance

The thickness of the prepared film formulations was measured by digital micrometer (Mitutoyo, Japan). An average reading was taken after measuring the film thickness at various places. Folding endurance of the film was then tested till the film breaks apart and the result was recorded [28].

2.4 Swelling and erosion study

The hydration and swelling of 1 × 1 cm pre-weighed film piece was carried out on a glass slide. About 40 ml of simulated tear fluid (pH 6.8) was poured on the glass slide and weighed at regular time interval after wiping out the excess phosphate buffer solution [29]. The hydration percentage was calculated by using the following formula.

$$\text{Dynamic hydration (\%)} = \frac{(\text{weight after hydration} - \text{initial dry weight before hydration})}{\text{Hydrated weight}} \times 100$$

The swelling rate (K_s) was calculated by slope of the linear profile of % swelling index versus time plot.

Erosion study was done by placing the hydrated films in an oven overnight at 60 °C. The film was then placed over activated silica in the desiccator gel for 24 h in order to remove moisture, if any. The difference between the initial weight and the dried weight was taken to estimate the erosion percentage using following formula:

$$\%\ \text{Erosion} = \frac{(\text{dry weight before hydration} - \text{dry weight after after hydration})}{\text{dry weight before hydration}} \times 100$$

2.5 Moisture content and uptake

The initial weight of a piece of the prepared film was taken and kept in a desiccator over activated silica gel. The film was then weighed after 24 h and the weight difference was used to evaluate the moisture content value.

$$(\%)\ \text{Moisture Content} = \frac{(\text{Final weight} - \text{initial weight})}{\text{Final weight}} \times 100$$

A pre-weighed film was placed in a closed desiccator maintained at the relative humidity of 75% and the final weight was taken after achieving equilibrium (till constant weight). A head space of 75% relative humidity was maintained inside the closed desiccator containing supersaturated NaCl slurry [30]. Moisture uptake of the film was estimated using the following formula:

$$(\%)\ \text{Moisture uptake} = \frac{(\text{Final weight} - \text{initial weight})}{\text{intial weight}} \times 100$$

2.6 Drug content estimation

Accurately weighed randomly cut pieces of the film formulation were dissolved in phosphate buffer solution (pH 6.8) and sonicated for 1 h to obtain a clear solution. For estimating drug content the solution was made ready by passing through a syringe driven filter (0.22 µm, Whatman Uniflo). Absorbance was measured at 197 nm in UV spectrophotometer (JASCO V-630 spectrophotometer).

2.7 Fourier transform infrared spectroscopy

FTIR spectra of the pure drug as well as of the prepared films were carried out. The formulated films were cut into very fine pieces and subjected to KBr pellet method. The scan was done in the region of 4000–400 cm^{-1} in JASCO FTIR 4100 (type A) and an average of 80 scans was taken.

2.8 X-ray diffraction

X-ray diffraction has been studied for the crystal structure analysis of the pure drug and the film formulation. Any changes in the crystalline intensities in the films have been confirmed in this study. The diffraction pattern was recorded using the powder X-ray diffractometer (Rigaku, Ultima IV) equipped with a Cu X-ray source radiation wavelength of 1.5406 Å. Diffraction was measured at a scan speed of 1° per min in between 5 and 70° 2θ applying 40 kV as voltage and 15 mA as current.

2.9 Differential scanning calorimetry

Differential Scanning Calorimetry measurements were performed for the powder drug and the films. Sample weight was taken in the range of 2–3 mg for the analysis. The sample was placed in a sealed aluminum sample holder having a single perforation in the lid to eliminate the vapor which was most likely to be generated during the process. The whole operation was done under a nitrogen atmosphere to maintain inertness during the thermal analysis (METTLER TOLEDO DSC 1, STAR^e SYSTEM).

2.10 *In vitro* drug release study

The *in vitro* release study was carried out in USP type 2 paddle type dissolution apparatus (Electrolab, dissolution tester USP, TDT06L, India) [31]. Accurately weighed piece of film was fixed on a glass slide by using cyanoacrylate adhesive which then fully merged into the simulated tear fluid (phosphate buffer: pH 7.4). The bath temperature was set at 34.0 ± 0.5 °C with a paddle rotation speed of 50 rpm [30, 32, 33]. Aliquots were drawn at predetermined time intervals, passed through a syringe driven filter of 0.45 µm. The filtered liquid was then analyzed at 197 nm.

2.11 *Ex vivo* permeation study

Freshly excised goat eyes were collected from the local slaughter house in phosphate buffer (pH 6.8) for the study [34]. The undamaged corneas were separated and rinsed thoroughly in phosphate buffer (pH 6.8). The ocular membranes then attached to the modified franz diffusion cell. The *ex vivo* ocular permeation study then carried out in 200 ml of phosphate buffer medium (pH 6.8) at 34 ± 0.2 °C. Aliquots were drawn in particular time intervals and replenished with fresh medium which then subjected to UV–V is spectra analysis. The procedure was continued for 6 h [31, 35].

The permeability co-efficient (P_{ss}) was calculated by:

$$P_{ss} = \frac{J_s}{C}$$

where, J_s the flux at the steady-state, C the concentration of the drug in the film.

2.12 Anti-inflammatory activity study

The animal experimentation were approved by the institutional animal ethical committee (IAEC) [IAEC/SPS/SOA/03/2019; dated: 29th June, 2019]. The guidelines of the Committee for the Purpose of Control and Supervision of Experiments on Animals (CPCSEA), India were followed [Institution registration number: 1171/PO/RE/S/08/CPCSEA].

New-zealand white rabbit (*Oryctolagus cuniculus*) of average weight of 1.6–2.0 kg was kept in the laboratory environment for their adaptation before experiments. Food was supplied according to their daily schedule and water *ad libitum*. Carrageenan was (100 µl of 3% w/v) injected by a

30 gauge needle into the upper palpebral region of the rabbit eye after instilling Proparacaine HCl Ophthalmic Solution USP (0.5%) for local anesthesia [36, 37]. Acute inflammation induced by carrageenan is believed to be disappeared within 24 h [38, 39]. A small piece of film formulation (VHD) was sterilized by UV exposure for 10 min at a distance of 25 cm from UV source and placed in the cul-de-sac carefully after 1 h of the injection when redness in the eye was noticed [18]. The anti-inflammatory activity was examined by the reduction of redness and tear discharge.

3 Results and discussion

All the films were found of uniform thickness in between 85 and 125 μm and are appropriate for ocular application [40]. Folding endurance value of >200 suggested enough strength and durability of the films [30]. Moisture content of the films varied from 5.52 to 7.67% at laboratory ambient condition. Where, the presence of PEG 400 (VHP) contributed to a higher moisture content than the

Table 1: Physicochemical properties of ocular film.

Film code	Plasticizer (20% w/w)	Moisture content (%)	RH (75%)	Thickness (μm)	Folding endurance
VHT	Triethanolamine	5.52 ± 0.47	11.22 ± 0.44	84.2 ± 0.005	>200
VHD	Dimethyl sulfoxide	6.85 ± 0.75	15.72 ± 0.54	110.8 ± 0.004	>200
VHP	Polyethylene glycol 400	7.67 ± 1.13	13.74 ± 0.49	125.2 ± 0.002	>200

others. The physical properties are given in Table 1. The moisture uptake of the film containing TEA (VHT) was slightly less (11.32% w/w at 75% RH) in comparison with that of the other films (VHD and VHP) at the same RH.

3.1 Swelling and erosion study

Swelling profile of the VID film as a function of time till 6 h has been depicted in Figure 1. Hydration and erosion after 6 h of swelling in presence of simulated tear fluid have also been exhibited in Figure 2. Hydration and erosion are the controlling factors of drug release particularly in gel-forming thin matrix film formulation. Values of swelling rate, K_s (174–363 h^{-1}), hydration level after 6 h of swelling (1684–2845%) and rate of erosion (16.16–24.12%) of the films are the dominating factors in the process of drug release. The film VHT has shown maximum swelling rate (K_s) of 363 h^{-1} compared to other formulation of VHD and

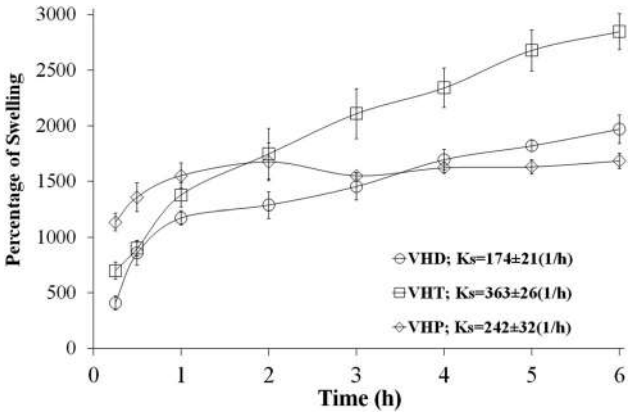

Figure 1: Swelling profile of VID film formulation containing DMSO TEA and PEG 400 as plasticizer.

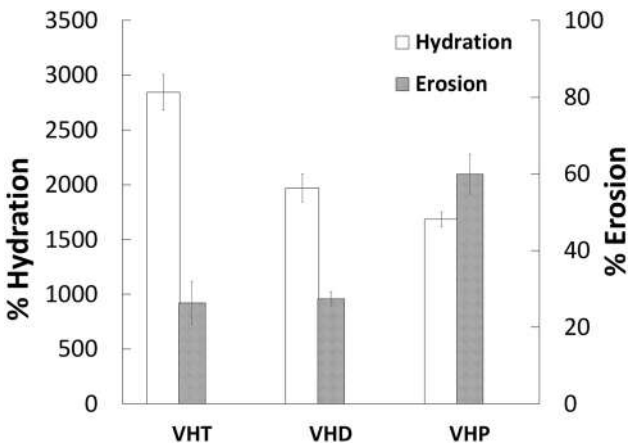

Figure 2: Hydration and erosion after 6 h of swelling in presence of simulated tear fluid.

VHP (174 and 242 h^{-1} respectively). The same film VHT exhibited least rate of erosion due to the presence of triethanolamine as the plasticizer rather than that of others containing DMSO and PEG 400. That means that swelling rate and hydration level are inversely related with the rate of erosion.

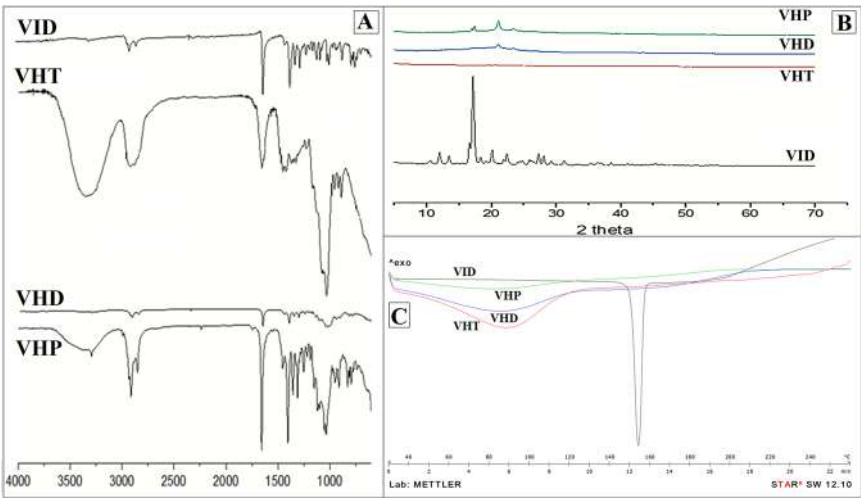

Figure 3: FTIR, DSC, and XRD study of VID and formulated films.

3.2 Fourier transform infrared spectroscopy

The characteristic peaks in the FTIR spectra of vildagliptin attributed to OH and N–H stretching vibrations were found at 3011–3370 and 3294 cm^{-1} respectively (Figure 3A). The peaks at 1663 and 1248 cm^{-1} were assigned to amide C=O, and C–N stretching [41, 42]. Vildagliptin containing film formulations showed a lower intensity peak of amide C=O stretching compared to the drug and a broad band in the region of 4000–3000 cm^{-1} probably because of OH stretching vibration of the intermolecular hydrogen bonds between polymer and drug. Incompatibility issue between the drug and the polymers may be ruled out as no significant change has been observed.

3.3 X-ray diffractometry

The XRD of VID and the formulations are represented in Figure 3B. The crystalline pattern showed characteristic peaks of the pure drug [43]. Vildagliptin showed intense characteristic peaks at 10.99, 12.45, 16.21, 19.15, 21.43, 26.33 and 28.30 2θ [41].

In the film formulations, VHT, VHD and VHP, the diffraction peaks were almost absent, representing the disappearance of crystals may be due to the presence of HPMC as the crystal growth inhibiting matrix polymer [44].

3.4 Differential scanning calorimetry

DSC of VID and all formulations are depicted in Figure 3C. A sharp endothermic peak of the pure vildagliptin was observed at 152.04 °C [45]. Due to moisture

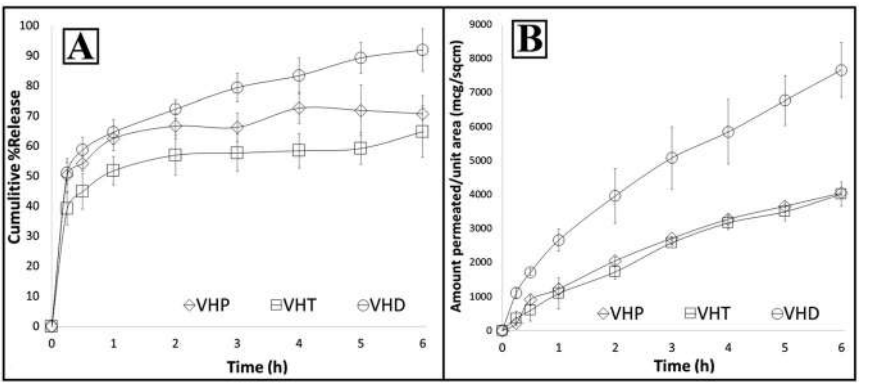

Figure 4: *In vitro* drug release and *ex vivo* permeation study of the film formulations.

evaporation from the polymeric matrix, a broad endothermic peak was found in the thermogram in the range of 60–110 °C [40, 46]. In the film formulations the sharp endothermic peak was absent, which established that the drug was almost completely amorphized.

3.5 *In vitro* drug release

In vitro release pattern has been presented in Figure 4A. The release initiated with a high rate may be due to the presence of HPMC as the hydrogel forming polymer matrix [47, 48]. Initially, the release of vildagliptin in the first hour was found to be more than 50% (51.8–65.5%) and reached to 64.8–91.9% at 6 h. DMSO plasticizer containing film (VHD) exhibited fastest release throughout compared to triethanolamine and polyethylene glycol 400 plasticized film formulations (VHT and VHP respectively).

Table 2: *In vitro* and *ex vivo* kinetics and permeation parameters.

Film code	*In vitro* release					Tissue permeation					Permeation parameters	
	First order	Higuchi		Peppas		First order	Higuchi		Peppas		J_s (μg/min)	$P_{ss} \times 10^2$ (cm/min)
	r^2	K	r^2	n	r^2	r^2	K	r^2	n	r^2	(mean ± sd) (n = 3)	(mean ± sd) (n = 3)
VHT	0.825	19.24	0.976	0.159	0.973	0.937	44.17	0.992	0.751	0.999	463 (94)	1.15 (0.001)
VHD	0.946	20.74	0.983	0.175	0.983	0.972	39.72	0.998	0.645	0.999	867 (54)	2.16 (0.002)
VHP	0.955	21.82	0.990	0.187	0.996	0.935	41.87	0.990	0.643	0.995	438 (38)	1.09 (0.001)

J_s = flux; P_{ss} = Permeability co-efficient.

3.6 *Ex vivo* permeation study

A sustained pattern of *ex vivo* permeation was observed from all the formulations (Figure 4B) because of the presence of lipophilic epithelial layer in the cornea. VHD showed maximum cumulative amount permeated throughout the period of 6 h than that of other formulations due to presence of DMSO as the plasticizer. DMSO might have interacted with the lipids of epithelial layer of cornea facilitating the permeation.

As per fitting of model test, it is understood that the kinetics of drug release and corneal permeation have followed both Higuchi and Korsmeyer-Peppas model (r^2 values in the range of 0.973–0.999) compared to relatively poor fitting with first order model (r^2 in the range of 0.825–0.972) as summarized in Table 2. The '*n*' values were found to be in the range of 0.159–0.187 (<0.5) depicting the probability of diffusion controlled release system [30]. In the case of *ex vivo* permeation study the obtained *n* values from the regression line of Korsmeyer-Peppas model were found in the range of 0.643–0.751 which is the evident of the system being partially

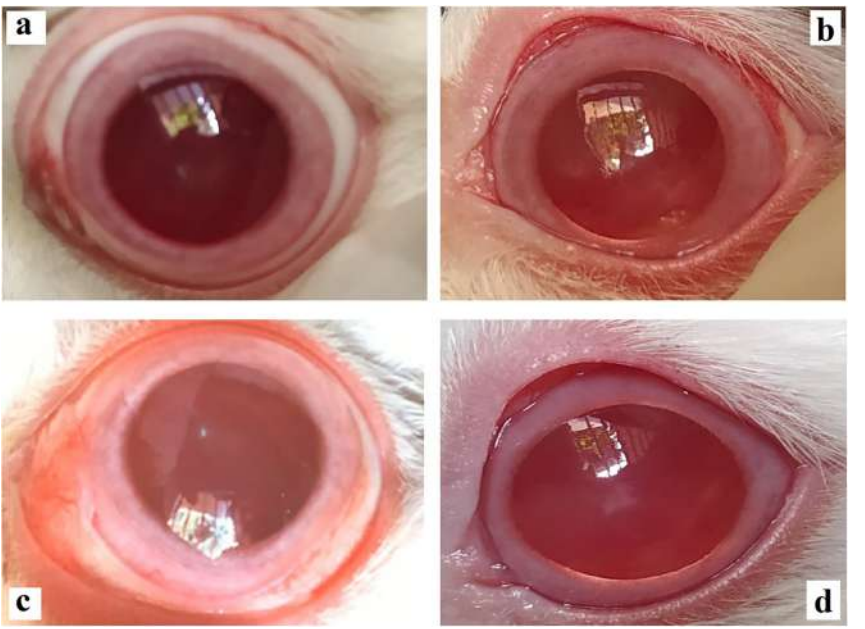

Figure 5: (a) Eye indicating no inflammation (b) after 45 min induce carrageenan eye appear redness and swelling (c) VID solution induced the rabbit eye in the cul-de-sac (d) untreated eye after 2 h.

diffusion and partially erosion controlled. Gel strength of the HPMC matrix film might have affected to some extent due to mucoadhesion during the corneal permeation and brought about partial erosion of the film [49]. Increased flux (J_s) and increased permeability co-efficient (P_{ss}) of VHD have also been resulted because of augmented permeation (867 μg/min and 2.16 cm/min respectively) compared to other films.

3.7 Anti-inflammation study

The normal and the inflamed eye are depicted in Figure 5a and 5b respectively. Significant lacrimation, reddening and swelling of the conjunctiva were noticed due to inflammation of the eye (Figure 5b). The redness of the rabbit eye almost disappeared within 2.5 h in the case of the treated one (Figure 5c). Whilst, symptoms of ocular inflammation continued to exist beyond 2.5 h in the untreated positive control rabbit eye (Figure 5d).

4 Conclusion

Triethanolamine, dimethyl sulphoxide, or polyethylene glycol 400 as plasticizer has been used successfully in HPMC based ocular film formulation of vildagliptin. Hydration level of swelling, swelling and erosion rate of the gel-forming thin matrix film played the controlling factor in the process of drug release, ocular residence and permeation. Maximum swelling rate of 363 h^{-1} has been exhibited by VHT compared to other formulation of VHD and VHP (174 and 242 h^{-1} respectively). The DSC and XRD study confirmed the absence of solid crystal structure of vildagliptin and presence of almost amorphized form in the film formulation. FTIR study has shown intermolecular hydrogen bonding between the polymer and the drug. The formulation containing DMSO (VHD) has shown highest *in vitro* release and *ex vivo* corneal permeation compared to other films. Ocular anti-inflammation of vildagliptin was observed by using VHD film formulation in the carrageenan induced ocular rabbit model. Plasticized vildagliptin film formulation could be utilized in the control and management of ocular inflammation in diabetic patients particularly with diabetic retinopathy after proper clinical studies with higher animal and human individual.

Acknowledgments: The authors are grateful to the Department of Science & Technology, Ministry of Science & Technology, New Delhi, India, for providing INSPIRE fellowship to Souvik Nandi (IF 180534). The authors are also very much

grateful to the President, Siksha O Anusandhan (Deemed to be University) for providing other facilities. The authors are also grateful to Glenmark Pharmaceutical Ltd. For the gift sample of vildagliptin.
Author contributions: All the authors have accepted responsibility for the entire content of this submitted manuscript and approved submission.
Research funding: None declared.
Conflict of interest statement: The authors declare no conflict of interest.

References

1. Shimodaira M., Niwa T., Nakajima K., Kobayashi M. Beneficial effects of vildagliptin on metabolic parameters in patients with type 2 diabetes. *Endocr. Metab. Immune Disord. – Drug Targets* 2015,*15*, 223–228.
2. Wang X., Hausding M., Weng S. Y., Kim Y. O., Steven S., Klein T., Daiber A., Schuppan D. Gliptins suppress inflammatory macrophage activation to mitigate inflammation, fibrosis, oxidative stress, and vascular dysfunction in models of nonalcoholic steatohepatitis and liver fibrosis. *Antioxidants Redox Signal.* 2018, *28*, 87–109.
3. Sudhakaran C., Kishore U., Anjana R. M., Unnikrishnan R., Mohan V. Effectiveness of sitagliptin in Asian Indian patients with type 2 diabetes—an Indian tertiary diabetes care center experience. *Diabetes Technol. Therapeut.* 2011, *13*, 27–32.
4. Kalra S. Emerging role of dipeptidyl peptidase-IV (DPP-4): inhibitor vildagliptin in the management of type 2 diabetes. *J. Assoc. Phys. India*. 2011, *59*, 237–245.
5. Yazbeck R., Howarth G. S., Abbott C. A. Dipeptidyl peptidase inhibitors, an emerging drug class for inflammatory disease. *Trends Pharmacol. Sci.* 2009, *30*, 600–607.
6. Wu Z., Wang S., Jin X., Bi Y., Ma S., Liu T. MiR-29a protects against cerebral ischemia injury by targeting DPP4 through TGF-β signaling pathway. *J. Neurosurg. Sci.* 2020, *64*, 586–587.
7. Chaudhuri A., Dandona P., Fonseca V. Cardiovascular benefits of exogenous insulin. *J. Clin. Endocrinol. Metab.* 2012, *97*, 3079–3091.
8. Forouhi N. G., Wareham N. J. Epidemiology of diabetes. *Medicine* 2010, *38*, 602–606.
9. Cho N., Shaw J. E., Karuranga S., Huang Y., da Rocha Fernandes J. D., Ohlrogge A. W., Malanda B. IDF Diabetes Atlas: global estimates of diabetes prevalence for 2017 and projections for 2045. *Diabetes Res. Clin. Pract.* 2018, *138*, 271–281.
10. Donath M. Y., Ehses J. A., Maedler K., Schumann D. M., Ellingsgaard H., Eppler E., Reinecke M. Mechanisms of β-cell death in type 2 diabetes. *Diabetes* 2005, *54*(Suppl. 2), S108–S113.
11. Ferreira L., Teixeira-de-Lemos E., Pinto F., Parada B., Mega C., Vala H., Pinto R., Garrido P., Sereno J., Fernandes R., Santos P. Effects of sitagliptin treatment on dysmetabolism, inflammation, and oxidative stress in an animal model of type 2 diabetes (ZDF rat). *Mediat. Inflamm.* 2010, *2010*; https://doi.org/10.1155/2010/592760.
12. Pollack R. M., Donath M. Y., LeRoith D., Leibowitz G. Anti-inflammatory agents in the treatment of diabetes and its vascular complications. *Diabetes Care* 2016, *39*(Suppl. 2), S244–S252.
13. Dobrian A. D., Ma Q., Lindsay J. W., Leone K. A., Ma K., Coben J., Galkina E. V., Nadler J. L. Dipeptidyl peptidase IV inhibitor sitagliptin reduces local inflammation in adipose tissue and in pancreatic islets of obese mice. *Am. J. Physiol. Endocrinol. Metab.* 2011, *300*, E410–E421.

14. Panina G. The DPP-4 inhibitor vildagliptin: robust glycaemic control in type 2 diabetes and beyond. *Diabetes Obes. Metabol.* 2007, (Suppl. 1), 32–39; https://doi.org/10.1111/j.1463-1326.2007.00763.x.
15. Katara R., Sachdeva S., Majumdar D. K. Aceclofenac oil drops: characterization and evaluation against ocular inflammation. *Pharmaceut. Dev. Technol.* 2017, *23*, 240–246.
16. Wirostko B., Mann B. K., Williams D. L., Prestwich G. D. Ophthalmic uses of a thiol-modified hyaluronan-based hydrogel. *Adv. Wound Care* 2014, *3*, 708–716.
17. Rocha E. D., Ferreira M. R. S., dos Santos Neto E., Barbosa E. J., Löbenberg R., Lourenço F. R., Bou-Chacra N. Enhanced in vitro antimicrobial activity of polymyxin B–coated nanostructured lipid carrier containing dexamethasone acetate. *J. Pharm. Innov.* 2020, *16*, 125–135.
18. Nanda A., Sahoo R. N., Pramanik A., Mohapatra R., Pradhan S. K., Thirumurugan A., Das D., Mallick S. Drug-in-mucoadhesive type film for ocular anti-inflammatory potential of amlodipine: effect of sulphobutyl-ether-beta-cyclodextrin on permeation and molecular docking characterization. *Colloids Surf. B Biointerfaces* 2018, *172*, 555–564.
19. Ariturk N. S., Oge I., Erkan D., Süllü Y., Şahin M. The effects of nasolacrimal canal blockage on topical medications for glaucoma. *Acta Ophthalmol. Scand.* 1996, *74*, 411–413.
20. Agrawal A. K., Das M., Jain S. In situ gel systems as 'smart'carriers for sustained ocular drug delivery. *Expet Opin. Drug Deliv.* 2012, *9*, 383–402.
21. El-Sousi S., Nácher A., Mura C., Catalán-Latorre A., Merino V., Merino-Sanjuán M., Díez-Sales O. Hydroxypropylmethylcellulose films for the ophthalmic delivery of diclofenac sodium. *J. Pharm. Pharmacol.* 2012, *65*, 193–200.
22. Mohapatra R., Senapati S., Sahoo C., Mallick S. Thermodynamic properties of ocular permeation of diclofenac: effect of triethanolamine. *FARMACIA* 2016, *64*, 72–81.
23. Bazuin C. G., Eisenberg A. Dynamic mechanical properties of plasticized polystyrene-based ionomers. I. Glassy to rubbery zones. *J. Polym. Sci, Part B: Polym. Phys.* 1986, *24*, 1137–1153.
24. Oh H. J., McGrath J. E., Paul D. R. Kinetics of poly(ethylene glycol) extraction into water from plasticized disulfonated poly(arylene ether sulfone) desalination membranes prepared by solvent-free melt processing. *J. Membr. Sci.* 2017, *524*, 257–264.
25. Panda B., Parihar A. S., Mallick S. Effect of plasticizer on drug crystallinity of hydroxypropyl methylcellulose matrix film. *Int. J. Biol. Macromol.* 2014, *67*, 295–302.
26. Hamid A., Khan M., Hussain F., Zada A., Li T., Alei D., Ali A. Synthesis and physiochemical performances of PVC-sodium polyacrylate and PVC-sodium polyacrylate-graphite composite polymer membrane. *Z. Phys. Chem.* 2021; https://doi.org/10.1515/zpch-2020-1763 [Ahead of Print/Just Accepted].
27. Swain K., Pattnaik S., Sahu S. C., Patnaik K. K., Mallick S. Drug in adhesive type transdermal matrix systems of ondansetron hydrochloride: optimization of permeation pattern using response surface methodology. *J. Drug Target.* 2010, *18*, 106–114.
28. Preis M., Woertz C., Kleinebudde P., Breitkreutz J. Oromucosal film preparations: classification and characterization methods. *Expet Opin. Drug Deliv.* 2013, *10*, 1303–1317.
29. Tanuma H., Saito T., Nishikawa K., Dong T., Yazawa K., Inoue Y. Preparation and characterization of PEG-cross-linked chitosan hydrogel films with controllable swelling and enzymatic degradation behavior. *Carbohydr. Polym.* 2010, *80*, 260–265.
30. Pramanik A., Sahoo R. N., Nanda A., Mohapatra R., Singh R., Mallick S. Ocular permeation and sustained anti-inflammatory activity of dexamethasone from kaolin nanodispersion hydrogel system. *Curr. Eye Res.* 2018, *43*, 828–838.

31. Kesarwani A., Yadav A. K., Singh S., Gautam H., Singh H. N., Sharma A., Yadav C. Theoretical aspects of transdermal drug delivery system. *Bull. Pharmaceut. Res.* 2013, *3*, 78–89.
32. Abdelrahman A. A., Salem H. F., Khallaf R. A., Ali A. M. Modeling, optimization, and in vitro corneal permeation of chitosan-lomefloxacin HCl nanosuspension intended for ophthalmic delivery. *J. Pharm. Innov.* 2015, *10*, 254–268.
33. Xu Y., Zhang C., Zhu X., Wang X., Wang H., Hu G., Fu Q., He Z. Chloramphenicol/sulfobutyl ether-β-cyclodextrin complexes in an ophthalmic delivery system: prolonged residence time and enhanced bioavailability in the conjunctival sac. *Expet Opin. Drug Deliv.* 2019, *16*, 657–666.
34. Abd-Elal R. M., Elosaily G. H., Gad S., Khafagy E. S., Mostafa Y. Full factorial design, optimization, in vitro and ex vivo studies of ocular timolol-loaded microsponges. *J. Pharm. Innov.* 2020, *15*, 651–663.
35. Fujishima H., Toda I., Yamada M., Sato N., Tsubota K. Corneal temperature in patients with dry eye evaluated by infrared radiation thermometry. *Br. J. Ophthalmol.* 1996, *80*, 29–32.
36. Mohapatra R., Mallick S., Nanda A., Sahoo R. N., Pramanik A., Bose A., Das D., Pattnaik L. Analysis of steady state and non-steady state corneal permeation of diclofenac. *RSC Adv.* 2016, *6*, 31976–31987.
37. Kato M., Hagiwara Y., Oda T., Imamura-Takai M., Aono H., Nakamura M. Beneficial pharmacological effects of selective glucocorticoid receptor agonist in external eye diseases. *J. Ocul. Pharmacol.* 2011, *27*, 353–360.
38. Fehrenbacher, J. C., Vasko, M. R., Duarte, D. B. Models of inflammation: carrageenan or complete freund's adjuvant (CFA) induced edema and hypersensitivity in the rat. *Curr. Protoc. Pharmacol.* 2012, *56*, 5.4.1–5.4.7.
39. Pattanaik S., Nandi S., Sahoo R. N., Nanda A., Swain R., Das S. Budesonide-cyclodextrin in hydrogel system: impact of quaternary surfactant on in vitro-in vivo assessment of mucosal drug delivery. *Rev. Chim. (Bucharest)* 2020, *71*, 332–345.
40. Mohapatra R., Senapati S., Sahoo C., Mallick S. Transcorneal permeation of diclofenac as a function of temperature from film formulation in presence of triethanolamine and benzalkonium chloride. *Colloids Surf. B Biointerfaces* 2014, *123*, 170–180.
41. Waghulde M., Naik J. Comparative study of encapsulated vildagliptin microparticles produced by spray drying and solvent evaporation technique. *Dry. Technol.* 2017, *35*, 1644–1654.
42. Nisar J., Iqbal M., Iqbal M., Shah A., Akhter M. S., Khan R. A., Uddin I., Shah L. A., Khan M. S. Decomposition kinetics of levofloxacin: drug-excipient interaction. *Z. Phys. Chem.* 2020, *234*, 117–128.
43. Kapor A., Nikolić V., Nikolić L., Stanković M., Cakić M., Stanojević L., Ilić D. Inclusion complexes of amlodipine besylate and cyclodextrins. *Cent. Eur. J. Chem.* 2010, *8*, 834–841.
44. Kumar Y. M., Bhagyasree K., Gopal N. O., Ramu C., Nagabhushana H. Structural, thermal and optical properties of Mn2+ doped methacrylic acid–ethyl acrylate (MAA: EA) copolymer films. *Z. Phys. Chem.* 2017, *231*, 1039–1055.
45. Baig M. M., Khan S., Naeem M. A., Khan G. J., Ansari M. T. Vildagliptin loaded triangular DNA nanospheres coated with eudragit for oral delivery and better glycemic control in type 2 diabetes mellitus. *Biomed. Pharmacother.* 2018, *97*, 1250–1258.
46. Castro-Hermida J. A., GóMez-Couso H., Ares-Mazás M. E., Gonzalez-Bedia M. M., CastañEda-Cancio N., Otero-Espinar F. J., Blanco-Mendez J. Anticryptosporidial activity of furan derivative G1 and its inclusion complex with beta-cyclodextrin. *J. Pharm. Sci.* 2004, *93*, 197–206.

47. Mura P., Zerrouk N., Faucci M. T., Maestrelli F., Chemtob C. Comparative study of ibuproxam complexation with amorphous β-cyclodextrin derivatives in solution and in the solid state. *Eur. J. Pharm. Biopharm.* 2002, *54*, 181–191.
48. Londhe V. Y., Umalkar K. B. Formulation development and evaluation of fast dissolving film of telmisartan. *Indian J. Pharmaceut. Sci.* 2012, *74*, 122–126.
49. Caccavo D., Cascone S., Lamberti G., Barba A. A., Larsson A. Swellable hydrogel-based systems for controlled drug delivery. *IntechOpen* 2016, *10*, 237–303.

Scientific paper

Influence of TiO_2 on Mucosal Permeation of Aceclofenac: Analysis of Crystal Strain and Dislocation Density

Souvik Nandi, Satyaki Aparajit Mishra, Rudra Narayan Sahoo, Rakesh Swain and Subrata Mallick*

School of Pharmaceutical Sciences, Siksha 'O' Anusandhan (Deemed to be University), Bhubaneswar, Odisha, India, 751003

** Corresponding author: E-mail: profsmallick@gmail.com; subratamallick@soa.ac.in*
Fax: +91-674-2350642, Tel: +91-674-2350635

Received: 05-22-2020

Abstract

Titanium dioxide can adhere with human epithelial cells and have good tolerability. Present work has been undertaken to explore the influence of TiO_2 on mucosal permeation of aceclofenac. Mucosal permeation of aeclofenac solution containing TiO_2 has been carried out. In fourier transform infrared spectrosopy (FTIR), the intensity of the peaks has decreased along with the increase of TiO_2 content in the formulation indicating a possible binding between drug and TiO_2. Melting enthalpy has been decreased with the increased content of TiO_2 in the solid. The status of crystal strain and dislocation density of TiO_2 and aceclofenac in the solid state formulation has also been evaluated from Xray Diffraction data using Debye-Scherrer's equation. Mucosal permeation of aceclofenac has shown sustained effect for more than 20 h in presence of titanium dioxide. Titanium dioxide could be used in designing formulation for sustaining mucosal aceclofenac delivery after performing risk assessment study.

Keywords: Aceclofenac; titanium dioxide; mucosal permeation; crystal strain; dislocation density; in vitro diffusion.

1. Introduction

Titanium Dioxide (TiO_2) is a biocompatible and stable material,[1] and has a wide range of application in various kinds of cosmetics. TiO_2 is accepted as food additive and also approved by Food and Drug Administration to be used in toothpaste, oral formulations etc.[2] Chen et al, 2011 described that TiO_2 is responsible for increasing intracellular Ca^{2+} concentration leading to elevated secretion of mucin.[3] TiO_2 coating is very much useful to adhere on epithelial tissues.[4] Masa and his colleagues, 2018 reported that TiO_2 has a property to attach with human epithelial cells along with a good tolerability.[5] TiO_2 nanoparticles interact instantly with the buccal mucosa upon contact and show a long residence time in the oral cavity.[6]

Aceclofenac is a widely used Biopharmaceutics Classification System (BCS) class II non-steroidal anti-inflammatory drug (NSAID).[7–9] It suffers from shorter elimination half-life and low oral bioavailability because of low aqueous solubility.[10–12] The toxic effects of this NSAID include gastric abnormalities like abdominal pain, gastric bleeding, dyspepsia etc. It is known that if the first pass metabolism is bypassed avoiding oral administration, improved bioavailability could be observed.[13] Aceclofenac eye drop has shown a marked reduction in ocular inflammation in post-operative cases of cataract operation.[14] Topical administration has been done frequently (2 hourly) for improved permeation through ocular mucosa. In vitro prolonged release has been studied for transmucosal delivery of aceclofenac using mucoadhesive dillenia fruit gum.[15] Katara et al., prepared a nano particle formulation of aceclofenac and claimed that the drug efficacy in local action can be improved if residence time of the formulation is amplified.[16]

In this present study the influence of TiO_2 has been explored on the mucosal permeation of aceclofenac in liquid formulation after topical administration. Any sort of sustained permeation of drug due to long residence time of TiO_2 upon interacting with the mucosal tissue has been examined. Solid state crystal strain and dislocation density have also been analysed.

2. Experimental

2. 1. Materials

Aceclofenac was received from Mannequin Pharmaceuticals Pvt. Ltd., (Bhubaneswar, India) as a gift sample. Titanium Dioxide was procured from Merck Specialities Pvt. Ltd, (Mumbai India).

2. 2. Preparation of Aceclofenac TiO_2 Kneaded Mixture

Aceclofenac was dissolved in a minimal amount of acetone and a kneaded mixture was prepared with titanium dioxide at different ratios (Table 1). [17,18] The mass was dried at 50 °C until constant weight and preserved in a desiccator.

2. 3. FTIR Study

KBR pellet method was used to carry out the FTIR study of pure drug and formulated powders.[19] A mean of 80 times was taken to obtain the average FTIR spectrum from 400 to 4000 cm^{-1} (Model: JASCO FTIR 4100 type A).

2. 4. DSC Study

Differential scanning calorimetry (DSC) cell was calibrated with Indium (melting point: 156.5 C, ΔH_{fus} = 28.54 J/g).[20] The thermogram was recorded under nitrogen atmosphere (50 ml/min) while taking a sample weighing between 4–6 mg in an aluminium crucible. The rate of heating was 10 °C/min and the upper limit was set as 200 °C. [21,22]

2. 5. XRD Study

X-ray diffraction pattern of pure aceclofenac and kneaded mixtures were subjected for XRD study. The scan was carried out at a speed of 1°/ min from 5–70° in Rigaku Ultima IV. CU was used as a source for Xray.

2. 6. *In vitro* Drug Release Study

In vitro drug diffusion study was done in both side open glass tube using dialysis membrane (HIMEDIA Dialysis Membrane-150) (surface area of diffusion = 1.54 cm^2). Acurately weighed amount of the powder samples were taken inside the diffusion tube with 2 ml of fresh liquid medium. The dialysis tube was placed in vessel containing 200 ml phosphate buffer (pH 7.4 at 34 ± 0.5 °C) under a paddle speed of 50 rpm.[23,24] Aliquot of 10 ml was drawn at particular time intervals and replaced with same volume of fresh medium. The absorbance was checked in a UV-Visible spectrophotometer (JASCO V-630 UV-Visible spectrophotometer) at 274 nm.

2. 7. *Ex vivo* Permeation Study

The similar diffusion system was used to study drug permeation through the corneal mucosa. Whole fresh eye ball of goat was brought from the local butcher shop. The cornea was carefully separated out along with 2 to 4 mm of surrounding sclera tissue and washed thoroughly. The cornea was tied tightly with thread along the circumference of vertical cylindrical diffusion tube to prevent any kind of leakage. Powder samples were taken inside the tube with 2 ml of fresh liquid medium and the tube was placed in vessel containing 200 ml phosphate buffer (pH 7.4 at 34 ± 0.5 °C) under a paddle speed of 50 rpm. The tubes were attached with paddle using adhesive tapes and paddles were put down as the as the cornea just touches the dissolution medium. Samples (10 ml) were withdrawn at 0.5, 1, 2, 3, 4, 5, 6, 7, 11, 20 h and replenished with 10 ml of fresh medium. The samples were filtered through 0.45 µm syringe driven filter and analysed by UV-Visible spectrophotometer. The studies of all formulations were performed in triplicate.[25]

3. Results and Discussion

3. 1. FTIR

As depicted in Figure 1, an intense peak was observed at 3317 cm^{-1} may be due to the amine group.[26] Peaks at 1715 and 1771 cm^{-1} may be formed due to stretch-

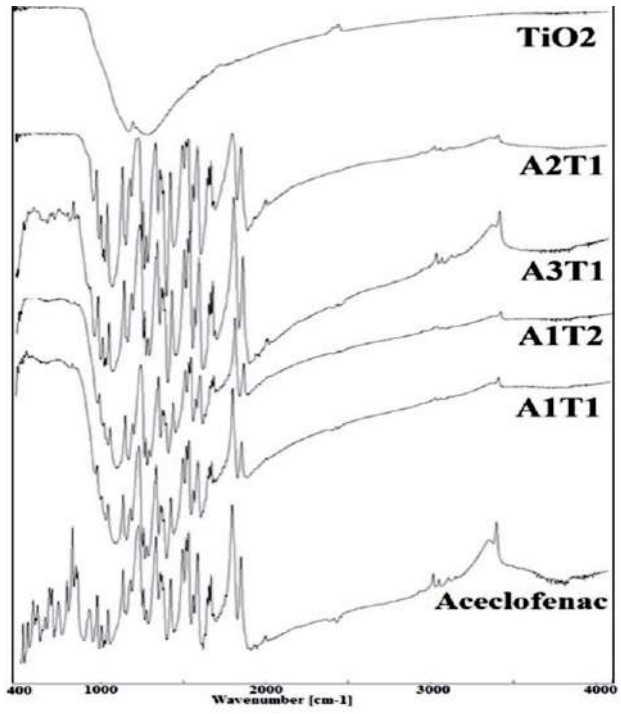

Figure 1. FTIR spectra of pure aceclofenac, TiO_2 and solid formulations.

ing of two carbonyl (C=O) groups in the drug structure.[27,28] The peak at 2969 cm^{-1} may be because of symmetric stretching of CH2 in both pure drug and formulations.[29] In the formulations, the intensity of the peaks has decreased along with the increase of TiO_2 indicating a possible binding between drug and TiO_2. The decrease of the peak intensity at 3317 with the increase of TiO_2 may be considered as the possible binding site with the oxygen present in titanium dioxide with the amine group of aceclofenac.

3. 2. DSC

The pure drug has shown a sharp melting point at 152.97 °C (Figure 2). The formulations have showed a ± 2 °C shifting of melting point along with lower peak intensity comparing to the pure drug. The pure drug has the highest enthalpy of melting (–155.76 jg^{-1}), where the enthalpy has reduced along with the decreased content of aceclofenac and increased content of TiO2 (Table 1). Probably the bond formation between TiO2 and aceclofenac is the cause of the decreased enthalpy of the formulations.

Table 1. Thermal behaviour of TiO_2 kneaded aceclofenac formulation

Formulation Code (Drug:TiO2)	Onset of Melting (°C)	Endset of Melting (°C)	Melting Point (°C)	Enthalpy (jg^{-1})
Aceclofenac	152.01	156.77	152.97	–155.76
A1T1 (1:1)	149.50	156.44	153.73	–62.11
A1T2 (1:2)	147.15	155.02	151.57	–32.23
A2T1 (2:1)	149.07	157.31	153.83	–66.67
A3T1 (3:1)	150.81	155.83	153.16	–153.09

3. 3. XRD Study

X ray diffraction data is portrayed in Figure 3. The TiO_2 as well as the formulations has shown a particular kind of diffraction pattern at 38.5° and 55° 2θ. The diffraction position and pattern proved that the TiO_2 anatase crystals has not changed in the formulations.[30] The most intense peaks then subjected to further calculation and an average value was taken as a representation for the whole formulation. The particle size was determined from the Debye-Scherrer's equation.[31]

$$D = \frac{K\lambda}{\beta Cos\theta} \quad (1)$$

Where, D is the crystal size (nm), K is a constant with a value of 0.9, λ is the wavelength of the Xray (0.1541 nm) and β is the value of FWHM (full width at half maxima) in radian. The X-ray diffraction pattern of TiO2 is evident to be at anatase phase[30,31] and the typical anatase TiO2 crystals have the octahedral structure.[32] Typically the K value can be considered as 0.9 and Anku et al., (2016) also estimated particle size of TiO2 anatase using Scherrer's Formula considering the shape factor 'K' as 0.9.[33]

Other characteristic properties of the formulations like, strain and dislocation density are tabulated in Table 2. Dislocation density can be described as the length of dislocation lines per unit volume of the crystals where dislocation is a linear defect found in crystals[34]. The untreated and treated pure TiO_2 has shown dislocation density of 0.80 and 0.71 respectively whereas the formulation with highest content of aceclofenac has shown almost 1.4 times higher dislocation lines per unit area. The similarity has also followed in the case of pure TiO_2 crystal strain (0.73) and the formulation, A3T1 has

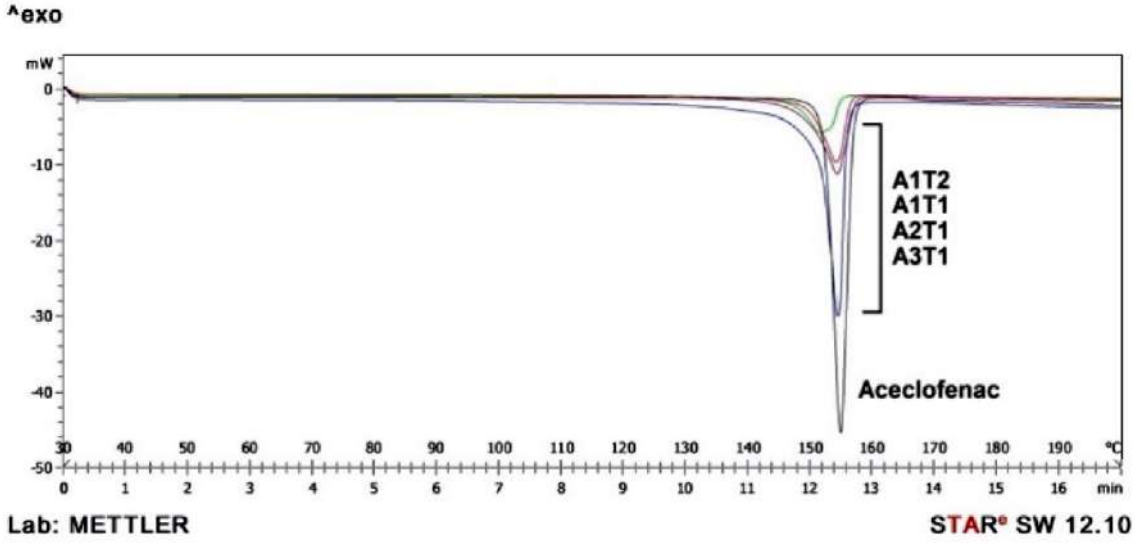

Figure 2. DSC Thermogram of aceclofenac and the formulations.

Table 2. Solid state particle properties of aceclofenac-titanium dioxide kneaded products

Formulation Code	TiO_2			Aceclofenac		
	Particle Size (nm)	Strain	Dislocation Density*10^{-3}	Particle Size (nm)	Strain	Dislocation Density *10^{-3}
Aceclofenac	–	–	–	98.08 ± 16.5	0.114 ± 0.014	0.44 ± 0.10
T1 (untreated TiO_2)	70.89 ± 3.64	0.073 ± 0.016	0.80 ± 0.088	–	–	–
T2 (Acetone treated TiO_2)	74.87 ± 1.60	0.068 ± 0.012	0.71 ± 0.030	–	–	–
A1T1	68.65 ± 0.84	0.075 ± 0.013	0.84 ± 0.021	73.47 ± 19.46	0.157 ± 0.037	0.90 ± 0.50
A1T2	64.44 ± 1.34	0.079 ± 0.015	0.96 ± 0.040	59.67 ± 11.56	0.132 ± 0.054	1.22 ± 0.40
A2T1	65.88 ± 3.15	0.077 ± 0.010	0.92 ± 0.092	71.09 ± 14.81	0.158 ± 0.054	0.98 ± 0.40
A3T1	63.01 ± 1.25	0.081 ± 0.013	1.00 ± 0.041	70.88 ± 14.58	0.149 ± 0.036	0.87 ± 0.30

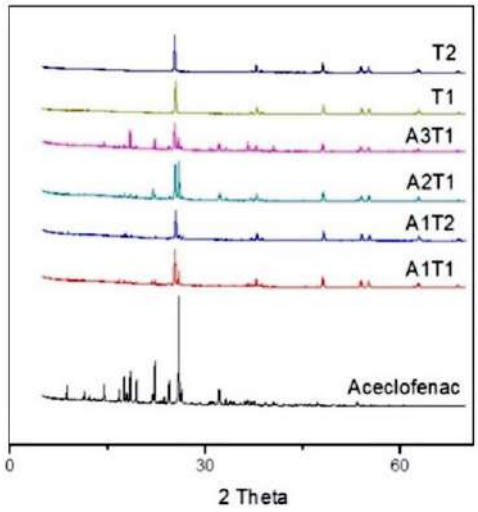

Figure 3. Powder Xray diffraction overlay of pure drug, formulation, untreated and treated titanium dioxide (T1 and T2 respectively).

shown the highest strain. The above mentioned changes may have occurred due to the binding of aceclofenac with titanium dioxide.[19] A similar phenomenon was noticeable in the case of aceclofenac where the dislocation density of A1T2 was higher than any other formulations or the pure drug itself. Particle size was found to be lowest in the case of the A1T2 formulation than the pure drug (98.08 nm).

3. 4. *In vitro* Diffusion Study

The observation was replicated in triplicate and the mean value is used to prepare the time vs cumulative percent release in Figure 4. The highest release was found in the case of A2T1 (89.88%) at 2 hours followed by A1T1 (89.13%). The formulation containing highest amount of TiO2 (A1T2) has shown lowest amount of drug release 82.55% in contrast to others at 120 mins.

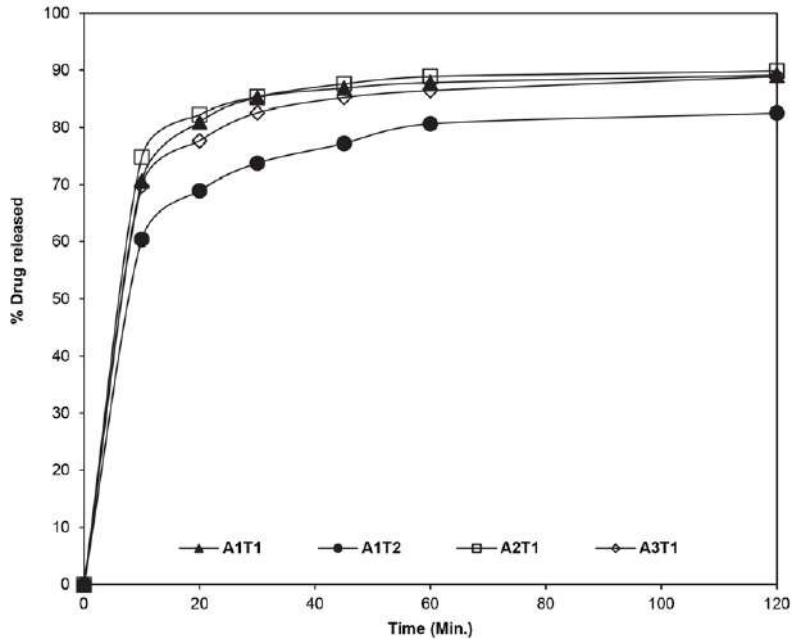

Figure 4. *In vitro* drug diffusion profile of the formulation

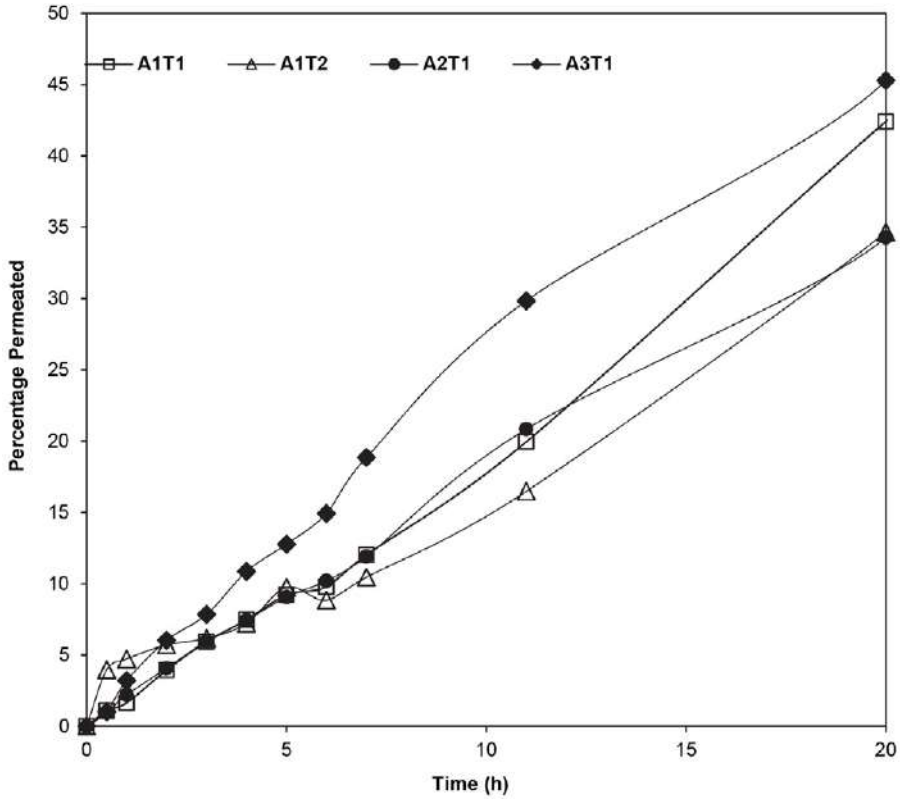

Figure 5. *Ex vivo* permeation study of the formulations through goat corneal mucosa

3. 5. *Ex vivo* Permeation Study

The data was presented as a plot of time vs percentage permeated in Figure 5. The highest release was found in the case of A3T1 (45.29 %) at 20 hours followed by A1T1 (42.40 %). In all of the formulations the permeation was continued up to 20 hours while maintaining an increasing order. Aceclofenac 0.1 % solution exhibited goat corneal permeation of almost 50–90 % within 2 h only in the pH range of 7–7.4.[14]

4. Conclusion

Influence of titanium dioxide on mucosal permeation of aceclofenac has been carried out in aqueous state. FTIR results revealed the decreased intensity of some characteristic peaks of aceclofenac in the formulation with the decreased content of aceclofenac and increased content of TiO_2 indicating possible binding between drug and TiO_2. Thermal analysis has also exhibited decreased melting enthalpy with the decrease of aceclofenac and increase of TiO_2 content in the solid. The change in crystal strain and dislocation density of TiO_2 and aceclofenac in the solid formulation has been noticed. Sustained mucosal permeation of aceclofenac has been observed for more than 20 h in presence of titanium dioxide. Titanium dioxide could be used in designing formulation for sustaining and controlling mucosal delivery of aceclofenac after assessing risk factor associated with TiO_2.

Acknowledgement

The authors are grateful to the Department of Science & Technology, Ministry of Science & Technology, New Delhi, India, for providing INSPIRE fellowship to Souvik Nandi (IF 180534). The authors are also grateful to Dr. Monojranjan Nayak, President, Siksha 'O' Anusandhan (Deemed to be University) for other laboratory facilities. We are also grateful to receive Aceclofenac as a gift sample from Mannequin Pharmaceuticals Pvt. Ltd., Bhubaneswar, Odisha. The authors are also grateful to the anonymous reviewers for their critical comments and suggestions to improve the quality of the manuscript.

Conflict of Interest

The authors declare no conflict of interests.

5. References

1. H. M. A. Shawish, H. Tamous, S. Saadeh, A. Tbaza, *Acta Chim. Slov*. **2018**, *65*, 811–822. **DOI:**10.17344/acsi.2018.4383
2. M. Skocaj, M. Filipic, J. Petkovic, S. Novak, *Radiol. Oncol.* **2011**, *45*, 227–247. **DOI:**10.2478/v10019-011-0037-0

3. E. Y. Chen, M. Garnica, Y. C. Wang, C. S. Chen, W. C. Chin, *PloS one*. **2011**, *6*, e16198. **DOI:**10.1371/journal.pone.0016198
4. S. Riivari, K. Shahramian, I. Kangasniemi, J. Willberg, T. O. Närhi, *Int. J. Oral Maxillofac. Implants*. **2019**, *34*, 313–319. **DOI:**10.11607/jomi.6862
5. R. Masa, Á. Deák, G. Braunitzer, Z. Tóth, J. Kopniczky, I. Pelsőczi-Kovács, K. Ungvári, I. Dékány, K. Turzó, *J. Nanosci. Nanotechnol*. **2018**, *18*, 3916–3924. **DOI:**10.1166/jnn.2018.15261
6. B. J. Teubl, G. Leitinger, M. Schneider, C. M. Lehr, E. Fröhlich, A. Zimmer, E. Roblegg, *Nanotoxicology*, **2015**, *9*, 253–261. **DOI:**10.3109/17435390.2014.921343
7. T. Soni, C. Nagda, T. Gandhi, N. P.Chotai, *Dissolut. Technol.* **2008**, *15*, 31–35. **DOI:**10.14227/DT150208P31
8. M. Grau, J. Guasch, J. L. Montero, A. Felipe, E. Carrasco, S. Juliá, *Arzneim-Forsch Drug Res*, **1991**, *41*, 1265–1276.
9. N. Sethuraman, S. Shanmuganathan, K. Sandhya, B. Anbarasan, *Indian J. Pharm. Educ.* **2018**, *52*, 581–586. **DOI:**10.5530/ijper.52.4.67
10. R. Raj, P. Mongia, A. Ram, N. K. Jain, *Artif Cells Nanomed. Biotechnol*. **2016**, *44*, 1434–1439.
11. https://pubchem.ncbi.nlm.nih.gov/compound/Aceclofenac#section=Melting-Point
12. B. Tubić, A. Uzunović, S. Pilipović, Ž. Gagić, *Acta Chim. Slov*. **2016**, *63*, 193–9. **DOI:**10.17344/acsi.2015.2168
13. S. Korani, M. Korani, S. Bahrami, T. P. Johnston, A. E. Butler, M. Banach, A. Sahebkar, *Drug Discov. Today*. **2019**, *24*, 567–574. **DOI:**10.1016/j.drudis.2018.09.023
14. V. Dave, S. Paliwal, *Saudi Pharm. J*. **2014**, *22*, 240–245. **DOI:**10.1016/j.jsps.2013.03.001
15. M. S. Hasnain, P. Rishishwar, S. Ali, A. K. Nayak, *SN App. Sci.* **2020**, *2*, 1–8. **DOI:**10.1007/s42452-019-1756-x
16. R. Katara, D. K. Majumdar, *Colloid Surface B*. **2013**, *103*, 455–462. **DOI:**10.1016/j.colsurfb.2012.10.056
17. A. Modi, P. Tayade, *AAPS PharmSciTech*. **2006**, *7*, E87. **DOI:**10.1208/pt070368
18. S. Nandi, S. A. Mishra, R. N. Sahoo, R. Swain, S. Mallick, *Indian J. Pharm. Educ.* **2020**, *54*, 68–72. **DOI:**10.5530/ijper.54.1.8
19. M. Starsinic, R. L. Taylor, P. L. Walker Jr, P. C.Painter, *Carbon*. **1982**, *21*, 69–74. **DOI:**10.1016/0008-6223(83)90158-6
20. G. Vanden, V. B. F.Mathot, *Thermochim. Acta*. **2006**, *446*, 41–54. **DOI:**10.1016/j.tca.2006.02.022
21. R. N. Sahoo, A. Nanda, A. Pramanik, S. Nandi, R. Swain, S. K. Pradhan, S. Mallick, *Acta Chim. Slov.* **2019**, *66*, 923–933. **DOI:**10.17344/acsi.2019.5139
22. M. Acharya, S. Mishra, R. N. Sahoo, S. Mallick, *Acta Chim. Slov.* **2017**, *64*, 45–54. **DOI:**10.17344/acsi.2016.2772
23. S. A. Agnihotri, T. M. Aminabhavi, *J. Control. Release.* **2004**, *96*, 245–259. **DOI:**10.1016/j.jconrel.2004.01.025
24. M. S. Bhandari, S. M. Wairkar, U. S. Patil, N. R. Jadhav, *Acta Chim. Slov*, **2018**, *65*, 492–501. **DOI:**10.17344/acsi.2017.3822
25. M. S. Kaynak, M. Celebier, S. Sahin, S. Altinöz, *Rev. Chim. (Bucharest).* **2013**, *64*, 27–30.
26. R. Mohapatra, S. Senapati, C. Sahoo, S. Mallick, *Farmacia*. **2016**, *64*, 72–81.
27. C. Y. Won, C. C. Chu, J. D. Lee, *Polymer*, **1998**, *39*, 6677–6681. **DOI:**10.1016/S0032-3861(98)00032-9
28. W. J. Ray, J. E. Katon, B. Phillips, *J. Mol. Struct.* **1981**, *74*, 75–84. **DOI:**10.1016/0022-2860(81)80009-9
29. P. S. Thomas, J. Guerbois, G. F. Russell, B. J.Briscoe, *J. Therm. Anal. Cal.* **2001**, *64*, 501–508. **DOI:**10.1023/A:1011578514047
30. A. Di Paola, M. Bellardita, B. Megna, F. Parrino, L. Palmisano, *Catal. Today.* **2015**, *252*, 195–200. **DOI:**10.1016/j.cattod.2014.09.012
31. W. Anku, S. O. Oppong, S. K. Shukla, P. P. Govender, *Acta Chim. Slov.* **2016**, *63*, 380–391. **DOI:**10.17344/acsi.2016.2385
32. S. Yang, N. Huang, Y. M. Jin, H. Q. Zhang, Y. H. Su, H. G. Yang, *Cryst. Eng. Comm.*, **2015**;*17*, 6617–6631. **DOI:**10.1039/C5CE00804B
33. A. Bishnoi, S. Kumar, N. Joshi, in: Microscopy Methods in Nanomaterials Characterization, Elsevier, **2017**, pp. 313–337. **DOI:**10.1016/B978-0-323-46141-2.00009-
34. I. Boukhoubza, M. Khenfouch, M. Achehboune, B. M. Mothudi, I. Zorkani, A. Jorio, in: *J. Phy.: Conference Series*, IOP Publishing, **2019**, *1292*, 012011. **DOI:**10.1088/1742-6596/1292/1/012011

Povzetek

Titanov dioksid se lahko adherira na človeške epitelijske celice in se dobro prenaša. Opisano delo je proučevalo vpliv TiO_2 na prepustnost sluznice za aceklofenak. Izvedena je bila študija prepustnosti sluznice za raztopino aceklofenaka, ki je vsebovala TiO_2. Pri infrardeči spektroskopiji s Fourierjevo transformacijo (FTIR) se je intenzivnost vrhov zmanjšala hkrati s povečanjem vsebnosti TiO_2 v formulaciji, kar kaže na morebitno vezavo med učinkovino in TiO_2. Entalpija taljenja se je zmanjšala s povečanjem vsebnosti TiO_2 v trdni snovi. Stanje kristalne oblike in dislokacijska gostota TiO_2 in aceklofenaka v trdni formulaciji sta bila ocenjena iz podatkov rentgenske difrakcije z uporabo Debye-Scherrerjeve enačbe. Prepustnost sluznice za aceklofenak je v prisotnosti titanovega dioksida pokazala podaljšano delovanje za več kot 20 ur. Titanov dioksid bi se po izvedbi študije ocene tveganja lahko uporabil pri oblikovanju formulacije za zadrževanje acekolofenaka na sluznici.

Original Article

Quantitative Estimation of Tabletability of Aceclofenac after Incorporation of Titanium Dioxide using Area under the Curve

Souvik Nandi, Satyaki Aparajit Mishra, Rudra Narayan Sahoo, Rakesh Swain, Subrata Mallick*

School of Pharmaceutical Sciences, Siksha 'O' Anusandhan (Deemed to be University), Bhubaneswar, Odisha, INDIA.

ABSTRACT

Background: Tablet manufacturing with direct compression is one of the leading industrial technique that consumes less time, labour and economic also. But the choice of excipients are critical in this case which will allow the drug to get compressed without granulation techniques. **Purpose:** Aceclofenac is a BCS class II non-steroidal anti-inflammatory drug, which exerts a low oral bioavailability because of low solubility in aqueous medium. The drug also suffers from compressibility and also shows poor tabletibility. **Methods:** We have attempted to improve tabletability by incorporating titanium dioxide (TiO_2) through kneading and solvent evaporation technique. **Results:** In the FTIR study revealed that NH and Cl aromatic stretching of aceclofenac has been affected significantly due to binding with TiO_2. DSC thermogram ascertained the partial amorphization of the drug in the formulations. Evaluated tabletability from the area under the applied pressure vs tensile strength curve (AUTC) of A1T1 has shown a poor value in contrast to other formulations.

Key words: Aceclofenac, Tabletability, Titanium dioxide, Direct compression, Area under the curve.

INTRODUCTION

Tablet manufacturing with direct compression is one of the leading industrial techniques that consumes less time, labour and more economic also. But the choice of excipients are critical in the direct compression which allows the drug to get compressed without granulation techniques. The excipient must have symmetrical particle size distribution, must be compatible with the drug and other excipients and to bind a large amount of material while it is undergoing direct compression. Many research reports are available on directly compressible tablets but, quantitative estimation of tabletability using non-linear approach are very few in number.

Aceclofenac, a BCS class II non-steroidal anti-inflammatory drug possesses remarkable analgesic and antipyretic properties and used to treat rheumatoid and osteo arthritis.[1-3] The drug also suffers from compressibility and shows poor tabletability.[4,5] Talcum and magnesium stearate as the flow promoting agents even could not change in the flow properties of the drug in the presence of HPMC. The compression problem was observed in preparing aceclofenac mouth dissolving tablet by direct compression using microcrystalline cellulose and other excipients. Patil *et al.* 2012 has prepared aceclofenac agglomerates to improve its flowability and compressibility by emulsion solvent diffusion technique.[6] The major limitations associated with the technique are the significant drug loss and polymer loss.[7] Shete *et al.* 2018 have prepared cocrystals of Fenofibrate and Nicotinamide. In this study they have subjected the formulations to various tableting studies like hardness, thickness but they have not created any tabletability profile of those prepared tablets.[8]

This study deals with the tabletability behaviour of aceclofenac kneaded with TiO_2 in different ratios by direct compression

Submission Date: 31-05-2019;
Revision Date: 04-09-2019;
Accepted Date: 22-11-2019

DOI: 10.5530/ijper.54.1.8

Correspondence:
Prof. Subrata Mallick ,
School of Pharmaceutical Sciences, Siksha 'O' Anusandhan (Deemed to be University), Bhubaneswar-751003, Odisha, INDIA.
Phone: +91 0674 2386209
E-mail: profsmallick@gmail.com

www.ijper.org

technique. Quantitative estimation of tabletability has rarely been studied earlier for any tablet formulation by direct compression technique. Non-linear approach for estimation of tabletability quantitatively has been proposed in this work from simple relationship which is supposed to be more accurate relative to least square method. Titanium dioxide is having outstanding biocompatibility and the drug releasing performance can be tuned by designing formulation/medical implants.[9,10]

MATERIALS AND METHODS

Materials

Titanium dioxide was purchased from Merck Specialities Pvt. Ltd., Mumbai, India. Microcrystalling cellulose was obtained from HIMEDIA Laboratories Pvt. Ltd., Mumbai, India. Aceclofenac pure drug was obtained as a gift sample from Mannequin Pharmaceuticals Pvt. Ltd., Bhubaneswar, Odisha.

Preparation of Aceclofenac TiO_2 Kneaded mixture

Aceclofenac was dissolved in a minimal amount of acetone and a kneaded mixture was prepared with titanium dioxide at different ratios.[11] The mass was dried at 50°C until constant weight and preserved in a desiccator.

Characterization

FTIR Study

FTIR study of pure drug and formulated powder sample was done using KBr pellet method.[12] The FTIR spectrum was a mean of 80 times scan between the wave number of 400-4000cm^{-1} in (Model: JASCO FTIR 4100type A).[13]

Direct Compression

The prepared formulation was mixed with microcrystalline cellulose by maintaining a ratio of 1:2. 200 mg of the prepared mixture then subjected to the punching cavity manually. The pressure was varied while preparing the compacts by using the previously stated formulations. The pressures which have been used were 0.5,1, 1.5, 2 and 2.5 tons.[14] The dimensions and hardness was then measured for determination of various physical and mechanical properties.[8] Tensile strength was calculated by using formula:[15]

$$TS = \frac{2F}{\pi dh}$$

Here, F is compression force applied in Newton force (unit: $kg.m/S^2$); d= diameter in meter, h=thickness of the tablet in meter.

Kawakita model

To relate between compaction pressure and volume reduction Kawakita and Ludde has proposed model as follows:

$$\frac{P}{C} = \frac{P}{a} + \frac{1}{ab}$$

In the above equation the 'P' signifies applied pressure, 'a' and 'b' both are constants which gives an idea of the maximum volume reduction and an inclination towards volume reduction respectively. 'C' can be described as degree of volume reduction and can be calculated from

$$C = 1 - \frac{V}{V_0}$$

(where, V_0 is the initial volume of the powder column and V is the volume under pressure).[16,17]

RESULTS AND DISCUSSION

FTIR Study

An intense peak was observed at 3317 cm^{-1} probably because of the amine group.[18] (Figure 1) The peaks at 1715 and 1771 cm^{-1} may be formed due to stretching of two carbonyl (C=O) groups in the aceclofenac structure.[19,20] The peak at 2969 cm^{-1} in both pure drug and formulations indicates the symmetric stretching of CH_2.[21] In the formulations, the intensity of the peaks has decreased along with the increase of TiO_2 concentration which indicated a possible binding of TiO_2 and Acceclofenc.

Direct Compression

A model given by Sun *et al.* 2001 is mainly used in the case of expressing tabletability. The equation is as follows:[22]

$$TS = k_t P + C$$

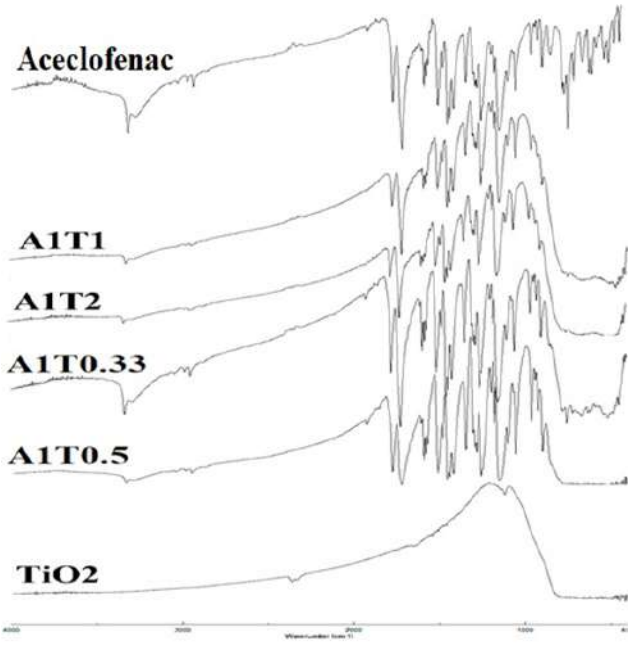

Figure 1: FTIR spectrum of aceclofenac and formulations

Tabletibility of the composite powder material can be expressed by applied pressure vs tensile strength curve (Figure 2) where the slope value 'k_t' signifies tabletability coefficient. It can be quantified by Area under the applied pressure vs tensile strength curve (AUTC). (Table 1) The plot has clearly shown that the 1:1 formulation is poor in tabletibility in contrast to the other formulations.[23]

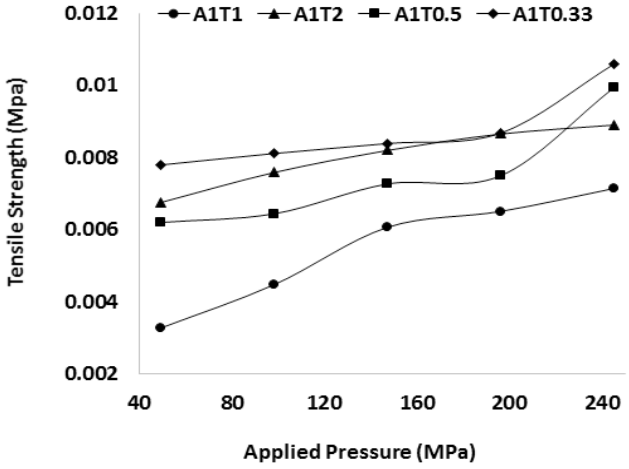

Figure 2: Tabletability profile of the formulations.

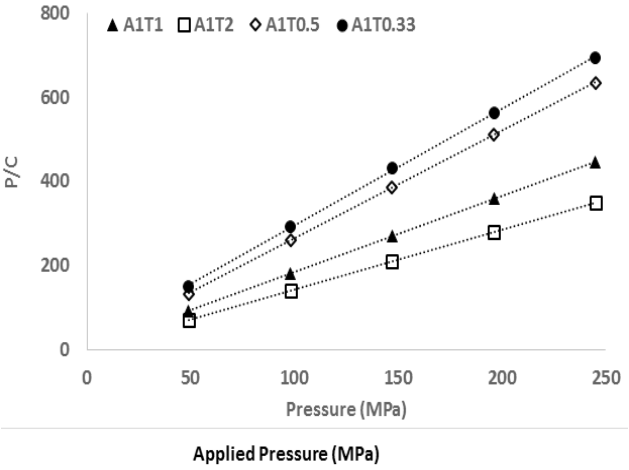

Figure 3: Kawakita pressure Plot of the prepared formulations.

Kawakita Model

As per Kawakita linearity model, the highest compressibility (a) and inclination towards volume reduction (b) are seen with the formulation A1T2 (Figure 3) (Table 2).

Proposed binding of Aceclofenac with TiO_2

Proposed binding between TiO_2 and aceclofenac has been depicted in Figure 4a, b. Binding could be possible in either of the two ways. Titanium is getting attached to Chlorines while the amine group is getting attached with the oxygen present in TiO_2. Chlorine may bind with the titanium by opposite charge attraction (4a) or formation of hydrogen bond between chlorine and titanium (4b).

CONCLUSION

Aceclofenac alone could not be tableted because of very poor compressibility by direct compression. Tabletability of A1T2, A1T0.5 and A1T0.33 formulations has been improved compared to A1T1. The kawakita parameters suggested that the inclination towards

Table 1: Tabletability parameters.

Formulation Code	K_t*10^6	AUTC
A1T0.33	12.49	1.685
A1T0.5	17.32	1.435
A1T1	19.80	1.091
A1T2	10.94	1.584

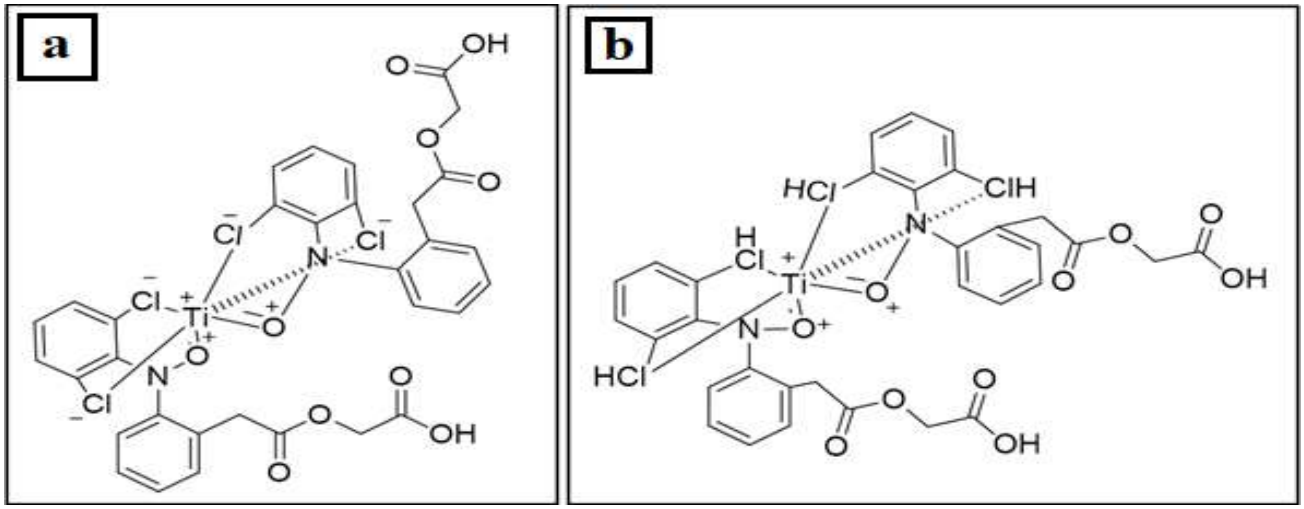

Figure 4: Proposed binding between TiO_2 and Aceclofenac. Chlorine may bind with the titanium by opposite charge attraction (4a) or formation of hydrogen bond between chlorine and titanium (4b).

Table 2. Kawakita Parameters of aceclofenac kneaded with TiO_2 in different ratios							
Formulation Code	**Drug:TiO_2 (w/w)**	**Equation**	**1/a**	**1/ab**	**a**	**ab**	**b**
A1T0.33	1:0.33	y=2.764x+19.17	2.764	19.176	0.361	0.052	0.144
A1T0.5	1:0.5	y=2.56x+8.16	2.560	8.160	0.390	0.122	0.313
A1T1	1:1	y=1.81x+3.14	1.810	3.146	0.552	0.317	0.575
A1T2	1:2	y=1.419x+1.26	1.419	1.261	0.704	0.793	1.125

volume reduction of the powder may be directly related to the amount of TiO_2 incorporation.

ACKNOWLEDGEMENT

The authors are grateful to Dr. Monojranjan Nayak, President, Siksha 'O'Anusandhan University for financial support and laboratory facility. We are also grateful to receive Aceclofenac as gift sample from Mannequin Pharmaceuticals Pvt. Ltd., Bhubaneswar, Odisha.

CONFLICT OF INTEREST

The authors declare no conflict of interest.

ABBREVIATIONS

BCS: Biopharmaceutical Classification System; **TiO_2:** Titanium Dioxide; **DSC:** Differential Scanning Calorimetry; **FTIR:** Fourier Transform Infrared Spectroscopy; **AUTC:** Area under the Tabletability Curve; **HPMC:** Hydroxypropylmethylcellulose; **TS:** Tensile Strength.

REFERENCES

1. Sethuraman N, Shanmuganathan S, Sandhya K, Anbarasan B. Design, Development and Characterization of Nano Structured Lipid Carrier for Topical Delivery of Aceclofenac. Indian J Pharm Educ. 2018;52(4):581-6.
2. Soni T, Nagda C, Gandhi T, Chotai NP. Development of Discriminating Method for Dissolution of Aceclofenac Marketed Formulations. Dissolut Technol. 2008;15(2):31-5.
3. Grau M, Guasch J, Montero JL, Felipe A, Carrasco E, Juliá S. Pharmacology of the Potent New Non-steroidal Anti-inflammatory Agent Aceclofenac. Arzneim-Forsch Drug Res. 1991;41(12):1265-76.
4. Mutalik S, Naha A, Usha AN, Ranjith AK, Musmade P, Manoj K, *et al.* Preparation, *in vitro*, Preclinical and Clinical Evaluations of Once Daily Sustained Release Tablets of Aceclofenac. Arch Pharm Res. 2007;30(2):222-34.
5. Solanki SS, Dahima R. Formulation and evaluation of aceclofenac mouth-dissolving tablet. J Adv Pharm Technol Res. 2011;2(2):128-31.
6. Patil SV, Sahoo SK. Improvement of Flowability, Compressibility and Dissolution of Aceclofenac by Emulsion Solvent Diffusion with Polyethylene Glycol. Ars Pharm. 2014;53(2):21-7.
7. Mallick S, Roy K, Chakraborty A, Saha S. Mechanism of *in vitro* Release Kinetics of Flurbiprofen Loaded Ethylcellulose Micropellets. Acta Pol Pharm. 2002;59(3):193-8.
8. Shete AS, Khandagale VV, Murthy SM, Vyankatrao A. Solid State Characterization and Tableting Studies of Ethanol Based Cocrystals of Fenofibrate with Nicotinamide. Indian J Pharm Educ. 2018;52(1):71-7.
9. Losic D, Aw MS, Santos A, Gulati, K, Bariana M. Titania nanotube arrays for local drug delivery: Recent advances and perspectives. Expert Opin Drug Deliv. 2015;12(1):103-27.
10. León A, Reuquen P, Garín C, Segura R, Vargas P, Zapata P, *et al.* FTIR and Raman Characterization of TiO_2 Nanoparticles Coated with Polyethylene Glycol as Carrier for 2-Methoxyestradiol. Appl Sci. 2017;7(1):49.
11. Modi A, Tayade P. Enhancement of Dissolution Profile by Solid Dispersion (Kneading) Technique. AAPS Pharm Sci Tech. 2006;7(3):1-6.
12. Starsinic M, Taylor RL, Jr W, Painter PC. FTIR Studies of Saran Chars. Carbon. 1982;21(1):69-74.
13. Swain RP, Nagamani A, Shankar PU. Formulation and Evaluation of Gastro-bilayer Floating Tablets of Ezetimibe as Immediate Release Layer and Atenolol as Sustained Release Layer. 2019;53(2).
14. Panda B, Digdarsini T, Mallick S. Physicomechanical and physicochemical characterizations of biexponential compaction process of paracetamol in the presence of talcum-lubricated-MCC. Powder Technol. 2015;273:91-101.
15. Sonnergaard JM. Quantification of the compactibility of pharmaceutical powders. Eur J Pharm Biopharm. 2006;63(3):270-7.
16. Kawakita K, Ludde KH. Some Considerations on Powder Compression Equations. Powder Technol. 1971;4(2):61-8.
17. Yamashiro M, Yuasa Y, Kawakita K. An Experimental Study on the Relationships between Compressibility, Fluidity and Cohesion of Powder Solids at Small Tapping Numbers. Powder Technol. 1983;34(2):225-31.
18. Won C, Chu C, Doo J. Novel biodegradable copolymers containing pendant amine functional groups based on aspartic acid and poly (ethylene glycol). Polymer. 1998;39(25):6677-81.
19. Ray WJ, Katon JE, Phillips B. Structure, Hydrogen Bonding and Vibrational Spectra of Pyruvic Acid. J Mol Struct. 1981;74(1):75-84.
20. Thomas PS, Guerbois J, Russell GF, Briscoe BJ. Ftir Study of the Thermal Degradation of Poly (Vinyl Alcohol). J Therm Anal Cal. 2001;64(2):501-8.
21. Silva DJD, Wiebeck H. Vibrational Spectroscopy Using PLS, iPLS and siPLS linear regressions to determine the composition of LDPE / HDPE blends: A comparison between confocal Raman and ATR-FTIR spectroscopies. Vib Spectrosc. 2017;92:259-66.

SUMMARY

Aceclofenac is a poorly compressible drug and has a low tabletability. We have tried to overcome these drawbacks by incorporating TiO_2 in the formulation. An increase in tablet ability has been observed after the addition of TiO_2. Kawakita parameters also suggested that the inclination towards volume reduction of the powdered formulation is directly proportional to the amount of TiO_2 added.

PICTORIAL ABSTRACT

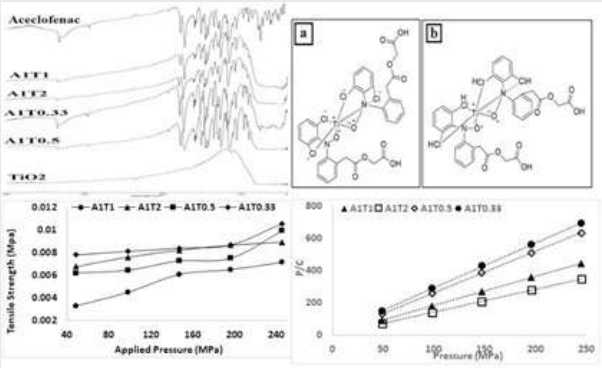

About Authors

Souvik Nandi, M.Pharm, currently engaged as a DST INSPIRE junior research fellow at School of Pharmaceutical Sciences, Siksha 'O' Anusandhan (Deemed to be University), Bhubaneswar, Odisha, India. His research area of interest is Formulation and Development, and Novel Drug Delivery Systems.

Satyaki Aparajit Mishra, M.Pharm from Siksha O Anusandhan (Deemed to be University), Bhubaneswar, Odisha, India.

Rudra Narayan Sahoo, M.Pharm, currently engaged as an INSPIRE Fellow under DST Government of India at School of Pharmaceutical Sciences, Siksha 'O' Anusandhan (Deemed to be University), Bhubaneswar, Odisha, India. His research area of interest is Formulation and Development, and Drug Delivery Systems.

Rakesh Swain, M.Pharm, currently engaged as a DST INSPIRE research fellow at School of Pharmaceutical Sciences, Siksha 'O' Anusandhan (Deemed to be University), Bhubaneswar, Odisha, India.

Subrata Mallick, (M.Pharm, Ph.D, PGDBM, FIC) is a life member of Association of Pharmaceutical Teachers of India, and Indian Pharmaceutical Association. At present he is the Professor and Heading the Department of Pharmaceutics, School of Pharmaceutical Sciences, Siksha 'O' Anusandhan (Deemed to be University), Bhubaneswar, India. He is the reviewer of Elsevier, Wiley, Informa Healthcare, Taylor and Francis, Bentham Science, Springer, IEEE Xplore, Dovepress etc. and editorial board member of several International Journals of America, Canada, UK, Thailand, India etc. He is also a member of doctoral committee of several universities. His current research areas of interest are: Ocular Drug Delivery Systems, Drug Stabilisation and Kinetics, Mucosal Delivey, Powder Compaction etc. More than 160 number of full research papers and conference proceedings are published in International and National levels under his guidance.

Cite this article: Nandi S, Mishra SA, Sahoo RN, Swain R, Mallick S. Quantitative Estimation of Tabletability of Aceclofenac after Incorporation of Titanium Dioxide using Area under the Curve. Indian J of Pharmaceutical Education and Research. 2020;54(1):68-72.

Scientific paper

Interactions between Ibuprofen and Silicified-MCC: Characterization, Drug Release and Modeling Approaches

Rudra Narayan Sahoo,[1] Ashirbad Nanda,[1] Arunima Pramanik,[1] Souvik Nandi,[1] Rakesh Swain,[1] Sukanta Kumar Pradhan[2] and Subrata Mallick[1,*]

[1] *School of Pharmaceutical Sciences, Siksha 'O' Anusandhan (Deemed to be University), Kalinganagar, Bhubaneswar- 751003, Odisha, India.*

[2] *Department of Bioinformatics, Orissa University of Agriculture and Technology, Bhubaneswar, Odisha, India.*

** Corresponding author: E-mail: profsmallick@gmail.com*
Fax: +91-674-2350642; Tel: +91-674-2350635

Received: 03-06-2019

Running Title: Docking analysis of ibuprofen with SMCC

Abstract

Analysis of the binding interactions of ibuprofen and silicified-microcrystalline cellulose (SMCC) has been undertaken. Co-processing of ibuprofen with SMCC was carried out by solid state ball milling, and aqueous state equilibration followed by freeze drying to investigate the effect of silicified-microcrystalline cellulose on ligand. Molecular docking study revealed that ibuprofen formed complex through hydrogen bond with microcrystalline cellulose (MCC) and silicon dioxide (SiO_2); the binding energy between MCC and SiO_2, and ibuprofen and SMCC were found as –1.11 and –1.73 kcal/mol respectively. The hydrogen bond lengths were varying from 2.028 to 2.056 Å. Interaction of Si atom of SMCC molecule with Pi-Orbital of ibuprofen has shown the bond length of 4.263 Å. Significant improvement in dissolution of ibuprofen has been observed as a result of interaction. Binary and ternary interactions revealed more stabilizing interactions with ibuprofen and SMCC compared to SMCC formation.

Keywords: Co-processing; silicified microcrystalline cellulose; molecular docking analysis; binary interaction; ternary interaction.

1. Introduction

Molecular docking experiment was used to predict the binding mode interactions between the molecules.[1] The program uses Lamarckian genetic algorithm, semi empirical free energy force field, grid box based method to allow rapid evaluation of the binding energy and pre-calculating the interaction between every atom type pair at every distance and result clustering procedures. The force field is based on a comprehensive thermodynamic model that allows incorporation of intramolecular energies into the predicted free energy of the binding.[2]

Rheumatoid arthritis, a systemic inflammatory disease causes pain, stiffness, and swelling of joints and, over the time, the disease has a severe, chronic and invalid progression with loss of mobility.[3,4] Ibuprofen could be considered as the drug of choice in the management and therapy of inflammation in rheumatoid arthritis.[5] Oral bioavailability of ibuprofen is very poor due to its poor water solubility.[6] Low oral bioavailability limits therapeutic efficacy of the drug.[7] Dissolution rate of ibuprofen (BCS class II) in gastrointestinal fluid is the rate limiting step in its oral absorption and often results in low and erratic oral bioavailability.[8,9] Many techniques have been reported to improve the bioavailability of poorly water-soluble drugs.[10,11] Solid state amorphization can achieve improved solubility.[12]

Microcrystalline cellulose is used in many solid oral dosage formulations in the pharmaceutical industry. Microcrystalline cellulose has outstanding compressibility properties and is commonly used in tablets. After silicification microcrystalline cellulose can improve binding capability and drug release as a material in tablet formula-

tions by direct compression, wet granulation, dry granulation, and extrusion/spheronization processes.[13–15] The present work was undertaken to analyze the binding interactions between ibuprofen and silicified-microcrystalline cellulose. Chemical structure of ibuprofen, silicon dioxide and microcrystalline cellulose is shown in Figure 1. Solid state ball milling, and aqueous state equilibration and freeze drying were the co-processing techniques applied to investigate the effect of silicified-microcrystalline cellulose on ligand. Interactions were monitored by FTIR, DSC and SEM followed by *in vitro* drug release studies. Molecular docking analysis of binary and ternary interactions would reveal stabilizing interactions of silicone dioxide-MCC (formation of SMCC) and ibuprofen-SMCC, which has not been found in extensive literature survey.

Infrared spectroscopy, a commanding technique gives a quantitative estimation of infrared intensity of absorption which is proportional to the magnitude of the change in the dipole moment of a bond during vibration.[16,17] Drug-excipient interaction study in the solid state has been reported very recently without any co-processing (physical mixture) using infrared spectroscopy and DSC studies.[16] Infrared spectroscopy results have been supported by differential scanning calorimetry (DSC) and scanning electron microscopy (SEM) in a report of drug excipient interaction study.[18]

AutoDock 4 programme was used to predict the binding mode interactions between ibuprofen as a ligand against MCC and silicon dioxide complex (SMCC). Docking calculations was performed with the grid box of the same size [(40 × 40 × 40)] with different grid centre to find out the potential binding conformations between ibuprofen, MCC and silicon dioxide. The least binding energy scored conformations were considered as the best conformation. The detailed procedure of molecular docking (using AutoDock) was adopted from a recent study.[19]

2. Experimental

2. 1. Materials

Ibuprofen, Colloidal Silicone Dioxide (Aerosil 200vv) was taken from Aristro Pharma as a gift sample, silicified microcrystalline cellulose were taken from Caplin Point, Chennai. All other chemical were used as analytical grade.

2. 2. Co-processing of Ibuprofen and Silicified Microcrystalline Cellulose

Ibuprofen and silicified microcrystalline cellulose were mixed for 10 minutes by blending process using mortar and spatula at laboratory ambient condition (~30 °C and 60 % RH). Physical mixture of ibuprofen and silicified microcrystalline cellulose at weight ratio of 1:1 was co-processed by ball-milling in the dry state, and aqueous state kneading and freeze drying and tabulated presented in Table 1.

Table 1. Formulation of co-processing of ibuprofen with silicified microcrystalline cellulose

Formulation code	Ibu : SMCC (by weight)	Co-processing
I_1S_1P	1:1	Physical mixture
I_1S_1B	1:1	Dry- state ball milling
I_1S_1F	1:1	Aqueous state kneading and freeze drying

(Ibuprofen = Ibu; Silicified microcrystalline cellulose = SMCC)

2. 3. Ball Milling

The physical mixture of ibuprofen and silicified microcrystalline cellulose in the solid state was placed into the cylindrical vessel of ball mill (Swastik Electro and Scientific Work, India) and 1 h period of constant milling was done at lab ambient condition at 100 rpm (Figure 2). The ball volume to the milling vessel volume was about 30 % and milling was carried out using balls of 4, 8, 14 and 20 mm in diameter. The milling experiments with constant set-up of ball-to-physical mixture mass ratio of 25:1 was used.[20]

2. 4. Freeze – Drying

Sufficient amount of distilled water was added in the physical powder mixture of ibuprofen and silicified microcrystalline cellulose to make slurry and kneaded well for a

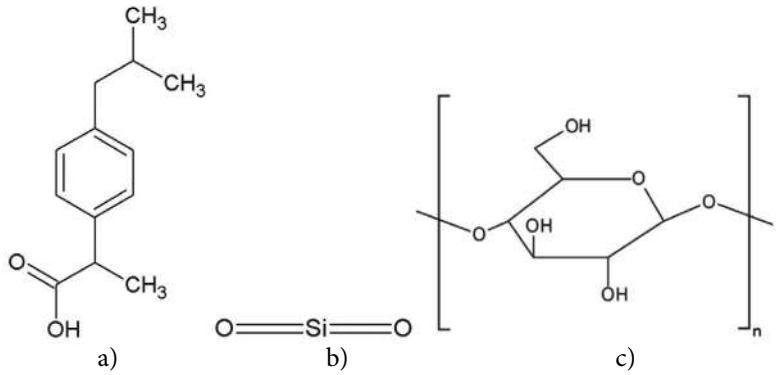

Fig. 1. Chemical structure of (a) ibuprofen, (b) silicon dioxide, and (c) microcrystalline cellulose.

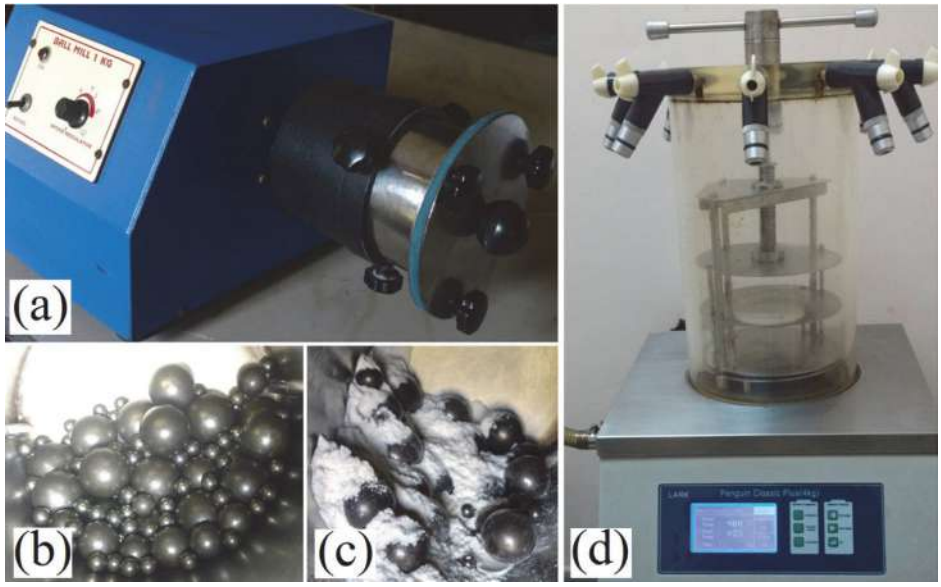

Fig. 2. Co-processing of ibuprofen with SMCC: (a) Laboratory Ball mill (1 kg) used for solid-state milling; (b) The balls charged for milling process; (c) Ibuprofen -SMCC physical mixture just after loading for the milling process; (d) Freeze dryer used for drying the physical mixer after aqueous state equilibration.

period of 30 min. The slurry then placed in the dark for a period of about 12 h at room ambient condition for equilibration. The kneaded samples were freeze dried for 12 hours for effective drying using a laboratory vacuum freeze dryer (4 kg, 220 V) with attached vacuum (220 V, 2.7 A, 370W, 1400 rpm, 50 Hz) (Lark, Penguin Classic Plus, India). Temperature maintained at –40 °C (approx.) and pressure during freeze-drying was adjusted to 15–20 Pa. The freeze dried samples were preserved in the desiccators till further analysis. The ball milled and freeze dried samples were placed at ambient condition for few hours and dried in an incubator (Labotech, India) at 50 °C. The dried powder were passed through mesh 44 (opening ~350 μm) and assayed for drug content determination from the absorbance measured at 222 nm (λ_{max}) in the UV visible spectrophotometer (Jasco-V630 UV spectrophotometer).

2. 5. FTIR Study

The FTIR spectra of pure ibuprofen and co-processed powder samples were performed for a comparative study between co-milling and co-freeze drying interaction. All the samples were thoroughly mixed with potassium bromide in the ratio 1:100. KBr discs were prepared by compressing the powders at a pressure of 6 tons for the 10 min in a hydraulic pellet press (Technosearch Instruments, Maharashtra, India). FTIR spectrometer (FTIR-4100 type A, Jasco, Tokyo, Japan) was used for collecting all scans from 4000–400 cm^{-1} of 80 accumulations at a resolution of 4 cm^{-1} and scanning of 2 mm/s. Spectra manager for windows software (Jasco, Tokyo, Japan) was used for data acquisition and holding.

2. 6. Surface Morphology and Thermal Analysis of the Particle

The surface morphology and crystalline nature of the particle samples were investigated by using Scanning Electron Microscope (Instrument: JSM-6390, Jeol, Tokyo, Japan). The dried samples were coated with gold and scanned at room temperature using voltage 10 kV (Wd 19 and spot size 48). Downloaded Imagej software (https://imagej.nih.gov/ij/download.html) was used for determining particle size distribution of the powder samples. Thermal behavior of powder samples were characterized by using Differential Scanning Calorimeter (DSC, Universal V4.2E TA Instrument). Powder samples approximately 2–4 mg were weighed accurately and put into crimped aluminum pans with a pin hole in the lid. All samples were heated at a heating rate of 10 °C/min in a nitrogen atmospheric condition up to 300 °C.

2. 7. In-vitro Dissolution Release

Powdered samples containing 10 mg equivalent of ibuprofen were dispersed in 900 ml of distilled water and drug release was carried out using USP XXIV type II dissolution apparatus (Electrolab dissolution tester USP) at a temperature of 37 ± 0.2 °C at an rpm of 100. Ibuprofen concentration was determined by UV absorbance at 222 nm. Samples were withdrawn at appropriate time intervals of 5, 10, 15, 30, 60, 90 and 120 min, and replaced with a fresh dissolution medium. After proper rinsing of the cuvette and filtration of the sample through a 0.45 μm membrane filter, absorbance was recorded using the UV visible spectrophotometer. Standard calibration curve was used

for calculating the respective concentration and the data were reported as the mean of not less than three determinations.

2. 8. Molecular Docking Analysis

The molecular visualizations and interaction analysis was performed using Discovery studio visualizer (Acceleris Inc.). The 3-D Structure file of ibuprofen was downloaded from Drug Bank (ID: DB01050) as PDB format. The 3-D structures of silicon dioxide and MCC were drawn by using marvin sketch[19,21] and saved as PDB extension files. The non-bonded H-atoms were merged, Kollman united atom type charges and solvation parameters were added. The PDBQT files of ibuprofen, MCC and silicon dioxide were prepared with the help of Auto Dock tools programme.[22] The ibuprofen non-steroidal anti-inflammatory drug was taken as a ligand to identify its binding affinity against the MCC and silicon dioxide complex (SMCC). In order to understand the interaction between MCC (receptor) with the ligand silicon dioxide another molecular docking experiment was carried out using these molecules. The docking complex stability was measured on the basis of binding constant and interaction energy.

3. Results and Discussion

The dry-state co-milling and aqueous state co-processing could be analogous to the commonly followed process in the tablet granulation department of pharmaceutical industries. Ball milling studies in different literature has shown different duration and speed of rotation. Median particle diameter has not been changed significantly upon milling of alfa-lactose monohydrate at a milling time of 60 and 300 min (ball-to-powder mass ratio of 25:1 and 13:1), and highest degree of amorphization was resulted at the ratio of 25:1.[20] In another milling study increasing powder loading decreased milling efficiency at a given rotation speed of 50, 100, and 153 rpm.[23] Hence, 1 h milling time and 100 rpm of milling speed could be justifiable or closely resembling to the dosage form processing. These processes are simple, effective and scalable for interaction study. Due to presence of varying amount of bound moisture in the native silicified microcrystalline cellulose the milled material became moisty in nature and needed drying. Instant character of freeze dried sample is to absorb moisture like a sponge when left at ambient condition of –60 % RH and 30 °C for few hours and drying in an incubator at 50 °C becomes necessary. The co-processed dried and equilibrated powder materials were passed through mesh of opening ~350 μm and assayed for actual drug content determination. Ibuprofen–silicified microcrystalline cellulose interaction study has been characterized by FTIR and the usefulness of this powerful technique has been supported by scanning electron microscopy and differential scanning calorimetry as described below. Drug release from the formulated dosage form is important and ultimately related to the bioavailability of the drug. Dissolution of ibuprofen from the co-processed material has also been described below.

3. 1. FTIR Analysis

Spectral figure and data of FTIR band assignments of ibuprofen and co-processed samples are tabulated presented in Table 2 and Figure 3 respectively. FTIR spectrum of ibuprofen has shown medium to very strong band at 3094, 2958 and 2901 cm^{-1} assigned to CH_2 asymmetric stretching, CH_3 asymmetric stretching and $CH_2 \cdot CH$ symmetric stretching respectively. Strong peaks in the region of 2800–3000 cm^{-1} of ibuprofen are still present when co-milled in

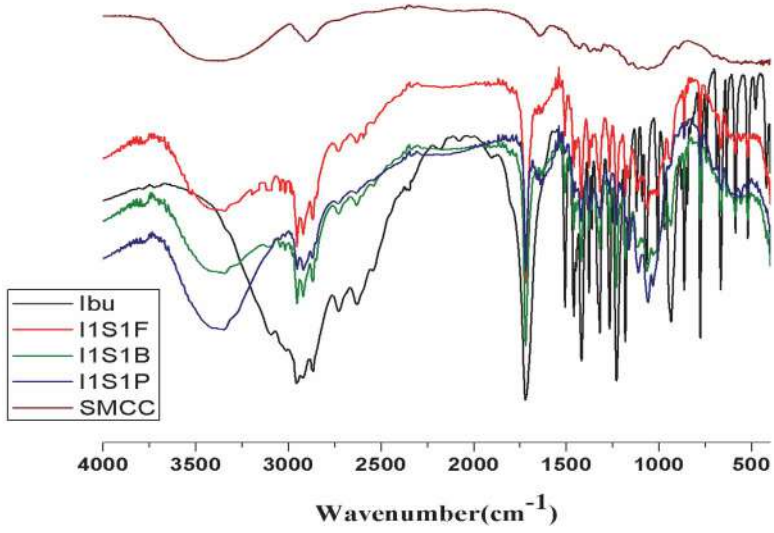

Fig. 3. FTIR Spectra of Ibuprofen co-processed with SMCC

Table 2. Spectral data of FTIR band assignments of ibuprofen and co-processed samples.

Band	Tentative assignment	Wave number (cm^{-1})				
		Ibuprofen	SMCC	I_1S_1B	I_1S_1F	I_1S_1P
1	OH stretching	Absent	3200–3550 bb	3200–3550 bb	3200–3550 bb	3200–3550 bb
2	CH_2 asym str	3094 m	–	absent	absent	absent
3	CH_3 asym str	2958 vs	–	2955 vs	2954 vs	2955 vs
4	CH_2 CH sym str	2901 s	2901 s	2901 s	2901 s	2901 s
5	CH_2 sym str	2868 m	–	2868 m	2869 m	2868 m
6	O–H …O valance str combination	2729 m	–	2730 m	2730 m	2728 m
7	O–H…O valance str combination	2630 m	–	2629 m	2629 m	2629 m
8	C=O str	1722 vs	–	1721 vs	1720 vs	1722 vs
9	conjugated C=O stretching mode	Absent	1645 s	1645 m	1645 m	1645 m
10	aromatic C=C str	1507 s	–	1508 s	1510 s	1507 s
11	CH_3 asym deformation, CH_2 scissoring	1462 s	–	1461 s	1461 s	1461 s
12	CH-CO deformation	1420 s	–	1420 s	1422 s	1420 s
13	CH3 sym str	1380 s	–	1379 s	1378 s	1379 s
14	OH in plane deformation	1321 s	–	1321 s	1321 s	1321 s
15	=C-H in plane deformation	1268 s	–	1267 s	1267 s	1268 s
16	C…C str	1230 vs	–	1231 vs	1231 vs	1231 vs
17	C-O str	1183 s	–	1183 s	1183 s	1183 s
18	Si-O-Si asym str	Absent	1059 bb	1066 bb	1059 bb	1075 bb
19	C-O-C str	970 m	–	–	–	Absent
20	C-H out of plane vibration	866 s	–	865 s	866 s	866 s
21	CH_2 rocking	779 s	–	780 s	780 s	779 s
22	CH_2 in plane rocking	522 m	–	521 m	521 m	521 m
23	O-Si-O bending	Absent	451 bb	461 bb	461 bb	451 bb

(s- strong; bb- broad band; mbb- medium broad band; w- weak; sym-symmetrical; asym-asymmetrical; str-stretching; m- medium; vs- very strong; vw – very weak; vvw – very very weak; aa- almost absent.)

the dry-state as well as co-freeze-dried after aqueous state kneading and equilibration with silicified microcrystalline cellulose assigned to the characteristic symmetric and asymmetric stretching vibrations of alkyl chain. High intensity carbonyl peak at 1722 cm^{-1} of ibuprofen became very weak after co-processing in the solid-state as well as wet-state with silicified microcrystalline cellulose.[24] The band at 1645 cm^{-1} of silicified microcrystalline cellulose designated to conjugated C=O in the aldehyde on the terminal anhydro-glucose unit is also present in co-processed samples. A strong CH_2 rocking vibration band is noticed at 779 cm^{-1} in ibuprofen and the intensity observed to be weaker and weaker after co-processing. CH_2 in plane rocking vibration (522 cm^{-1}) is identified in pure ibuprofen and became weaker when co-milled and freeze dried after co-kneading. C-O stretching at 1183, CH_2 scissoring vibration at 1462 and CH-CO deformation at 1420 cm^{-1} contributed their occurrence strongly in ibuprofen alone and weakly in the co-processed sample. A big broad band between 3200 to 3550 cm^{-1} attributed to the presence of the O-H stretching frequency of silanol group bonded to the inorganic structure of containing SiO_2 (SMCC), and also hydrogen bonds between adsorbed water and silanol.[25] This bulky broad band is not present in ibuprofen pure drug but consistently maintained in all the co-processed formulations might be due to intermolecular hydrogen bonding. The band related to the Si-O-Si (silanol) asymmetric stretching was found at 1059 cm^{-1} with elevated intensity in SMCC and also in the co-processed materials. Another peak at 451 cm^{-1} due to O-Si-O bending notably observed in the formulations. The small changes in the band orientation, band intensity and overlapping indicated only Vander Waals or dipole-dipole interactions between ibuprofen and silicified microcrystalline cellulose molecules.

3. 2. SEM and DSC

Scanning electron microscopy is a commanding tool for examining the inhibition of crystal growth morphology. Figure 4 shows distinctive plate like geometric layers of the initial samples of pure ibuprofen indicating crystalline nature. Slightly damaged morphology of the crystal geometry of ibuprofen is seen in the physical mixture of 1 : 1 ratio of I_1S_1P in presence of fine particles of SMCC. Crystal geometry of ibuprofen has been damaged appreciably after co-milling in the solid-state and co-freeze-drying after aqueous state kneading and equilibration with silicified microcrystalline cellulose. The Feret diameter and its distribution of the powder sample were evaluated opening the SEM image (Figure 5). Feret diameter is an estimate of a particle size along a specified direction and can be defined as the distance between the two parallel planes restricting the particle perpendicular to

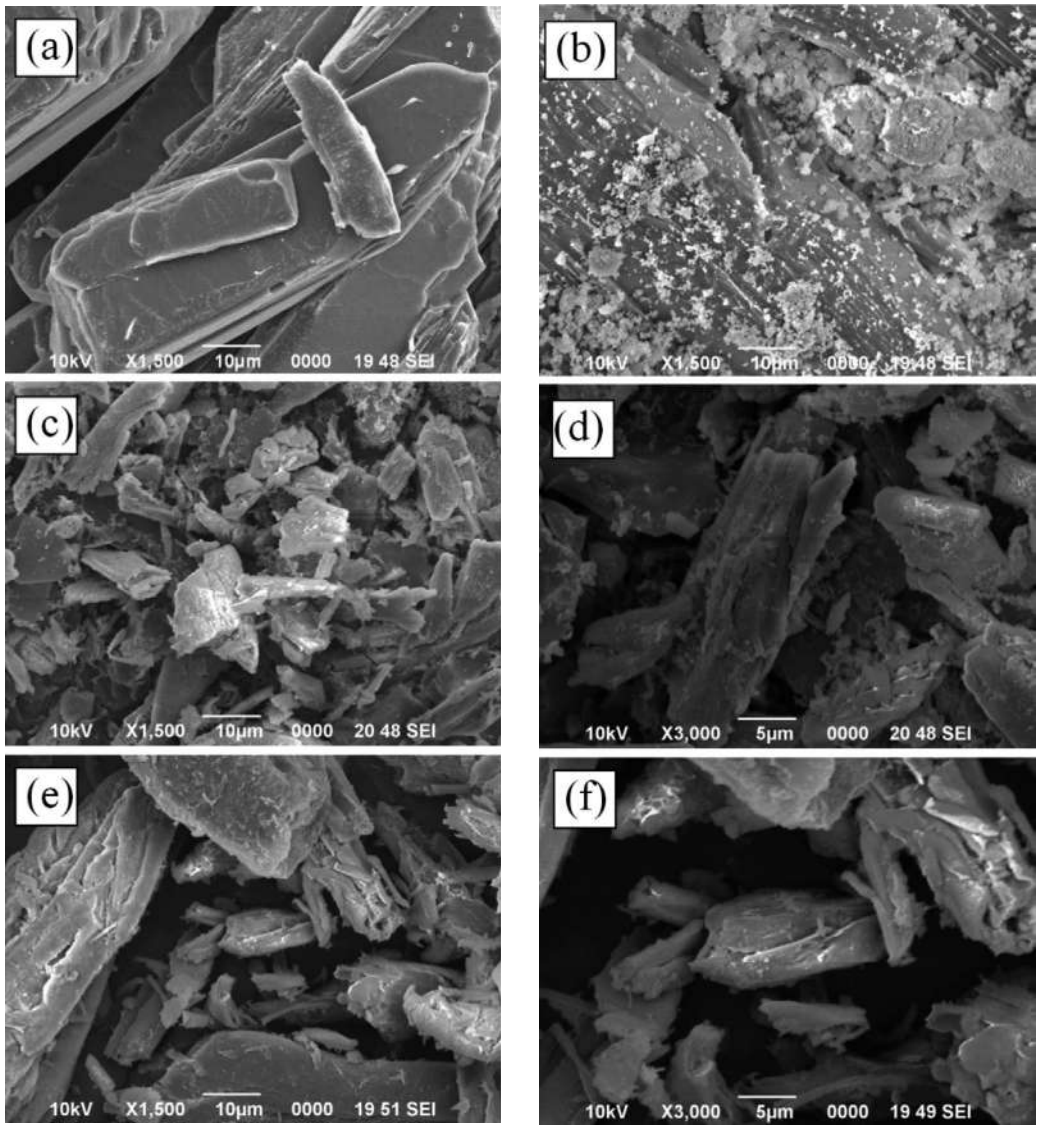

Fig. 4. SEM Images (a) Ibu; (b) I_1S_1P; (c) and (d) I_1S_1B; (e) and (f) I_1S_1F.

that direction. In both cases (I_1S_1B and I_1S_1F) particle size has been significantly reduced. Irregular particles in agglomerated and discrete forms are prominently seen after co-processing. These noticeable changes in morphology may be due to amorphization of ibuprofen to the large extent.

Differential scanning calorimetry is frequently used in pharmaceutical research as an analytical tool for the identification and interaction study of active drug after co-processing with other pharmaceutical compounds. It can explain the miscibility/incompatibility with its effects on thermal stability, yielding results promptly and efficiently.[26] Thermograms after differential scanning calorimetry of pure ibuprofen and co-processed powder samples are depicted in Figure 6. Pure ibuprofen has shown the melting endotherm at 76.66 °C which is approximately similar to the literature value.[27] The peak, onset and endset of melting of ibuprofen in the formulated powder samples have not been changed significantly (Table 3) but the enthalpy of melting (normalized, J/g) of ibuprofen (–322.55) decreased drastically after co-processing and that is the indication of amorphous transformation of ibuprofen in the co-processed formulations. Solid-state ball-milling sample exhibited lesser enthalpy content (–42.93) compared to freeze-dried material (–63.40). This result suggested that the extent of amorphization of ibuprofen is more in I_1S_1B rather than I_1S_1F material (relative crystallinity 13.31 and 19.66 % respectively with reference to pure drug ibuprofen). The physical mixture has shown only 22.49 %. The zero crystallinity corresponds to a totally amorphous particle. In our present work relative crystallinity (%) has been shown with reference to the pure drug ibuprofen which is highly crystalline (reference).

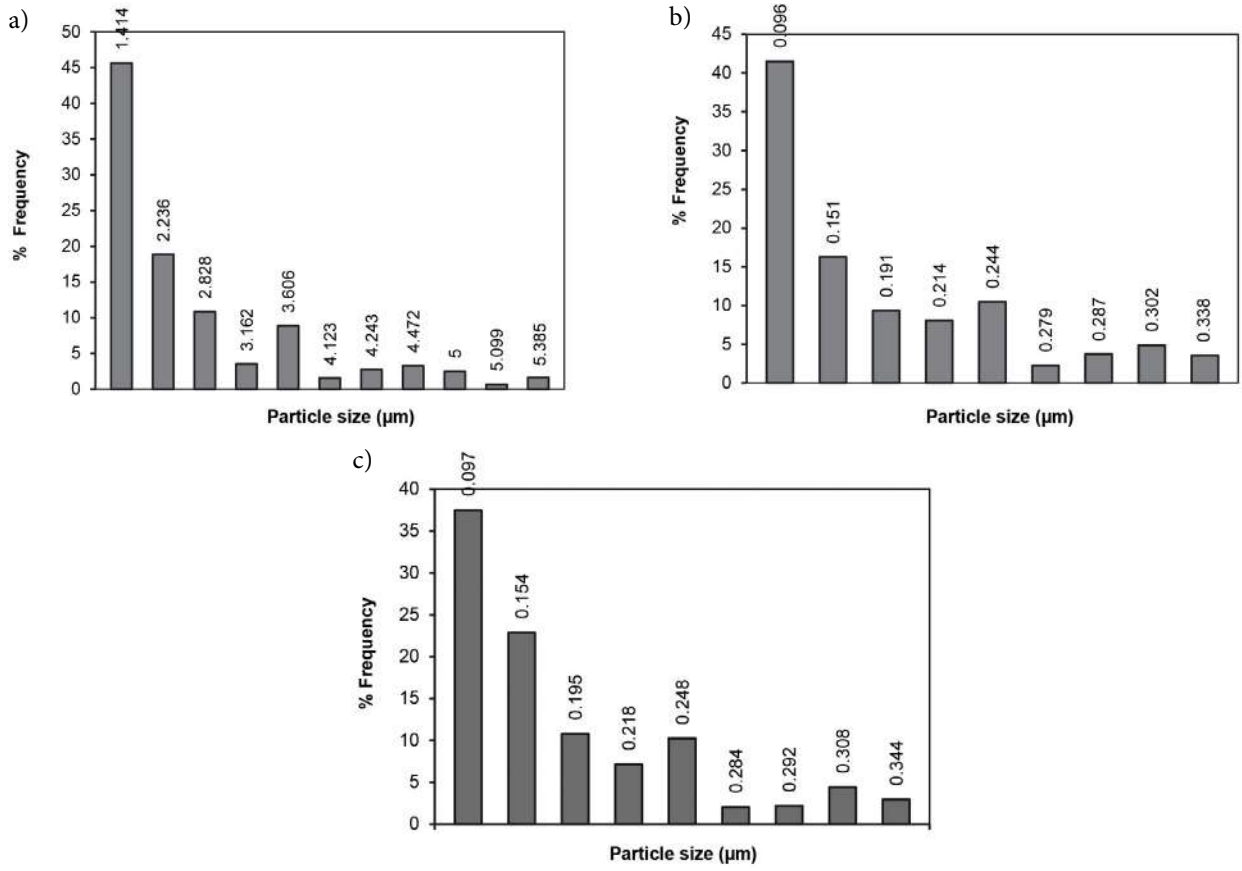

Fig. 5. Feret diameter and its distribution of the powder sample estimated from SEM image: (a) Ibu, (b) I_1S_1F, (c) I_1S_1B.

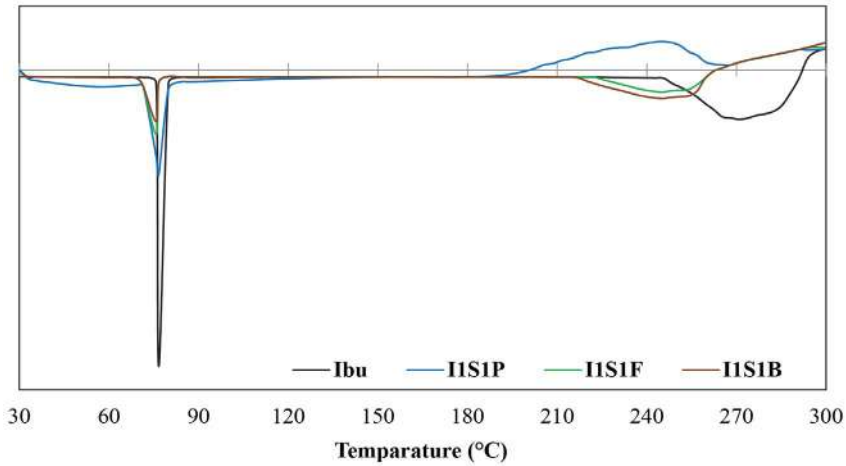

Fig. 6. DSC Thermogram of ibuprofen co-processed with SMCC.

Table 3. Thermal analysis after co-processing of ibuprofen with microcrystalline cellulose

Formulation	Peak melting (°C)	Onset melting (°C)	End set melting (°C)	Normalized (J/g)	Relative crystallinity (%)
Ibu	76.66	75.78	79.93	–322.55	Reference
I_1S_1P	76.56	73.03	80.43	–72.53	22.49
I_1S_1B	74.71	73.04	76.34	–42.93	13.31
I_1S_1F	75.66	73.03	77.99	–63.40	19.66

3. 3. In-vitro Drug Release

Many research reports used distilled water[28–30] as media to determine the solubility of drug substance. Ibuprofen drug release from microemulsion was studied also in distilled water by Hu et al.[31] Ibuprofen release profiles were similar for three kinds of microspheres in distilled water and with solution of low pH of 1.2 because of poor solubility of the drug.[32] Like ibuprofen many other non-steroidal anti-inflammatory drugs tend to self-associate by forming mixed-charged micelles or micelle-like structures and the solubility-pH profiles cannot be described properly with the Henderson-Hasselbalch eq.[33,34] However, release of ibuprofen in distilled water will give an idea about its overall improvement in dissolution. Figure 7 shows cumulative percentage release of ibuprofen in distilled water of the co-processed material up to 120 min. The powder materials have shown significantly improved dissolution of drug after co-processing. Comparison of two dissolution profiles is based on the determination of a model independent statistical method, the difference factor f_1 and the similarity factor f_2. Similarity or equivalence between two dissolution profiles is based on $f_1 \leq 15$ and $f_2 \geq 50$.[35–37] Significantly improved drug dissolution of solid state milling, and aqueous state kneading and freeze drying has been understood by using f_1 and f_2 values when pair wise formulation vs pure drug was compared (f_1: 32.75, & f_2: 13.29 and f_1: 15.05, & f_2: 28.93 respectively). Crystalline ibuprofen exhibited only 52.89 % dissolution whereas, dry-state co-milling and freeze dried co-processed material has improved dissolution to a great extent (85.84 and 81.35 % respectively). Silicified microcrystalline cellulose has shown more impact in solid state milling compared to aqueous state kneading and equilibration and brought about more amorphization of ibuprofen. As a result more improved dissolution has been achieved in ball milled product.[38]

Drug release mechanism has been predicted to develop a rational formulation utilizing mathematical models. The drug release data was analyzed by applying different kinetic models as First order, Higuchi, Korsmeyer–Peppas kinetics[39,40] using Origin Pro 8.0 (Originlab Corporation, US) software by non-linear regression analysis. These models are represented as follows:

$$\text{First order model: } Q = 100 - \exp((-K_F * t) + 4.605) \quad (1)$$

$$\text{Higuchi model: } Q = K_H \times \sqrt{t} \quad (2)$$

$$\text{Korsmeyer-Peppas model: } Q = K_p \times t^n \quad (3)$$

Q = Cumulative percent drug release at time t
K_F = First order release rate constant
K_H = Higuchi release rate constant,
K_P = Parameter reflecting the structural and geometric characteristics of the delivery device, or Peppas release rate constant,
n = Power law exponent, or release exponent.

This n value indicates drug release controlled by Fick's laws and also confirmed by the Higuchi model. Matrix controlled release has been followed (Figure 8). The kinetic parameters as per model are presented in the Table 4. As per Peppas model, n value 0.5 is referred to Fickian release pattern. The n value of I_1S_1P, I_1S_1F and I_1S_1B was found to be 0.400, 0.408 and 0.143 respectively (less than 0.5) which indicated the diffusion controlled release mechanism. The diffusion controlled release mechanism has also been supported by the fitting of Higuchi model (R^2 is 0.354–0.973).

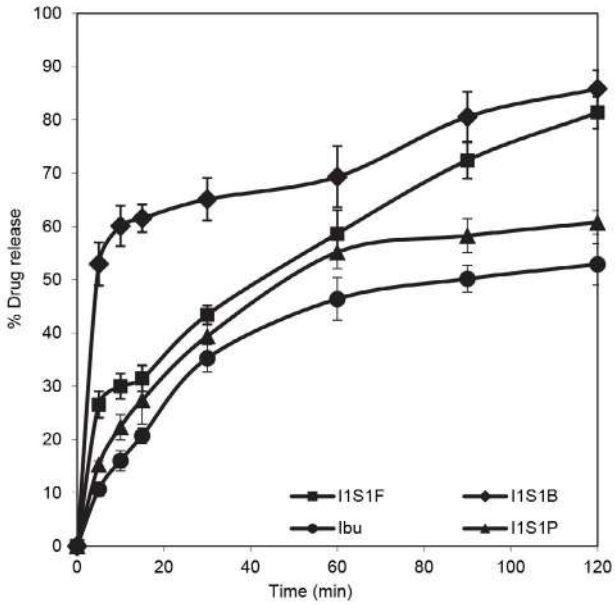

Fig. 7. Cumulative percentage release profiles of ibuprofen co-processed with SMCC.

Table 4. Model fitting and kinetic parameters of drug dissolution of ibuprofen co-processed material.

Formulation	f_1	f_2	First order			Higuchi			Korsmeyer–Peppas			
			K_F (min^{-1})	r^2	RSS	K_H (%.min$^{-1/2}$)	r^2	RSS	n	K_P	r^2	RSS
I_1S_1P	6.25	48.96	0.011	0.789	727	6.27	0.956	150	0.400	9.544	0.976	69
I_1S_1F	15.04	28.93	0.017	0.854	729	7.71	0.973	133	0.408	11.363	0.990	40
I_1S_1B	32.75	13.28	0.07	0.466	2590	9.52	0.354	3131	0.143	41.497	0.986	54

RSS = Sum of $(Q_{exp} - Q_{calc})^2$

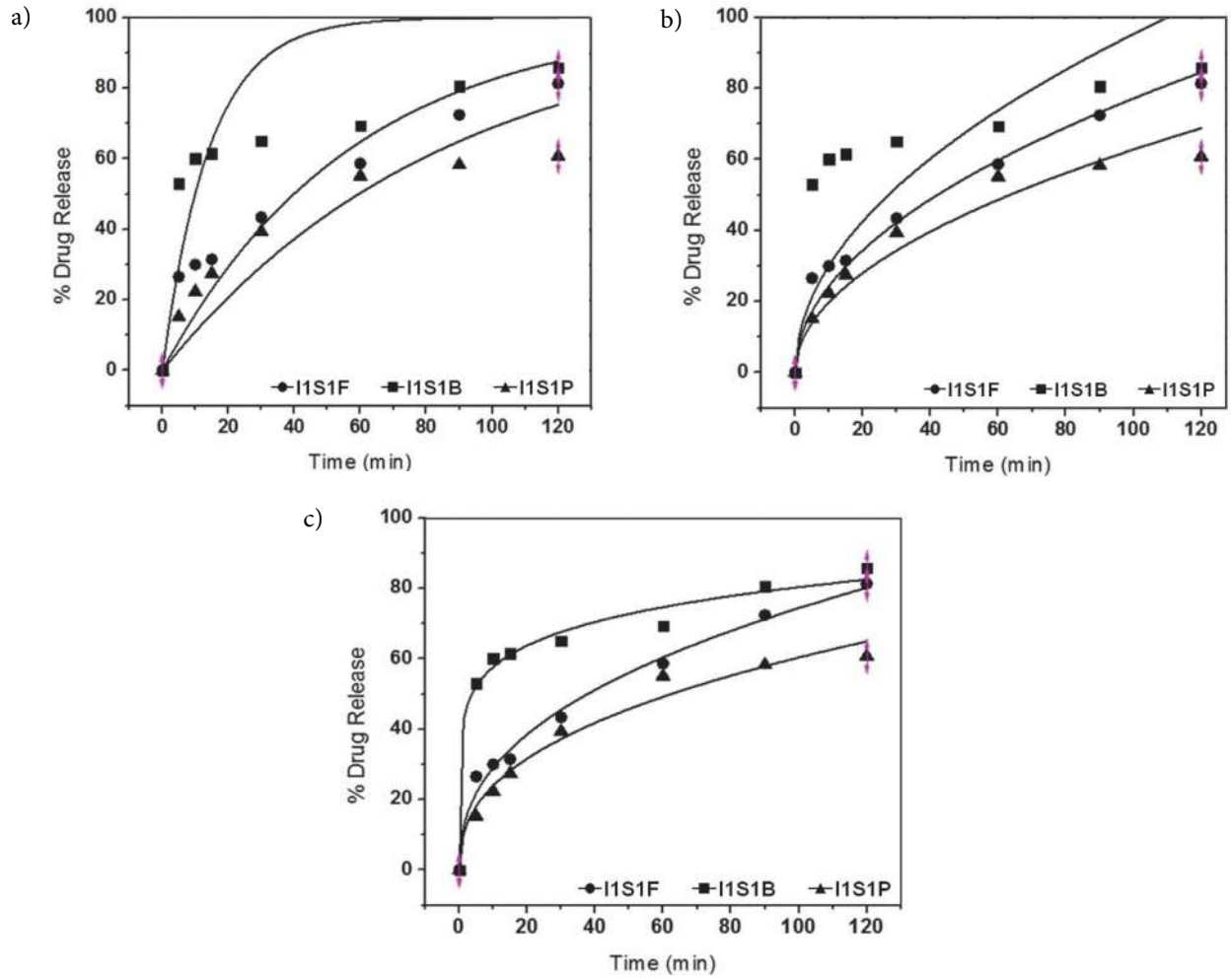

Fig. 8. Kinetics of drug release applying kinetic models to plot both the experimental data (symbols) and the models (curves): (a) First order (b) Higuchi (c) Korsmeyer–Peppas.

3. 4. Molecular Docking Analysis of the Complexes

The predicted co-ordinates of ibuprofen and silicone dioxide complex were monitored by molecular docking method Table 5 and Figure 9 respectively. The interaction between MCC-SiO_2 would be obtained from inter molecular hydrogen bonding between OH group of MCC and H atom of SiO_2. The hydrogen bond lengths are varying from 2.028 to 2.056 Å. The binding energy value was found –1.11kcal/mol. Hydrogen bonding plays a vital role in H-bonded network systems. Hydrogen bond length between ibuprofen and SMCC are ranging from 2.028 to 2.930 Å and the most interesting other probable interaction of Si atom of SMCC molecule with Pi-Orbital of ibuprofen showing bond length of 4.263 Å. The binding energy was found to be –1.73 kcal/mol. The higher negative binding energy values indicate stable interactions than

Table 5. Molecular docking and binding parameter interactions in the co-processing of ibuprofen with silicified microcrystalline cellulose

Binding Molecules	Binding energy (Kcal/mol)	Binding atoms	Bond name	Bond length (Å)
MCC – SiO_2	–1.11	OH --- O	Hydrogen Bond	2.028
(SMCC)		H --- O	Hydrogen Bond	2.056
SMCC – Ibuprofen	–1.73	OH --- O	Hydrogen Bond	2.028
		OH --- O	Hydrogen Bond	2.930
		H --- O	Hydrogen Bond	2.056
		Si --- Pi-orbital	Pi-Sulfur Bond	4.263

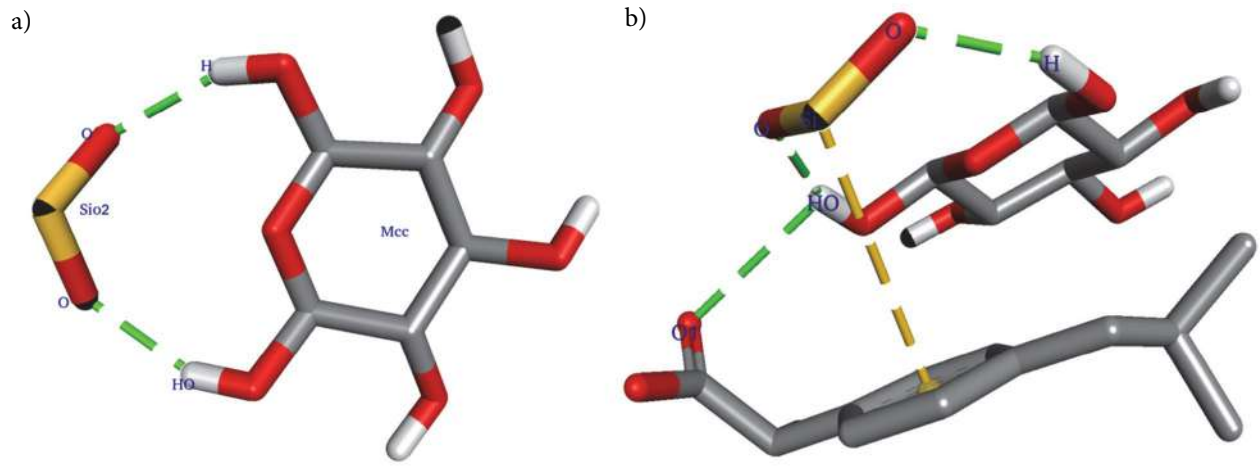

Fig. 9. Molecular docking study of (a) SMCC (binary); and (b) ibuprofen-microcrystalline cellulose -silicon dioxide (ternary).

that of lower negative values, which indicate destabilizing interactions.[21,41]

4. Conclusions

Binding interactions of ibuprofen and silicified-microcrystalline cellulose (SMCC) has been analysed. The dry-state and aqueous state co-processing of ibuprofen was performed by co-milling and co-freeze-drying after aqueous state kneading and equilibration with silicified microcrystalline cellulose in at laboratory scale to investigate the effect of silicified-microcrystalline cellulose on ligand. The changes in the band intensity, band orientation, and overlapping of FTIR indicated only the H-bond, Van der Waals and/or dipole-dipole interactions between ibuprofen and silicified microcrystalline cellulose molecules. SEM study revealed that the ibuprofen crystal morphology has been damaged appreciably after co-processing in the solid-state and wet-state with SMCC. Thermal analysis has shown significantly decreased enthalpy of melting of ibuprofen after co-processing with SMCC. Silicified microcrystalline cellulose has transformed more amorphization of ibuprofen by solid state milling compared to aqueous state kneading and freeze drying and brought about more improved dissolution of ibuprofen of ball milled product rather than freeze dried product. Matrix controlled release mechanism has been predicted utilizing mathematical kinetic models. Molecular docking study revealed the formation of ibuprofen complex through hydrogen bonding with MCC and silicon dioxide. The binding energy between MCC and SiO_2, and ibuprofen and SMCC were found as –1.11 and –1.73 kcal/mol respectively.

5. Acknowledgements

The authors are acknowledging gratefulness to the Department of Science & Technology, Ministry of Science & Technology, New Delhi, India, for providing INSPIRE fellowship to Rudra Narayan Sahoo (IF 150987). The authors are also very much grateful to Prof. Manoj Ranjan Nayak, President, Siksha O Anusandhan (Deemed to be University) for providing other facilities and encouragement.

Conflicts of interest

The authors declare that there is no conflict of interest.

6. References

1. W. P. Sohtun, A. Kannan, K. Hari Krishna, D. Saravanan, M. S. Kumar, M. Velusamy, *Acta Chim. Slov*. **2018**, *65*, 621–629. **DOI:**10.17344/acsi.2018.4275
2. G. M Morris, R. Huey, W. Lindstrom, M. F. Sanner, R. K. Belew, D. S. Goodsell, A. J. Olson, J. Comput. Chem. **2009**, *16*, 2785–2791. **DOI:**10.1002/jcc.21256
3. P. O. Carvalho, Q. B. Cass, S. A. Calafatti, F. J. Contesini, R. Bizaco, *Braz. J. Chem. Eng.* **2006**, *23*(03), 291–300. **DOI:**10.1590/S0104-66322006000300003
4. T. Chaban, V. V. Ogurtsov, V. S. Matiychuk, G. Chaban, L. Demchuk, A. Nektegayev, *Acta Chim. Slov*. **2019**, *66*, 103–111. **DOI:**10.17344/acsi.2018.4570
5. Q. Wei, H. Yuanzhi, G. Zhen, L. Zhang, W. Li, Y. Xianzhen, S. Shakya, A. Maharjan, T. Yan, Z. Weifeng, Z. Jiwen, *Asian J. Pharm. Sci*. **2018**, *4*, 1–9.
6. M. Mombeini, G. Saki, L. Khorsandi, N. Bavarsad, *Medicina*, **2018**, *54(*1), 1–9. **DOI:**10.3390/medicina54010001
7. R. Lobenberg, G. L Amidon, *Eur. J. Pharm. Biopharm*. **2000**, *50*(1), 3–12.
8. R. P. Swain, B. B. Subudhi, *Drug. Dev. Ind. Pharm*. **2019**, (Published online: 16 Feb 2019). **DOI:**10.1080/03639045.2019.1572183
9. S. Mallick, S. Pattnaik, K. Swain, P. K. De, *Drug Dev. Ind. Pharm*. **2007**, *33*, 535–541. **DOI:**10.1080/03639040601050130
10. S. Mallick, S. Pattnaik, K. Swain, P. K De, A. Saha, G. Ghoshal, A. Mondal, *Drug Dev. Ind. Pharm.* **2008**, *34*, 726–734. **DOI:**10.1080/03639040801901868

11. S. Mallick, A. Sahu, K. Pal, *Acta Pol. Pharm*. **2004**, *61*, 21–30.
12. R. H. Dave, Overview of Pharmaceutical Excipients used in tablets and capsules, https://www.drugtopics.com/hospital-health-system-pharmacy/overview-pharmaceutical-excipients-used-tablets-and-capsules, (assessed: March 13, 2019).
13. S. Lijun, L. Liping, S. Xiaoying, C. Honglang, Z. Shumin, C. Wenfeng, Z. Ruoxia, Z. Wenchang, *Asian J. Pharm. Sci*. **2018**, *19*(13), 1–10.
14. R. Vasluianu, D. A. Forna, M. Zaltariov, A. Murariu, *Rev. Chim.* (Bucharest). **2016**, *67*(12), 2475–2478.
15. M. S. Bhandari, S. M. Wairkar, U. S. Patil, N. R. Jadhav, *Acta Chim. Slov.* **2018,** *65*, 492–501. **DOI:**10.17344/acsi.2017.3822
16. F. Dragan, I. Kacso, S. Dreve, F. Martin, G. Borodi, I. Bratu, K. Earar, *Rev. Chim.* (Bucharest). **2015**, *66*(2), 191–195.
17. B. Tita, G. Furau, E. Marian, D. Tita, C. Furau, *Rev. Chim*. (Bucharest). **2016**, *67*(4), 706–710.
18. E. Marian, T. Jurca, B. Tita, P. Sfirloaga, D. Tita, N. Duteanu, *Rev. Chim*. (Bucharest). **2015**, *66*(4), 477–481.
19. J. Maharana, M. C. Patra, B. C. De, B. R. Sahoo, B. K. Behera, S. De, S. K Pradhan, *J. Mol. Recog.* **2014**, *27*(5), 260–275. **DOI:**10.1002/jmr.2357
20. S. Pazesha, J. Grasjo, J. Berggren, G. Alderborn, *Int. J. Pharm*. **2017**, *528*, 215–227. **DOI:**10.1016/j.ijpharm.2017.05.043
21. R. Mohapatra, S. Mallick, A. Nanda, R. N. Sahoo, A. Pramanik, A. Bose, D. Das, L. Pattnaik, *RSC Adv*. **2016**, *6*, 31976–31987. **DOI:**10.1039/C6RA03604J
22. G. M. Morris, D. S. Goodsell, R. S. Halliday, R. Huey, W. E. Hart, R. K. Belew, A. J. Olson, *J. Comput. Chem*. **1998**, *19*(14), 1639–1662. **DOI:**10.1002/(SICI)1096-987X(19981115)19:14<1639::AID-JCC10>3.0.CO;2-B
23. H. Shin, S. Lee, H. S. Jung, J. Kim, *Ceram. Int.* **2013**, *39*(8), 8963–8968. **DOI:**10.1016/j.ceramint.2013.04.093
24. S. Mallick, S. K. Pradhan, R. Mohapatra, *Int. J. Biol. Macromol*. **2013**, *60*, 148–155. **DOI:**10.1016/j.ijbiomac.2013.05.021
25. A. L. Balieiro, R. A. Santos, M. M. Pereira, R. T. Figueiredo, L. S. Freitas, O. L. S. de Alsina, A. S. Lima, C. M. F. Soares, *Braz. J. Chem. Eng*. **2016**, *33*(2), 361–372. **DOI:**10.1590/0104-6632.20160332s20140089
26. B. Panda, A. S. Parihar, S. Mallick, *Int. J. Biol. Macromol*. **2014**, *67*, 295–302. **DOI:**10.1016/j.ijbiomac.2014.03.033
27. S. Mallick, S. K. Pradhan, M. Chandran, M. Acharya, T. Digdarsini, R. Mohapatra, *Results Pharm. Sci*. **2011**, *1*(1), 1–10. **DOI:**10.1016/j.rinphs.2011.05.003
28. P. Arya, K. Pathak. *Int J Pharm*. **201**4, *460*(1–2), 1–12. **DOI:**10.1016/j.ijpharm.2013.10.045
29. F. L. Mota, A. P. Carneiro, A. J. Queimada, S. P. Pinho, E. A. Macedo. *Eur J Pharm Sci*. **2009**, *37(3–*4), 499–507. **DOI:**10.1016/j.ejps.2009.04.009
30. F. A. Maulvi, S. J. Dalwadi, V. T. Thakkar, T. G. Soni, M. C. Gohel, T. R. Gandhi. *Powder Technol*. **2011**, *207(1–3*), 47–54. **DOI:**10.1016/j.powtec.2010.10.009
31. L. Hu, J. Yang, W. Liu, L. Li, *Drug Deliv.* **2011,** *18(1*), 90-95, **DOI:**10.3109/10717544.2010.522613
32. Q. Wei, *Asian J. Pharm. Sci.* **2019**, *14*, 174–182. **DOI:**10.1016/j.ajps.2018.05.003
33. A. Avdeef, *ADMET DMPK*. **2014**, *2(1)*, 33–42. **DOI:**10.5599/admet.2.1.30
34. A. Fini, *Int. J. Pharm*. **1995**, *126(1–2*), 95–102. **DOI:**10.1016/0378-5173(95)04102-8
35. P. Costa, J. Manuel, S. Lobo, *Eur. J. Pharm. Sci*. **2001**, *13*, 123–133. **DOI:**10.1016/S0928-0987(01)00095-1
36. A. Pramanik, R. N. Sahoo, A. Nanda, R. Mohapatra, R. Singh, S. Mallick, *Curr. Eye Res*. **2018**, *43*(6), 828–838. **DOI:**10.1080/02713683.2018.1446534
37. D. Vetchy, M. Vetcha1, M. R. Artina, E. Gryczova, L. Bartošikova, *Medicina*, **2007**, *43*(4), 326–330. **DOI:**10.3390/medicina43040040
38. S. Mallick, S. Pattnaik, K. Swain, P. K. De, *Drug Dev. Ind. Pharm*. **2007**, *33*(8), 865–873. **DOI:**10.1080/03639040701429333
39. S. Mallick, K. Roy, A. Saha, *Acta Pol. Pharm*. **2002**,*59*(3), 193–198.
40. S. Mallick, B. K. Gupta, S. K. Ghoshal, *J. Sci. Ind. Res.* **1999**, *58*, 1010–1016.
41. A. Nanda, R. N. Sahoo, A. Pramanik, R. Mohapatra, S. K. Pradhan, A. Thirumurugan, D. Das, S. Mallick, *Colloids Surf. B Biointerfaces*. **2018**, *172*, 555–564. **DOI:**10.1016/j.colsurfb.2018.09.011

Povzetek

Opravili smo analizo veznih interakcij med ibuprofenom in silicificirano mikrokristalno celulozo (SMCC). Procesiranje ibuprofena s SMCC je bilo izvedeno z mletjem kroglic v trdnem stanju in ravnotežjem v vodni fazi, čemur je sledilo sušenje z zamrzovanjem. Želeli smo raziskati vpliv silificirane mikrokristalne celuloze na ligand. Z metodo molekulskega sidranja (»molecular docking«) smo pokazali, da ibuprofen tvori kompleks preko vodikove vezi z mikrokristalno celulozo (MCC) in silicijevim dioksidom (SiO_2); izračunana energija vezave med MCC in SiO_2 ter ibuprofenom in SMCC je bila kot –1,11 kcal/mol oziroma –1,73 kcal/mol. Dolžine vodikovih vezi so se gibale od 2,028 Å do 2,056 Å. Interakcije atoma Si SMCC molekule s π-orbitalmi ibuprofena smo zaznali na razdalji 4,263 Å. Kot rezultat interakcij smo opazili pomembno izboljšanje raztapljanja ibuprofena. Binarne in ternarne interakcije so pokazale bolj stabilne interakcije z ibuprofenom in SMCC v primerjavi s samo silificirano mikrokristalno celulozo (SMCC).

Original Article

Sustained Release Bioadhesive Suppository Formulation for Systemic Delivery of Ornidazole: *In-silico* Docking Study

Rasmita Dash, Rudra Narayan Sahoo, Souvik Nandi, Rakesh Swain, Subrata Mallick*

Department of Pharmaceutics, School of Pharmaceutical Sciences, Siksha O Anusandhan (Deemed to be University), Bhubaneswar, Odisha, INDIA.

ABSTRACT

Background and Objectives: Ornidazole is widely used as an antiprotozoal and anti-amoebic drug and its onset of action is within 2 h. The major extent of the drug is metabolized in the liver and excreted in the urine and faeces. Hence, the present study of suppository formulation for sustained systemic delivery of ornidazole is significant which could minimize abdominal disturbances and nausea and delayed onset of action particularly after oral administration. **Methods:** Bioadhesive suppository formulations were prepared for systemic delivery of ornidazole via rectal and vaginal route. **Results:** The physical drug-excipient-interaction was confirmed by *in-silico* docking study. The affinity between drug-HPMC and drug-PEG was found to be -2 and -0.9 k cal/mol respectively. *In vitro* drug release of the suppositories varied depending on the viscosity grade of HPMC used and all have followed mostly diffusion controlled mechanism. The formulation containing HPMC K100 showed the most sustained release of ornidazole in both the dissolution fluid of pH 7.4 and 4.5 (54.53 and 41.89 % respectively after 360 min). **Conclusion:** In conclusion, present bio adhesive suppositories could be utilized for sustained systemic delivery of ornidazole via rectal and vaginal route. The findings of this work will contribute to the current knowledge and encourage future pre-clinical research.

Key words: Ornidazole, Sustained release suppository, *In-silico* docking, Bioadhesive formulation, *in-vitro* dissolution.

INTRODUCTION

Ornidazole is widely used as an antiprotozoal and anti-amoebic drug and its onset of action is within 2 hr.[1] It prevents recurrence of peptic ulcer disease caused by *Helicobacter pylori*. It is also used effectively and safely for the treatment of inflammatory bowel disease.[2] Ornidazole is better tolerated than metronidazole; the major extent of the drug is metabolized in the liver and excreted in the urine and faeces.[3] The main adverse effects of ornidazole are headache, dizziness, anorexia, intestinal spasms, loose stools etc and the very common are significant abdominal disturbances, nausea etc.[4] Gastro retentive drug delivery systems were reported by increasing residence time to sustain the drug release in the g.i. tract for enhancing local action on *H. pylori*.[5,6] Other route of administration like rectal or vaginal could overcome these problems. The absorption of some drugs is notable from the vaginal wall.[7] Drugs used in the treatment of *Trichomonas* and *Candida* infections lead to systemic effect.[8] Prostaglandins, estrogens are hormones which are rapidly and extensively absorbed through the vaginal epithelium because of its large surface area. This route bypasses first pass metabolism so the rate of absorption is high.[9] Due to the mucoadhesive property it can attach to the mucus membrane of vagina and minimises the chance of detach and can sustain the drug release. Ornidazole suppository showed sustained release up to 90

Submission Date: 09-07-2019;
Revision Date: 18-09-2019;
Accepted Date: 17-10-2019

DOI: 10.5530/ijper.53.4s.153

Correspondence:
Prof. Subrata Mallick,
Department of Pharmaceutics, School of Pharmaceutical Sciences, Siksha O Anusandhan (Deemed to be University), Bhubaneswar, Odisha, INDIA.
Phone: +91 674 2386209
E-mail: profsmallick@gmail.com

www.ijper.org

min only as reported by Ozyazici *et al.*[10] The very common adverse effects of ornidazole are the significant abdominal disturbances, nausea etc. Abdominal disturbances and nausea and delayed onset of action particularly after oral administration could be minimized by using sustained and controlled release delivery of non-invasive suppository formulation of ornidazole compared to transdermal delivery.[11] Hard surface of the tablets may cause irritation of the vaginal epithelium in case of intravaginal application. The slippery and smooth surface of suppositories may facilitate application and thus the irritation will be less.[12,13] Therefore suppository preparations are also suitable dosage forms for vaginal administration. The HPMC is an inert and semi-synthetic polymer used to control the release rate of drug and may be used as controlled delivery component in different medicaments.[14] PEG has the property of maximum water solubility.[15] In this study, the rectal and vaginal suppositories were prepared using PEG 400, PEG4000, HPMC K100, HPMC K15, HPMC E5 in different ratios to sustain the release of ornidazole and compare their *in vitro* drug release properties.

MATERIALS AND METHODS

Materials

Ornidazole was taken as a gift sample from Jagannath Pharmaceuticals (Jagatpur, Cuttack, India). HPMC E5, HPMC K15 and HPMC K100 were purchased locally from Burgoyne and Co., Mumbai, India). PEG400 and PEG 4000 were collected from Merck Specialities Private limited, India.

Preparation of suppository

Suppository formulations were prepared by fusion molding and congealing technique. PEG 4000, PEG 400, HPMC (K15, K100, E5), ornidazole and water were used in different ratio to constitute a one-gram suppository (Table 1).

PEG 4000 and PEG 400 were taken in a 25ml beaker and melted at 30°C for 4 to 5 min. The melted content was transferred to a china dish containing ornidazole, HPMC and water. Then the content was triturated for 4 to 5 min to get a uniform mixture. The china dish was kept in a hot air oven at 30°C for 2 to 3 min and finally the content was transferred to the suppository forming mould and preserved in refrigerator to settle down and solidification for overnight period. Next morning the solidified suppositories were removed by simply pressing in a forward direction and utilized for further testing.

Differential Scanning Calorimetry (DSC)

Thermal analysis of pure ornidazole and formulations were analysed by differential scanning calorimetry (DSC-1, Mettler Toledo software) in the range of 30 to 105°C at constant heating rate under liquid nitrogen gas purge.

Fourier-Transform Infrared Spectroscopy (FTIR)

Samples of pure ornidazole and prepared suppository formulations for FTIR study were placed over zinc selenide crystal and pressed on to the attenuated total reflectance crystal (ATR crystal) by using the integrated pressure application device by using Bruker infrared analyser (Bruker alpha; Ettlingen, Germany).

Scanning Electron Microscopy (SEM)

The surface morphology and crystalline nature of the samples were investigated by using Scanning Electron Microscope (ESEM-FEI Quanta-250). The drug and suppository formulations were placed over carbon tape and scanned at room temperature with voltage of 10 kV at low vacuum (100Pa).

In-silico docking study

Auto Dock Vina 1.1.2 program was used to calculate the binding between drug and polymer. The programme helps in pre-calculating the interaction between ornidazole-HPMC and Ornidazole-PEG also the binding interaction between them. Protein Data Bank (PDB)

Table 1: Sustained release bioadhesive ornidazole suppository formulation.

Formulation codes	Ornidazole (mg)	PEG 4000 (mg)	PEG 400 (mg)	Water (ml)	HPMC (mg)		
					E5	K15	K100
ORHL5	200	320	400	0.075	5	--	--
ORHL10	200	325	400	0.075	10	--	--
ORHM5	200	320	400	0.075	--	5	--
ORHM10	200	325	400	0.075	--	10	--
ORHH5	200	320	400	0.075	--	--	5
ORHH10	200	325	400	0.075	--	--	10

and its 3-D visualization were generated by using MGL Tools (an Auto dock tool). Marvin sketch helped in drawing the 3-D structure of (OR, HPMC, PEG). By using Auto Dock tools programme the PDBQT files of OR, HPMC, PEG were prepared. The OR was taken as ligand in opposition to the receptors like HPMC, PEG. The stability was deliberated on the basis of interaction energy between the ligand and receptor. The more negative score the better will be the binding.

In vitro drug release

The *in-vitro* dissolution tests of ornidazole suppositories were performed with USP dissolution apparatus (type-2, paddle type). Accurately weighed suppository samples were placed over the dialysis membrane (Dialysis Membrane- 150, LA401-30MT) (Av. Flat width-37.70 mm, Av. diameter- 25.4 mm, Capacity approx- 5.07 ml/cm, molecular weight cut-off 12000-14000, Himedia Laboratory Pvt. Ltd., Mumbai) in a both side open diffusion tube and tied with thread tightly. Diffusion tube was attached with the paddle and *in vitro* drug release was carried out in phosphate buffer (pH-7.4) and sodium acetate buffer (pH-4.5).[16] Drug release was continued in 200ml medium with a rotation speed of 50rpm at 37°C. Samples were withdrawn at regular time intervals and analysed in a UV spectrometer (Thermo scientific, Evolution 201-uv-visible spectrophotometer) at 319nm.

RESULTS AND DISCUSSION

Suppositories were solidified and found smoothed surface (Figure 1) and studied characterizations are described below:

Differential Scanning Calorimetry (DSC)

A sharp endothermic peak of pure ornidazole was observed at 91.26°C indicating pure crystalline form (Figure 2). Formulationsshowed endothermicappearance in the range of 50 - 59°C due to presence of PEG.[17] Ornidazole melting peak has been disappeared in all the formulations indicating amorphous nature of the drug in the suppositories.

Fourier-Transform Infrared Spectroscopy (FTIR)

The peaks at 3172 and 3314 cm^{-1} in the FTIR spectrum of ornidazole are due to the C-H stretching and –O-H stretching mode respectively. The peaks at 1532 cm^{-1} and 1365-1264 cm^{-1} are due to asymmetric and symmetric stretching of NO_2 respectively. The C-O stretching vibration is confirmed by the presence of peak at 1186 cm^{-1}. The carbon connected with NO_2(C-N) has been credited by the presence of peaks at 824 and 732 cm^{-1} is due to the stretching frequency of C–Cl bond vibration. Peaks at 3500 and 3000 are due to O-H stretching of water and C-H stretching. Another peak at 1646 is due to N-H bending which signifies the interaction between polymer and drug through H-bonding (Figure 3).

Scanning Electron Microscopy (SEM)

The surface morphology of the pure drug and the suppositories are shown in Figure 4. Distinct brick shaped crystals were seen in the SEM image of ornidazole. The disappearance of definite crystal geometry is seen in the SEM images of all the suppository formulations. The disappearance of crystal geometry conforms the uniform distribution of drug throughout the formulations.

Analysis of molecular interaction (Docking)

The docking scores have been cited in Table 2. *In-silico* study gave an idea about the interaction between drug and carrier molecule (Figure 5). The physical interaction and possible conformation were well predicted by docking study. The binding interaction in between the Ornidazole and PEG showed lowest energy as compared to OR and HPMC. The negative energy in between drug and carrier indicates stable interaction. The more

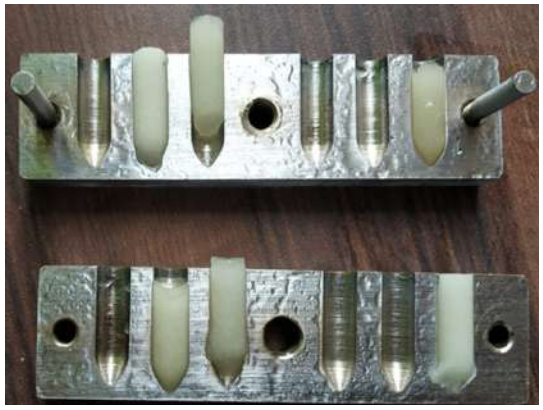

Figure 1: Prepared suppositories.

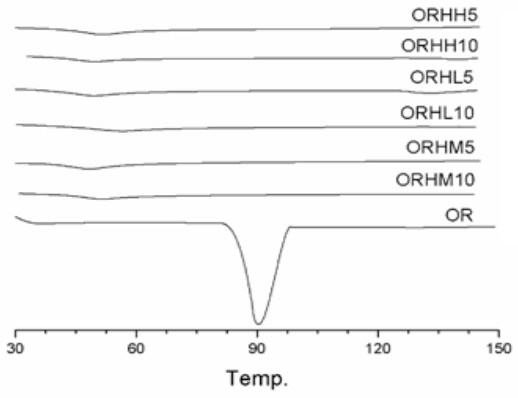

Figure 2: DSC thermo gram of ornidazole and the prepared suppositories.

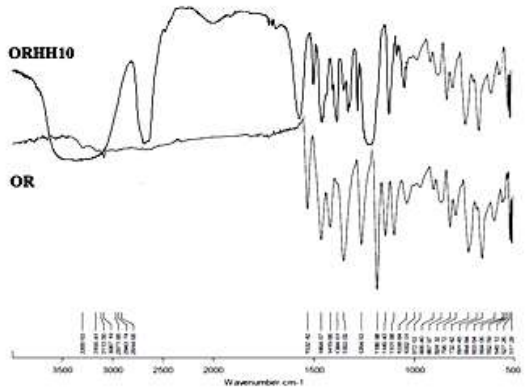

Figure 3: FTIR spectrum of OR and ORHH10.

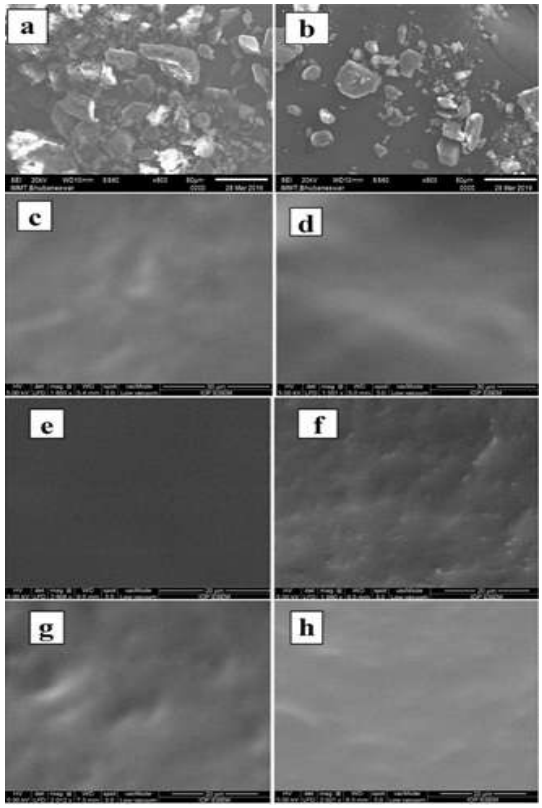

Figure 4: SEM image of pure crystalline drug ornidazole: (a) (magnification 500X), (b) (magnification 500); and suppository formulations: (c) ORHL5 (magnification 1655), (d) ORHL10 (magnification 1551); (e) ORHM5 (magnification 1551), (f) ORHM10 (magnification 1960); (g) ORHH5 (magnification 2012), (h) ORHH10 (magnification 2021).

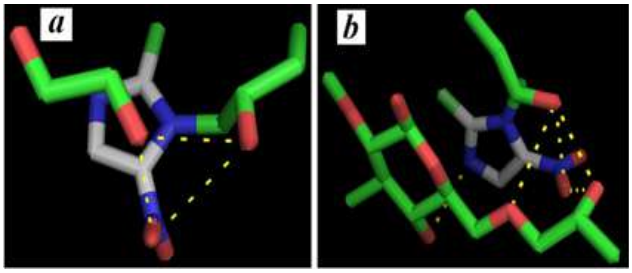

Figure 5: Docking interaction of (a) ornidazole-PEG and (b) ornidazole-HPMC.

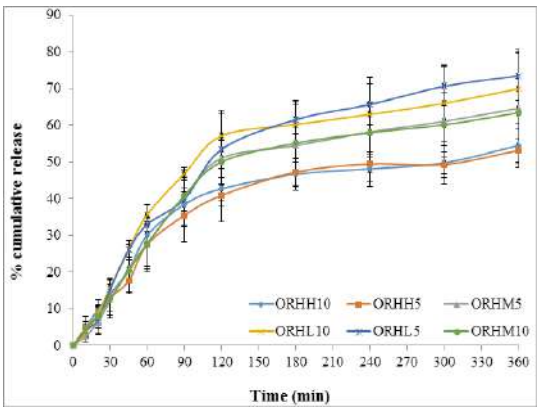

Figure 6: Ornidazole release from suppositories in phosphate buffer of pH 7.4(Results are mean ± SD of three independent experiments, *n*=3).

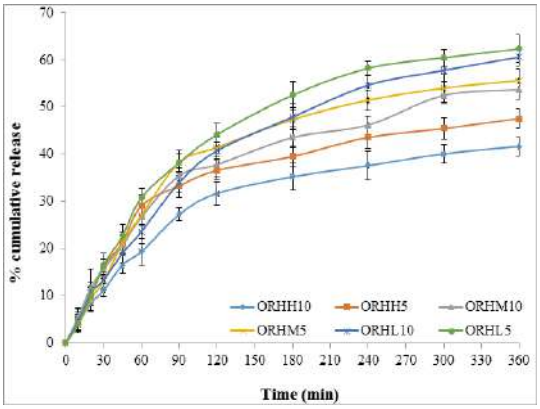

Figure 7: Ornidazole release from suppositories in phosphate buffer of pH 4.5(Results are mean ± SD of three independent experiments, *n*=3).

Table 2: Docking score of drug and polymer interaction.

Formulation	Docking score (Affinity)
OR-HPMC	-2.0
OR-PEG	-0.9

negative value indicates more stable binding than that of less negative value. The binding energy values for OR-HPMC and OR-PEG were -2.0 and -0.9 k cal/mol respectively. Figure 5 shows the docking interaction of ornidazole and the polymer.

In vitro drug release

The *in-vitro* release of ornidazole from suppositories containing bases of different composition were analysed in different time intervals. As shown in the Figure 6 and Figure 7 the diffusion of ornidazole from suppositories were in a sustained manner and continued to 6 h to release about 50-70%. Ornidazole release pattern from the suppositories were in the order of ORHH10>ORHH5>ORHM10>ORHM5>ORHL10>ORHL5.

Table 3: Drug release kinetics of ornidazole suppository formulations at pH 7.4.

Formulation code	Zero order		First order		Higuchi		Korsmeyer-Peppas		
	K_0 (%.min^{-1})	r^2	K_F (min^{-1})	r^2	K_H (%. min$^{-1/2}$)	r^2	n	Kp	r^2
ORHL5	0.207	0.859	1.955	0.946	4.739	0.959	0.787	0.012	0.950
ORHL10	0.191	0.791	1.935	0.881	2.205	0.926	0.757	0.002	0.973
ORHM5	0.182	0.825	1.953	0.896	4.337	0.938	0.797	0.099	0.946
ORHM10	0.178	0.824	1.949	0.890	0.343	0.939	0.790	0.024	0.965
ORHH5	0.143	0.806	1.948	0.859	1.073	0.937	0.711	0.039	0.972
ORHH10	0.140	0.782	1.940	0.844	0.342	0.927	0.705	0.072	0.964

Table 4: Drug release kinetics of ornidazole suppository formulations at pH 4.5.

Formulation code	Zero order		First order		Higuchi		Korsmeyer-Peppas		
	K_0 (%.min^{-1})	r^2	K_F (min^{-1})	r^2	K_H (%. min$^{-1/2}$)	r^2	n	Kp	r^2
ORHL5	0.171	0.848	1.947	0.920	1.932	0.964	0.741	0.038	0.969
ORHL10	0.161	0.893	1.960	0.950	3.352	0.979	0.723	0.037	0.986
ORHM5	0.151	0.822	1.947	0.885	1.316	0.949	0.726	0.027	0.968
ORHM10	0.139	0.845	1.946	0.908	0.351	0.969	0.681	0.116	0.970
ORHH5	0.119	0.778	1.940	0.839	1.927	0.934	0.672	0.105	0.954
ORHH10	0.110	0.832	1.958	0.874	0.167	0.959	0.659	0.049	0.977

The *in-vitro* release of ornidazole from suppository containing 10mg of HPMC K100 (ORHH10) showed the most sustained release as compare to all the formulation.[18] The drug release up to 360 min was considered as the main criterion for understanding the most sustaining effect. Drug release kinetics was not considered as the criterion for understanding the most sustaining effect. Suppository ORHH10 exhibited 41.68 % drug release whereas; ORHM10 has shown 53.75% up to 360 min.

Kinetics of drug release

Drug release mechanism has been predicted to develop a rational formulation utilizing mathematical models. Different kinetic models like Zero order, First order, Higuchi and Korsmeyer-Peppas model[19-31] were used to describe the kinetics of ornidazole release of suppository. The model that uses highest level of correlation (r^2) was used as the model-fitting kinetics. These models are represented as follows:

Zero order model: $Q=Q_0+K_0t$---------- (i)

First order model: $Log\ (100-Q)= \frac{K_F.t}{2.303}$---------- (ii)

Higuchi model: $Q=K_H\times\sqrt{t}$ ---------- (iii)

Korsmeyer-Peppas model: $Q=K_p\times t^n$

$LogQ=LogK_p+n.Logt$ ------ (iv)

Q = Cumulative percent drug release at time t

Q_0 = Cumulative percent drug release at time t = 0

K_0 = Zero order release rate constant

K_F = First order release rate constant

K_H = Higuchi release rate constant,

K_p = Peppas release rate constant or, Parameter reflecting the structural and geometric characteristics of the delivery device,

n = Power law exponent, or release exponent.

The kinetic parameters as per model are presented in the Table 3 and Table 4. Result indicates that the release kinetics of all the suppository formulations (pH 7.4 and pH 4.5) is mostly following the Korsmeyer-Peppas model because of higher r^2 value (0.946-0.986) compare to other models. The release exponent values (n= 0.659-0.797) are a sign of partially diffusion controlled and partially erosion controlled release. Fitting of release data with Higuchi model has shown r^2 values (0.926-0.929) closer to Korsmeyer-Peppas model indicating also diffusion controlled release to some extent.

CONCLUSION

The drug and polymer showed a significant interaction between them which was conformed from FTIR study and was supported by molecular level study (*in-silico* docking). The *in-vitro* release of ornidazole from suppository containing 10mg of HPMC K100 (ORHH10) showed the most sustained release as compare to all the formulation. Due to the presence of HPMC, it works as mucoadhesive so that it can attach to the mucus membrane of vagina and rectus for longer period of time. So this can be an approach in sustaining the release of ornidazole up to 6 hr and minimises the repeating of dose.

ACKNOWLEDGEMENT

The authors are grateful to Prof. (Dr) Monojranjan Nayak, President, Siksha 'O' Anusandhan (Deemed to be University) for financial support and laboratory facility. We are also grateful to receive Ornidazole as gift sample from Jagannath Pharmaceuticals, Cuttack, Odisha.

CONFLICT OF INTEREST

The authors declare no conflict of interest.

ABBREVIATIONS

HPMC: Hydroxy Propyl Methyl Cellulose; **PEG:** Poly Ethylene Glycol; **SD:** Standard Deviation.

REFERENCES

1. https://www.medicineindia.org/pharmacology-for-generic/474/ornidazole.
2. Triantafillidis JK, Antoniou A, Emmanoulidis A, Nicolakis D, Barbatzas C, Cheracakis P. Ornidazole in the prevention of recurrence of crohn's disease. Ital J Gastroenterol. 1998;30(4):446-47.
3. Taburet AM, Delion F, Attali P, Thebault JJ, Singlas E. Pharmacokinetics of ornidazole in patients with severe liver cirrhosis. Clin Pharmacol Ther. 1986;40(3):359-64.
4. https://www.lybrate.com/medicine/ornidazole/health-feed/questions.
5. Mallick S, Pattnaik S, Swain K, De PK, Saha A, Mazumdar P, *et al*. Physicochemical characterization of interaction of ibuprofen by solid-state milling with aluminum hydroxide. Drug Dev Ind Pharm. 2008;34(7):726-34.
6. Swain RP, Nagamani A, Shankar PU. Formulation and evaluation of gastro-bilayer floating tablets of ezetimibe as immediate release layer and atenolol as sustained release layer. Indian J Pharm Edu Res. 2019;53(2):S93-103.
7. Baloğlu E, Özyazıcı M, Baloğlu A, Ova L. A randomized controlled trial of a new ovule formulation of ornidazole for the treatment of bacterial vaginosis. Clin Pharm Ther. 2003;28(2):131-6.
8. Reddy RS, Kumar L, Pydi CR, Reddy MS, Verma R. Development of fluconazole suppositories for the treatment of candida infection of genitourinary tract. Indian J Pharm Edu Res. 2018;52(4):S16-22.Baria AH, Patel RP, Suthar AM, Parmar RB. Formulation development and evaluation of sustained release aceclofenac suppository. Int J Pharm Sci. 2009;1(2):71-3.
9. Ozyazíçí M, Gokçe E, Hizarcioglu SY, Taner MS, Koseoglu K, Ertan G. Dissolution and vaginal absorption characteristics of metronidazole and ornidazole. Pharmazie. 2006;61(10):855-61.
10. Fuh YM, Pham DC, Weng CF. Effects of sting plant extracts as penetration enhancers on transdermal delivery of hypoglycemic compounds. Medicina. 2019;55(5):121.
11. Havaldar VD, Yadav AV, Dias RJ, Mali KK, Kale SS, Pujari PP. Rectal suppository of mucoadhesive microspheres of alverine citrate for irritable bowel disease: *In vitro* evaluation. Res J Pharm Technol. 2018;11(7):3091-8.
12. Mallick S, Dey PK, Sannigrahi S, Mitra A. Crystallization of a non-steroidal anti-inflammatory drug from ethanol-water solution in presence of polymers: Physicochemical characterization and release behaviour from suppositories. Acta Pol Pharm. 2004;61:447-53.
13. Nanda A, Sahoo RN, Pramanik A, Mohapatra R, Pradhan SK, Thirumurugan A, *et al*. Drug-in-mucoadhesive type film for ocular anti-inflammatory potential of amlodipine: Effect of sulphobutyl-ether-beta-cyclodextrin on permeation and molecular docking characterization. Colloids Surf B. 2018;172:555-64.
14. Allen C, Santos ND, Gallagher R, Chiu GNC, Shu Y, Li WM, *et al*. Controlling the physical behavior and biological performance of liposome formulations through use of surface grafted poly (ethylene glycol). Biosci Rep. 2002;22(2):225-50.
15. Gomaa E, Abu LAS, Hasan AA, Ghazy FES. Preparation and characterization of intravaginal vardenafil suppositories targeting a complementary treatment to boost *in vitro* fertilization process. Eur J Pharm Sci. 2018;111:113-20.
16. Das D, Ganguli AK. Design of nanostructured cadmium tantalate and niobate and their photocatalytic properties. RSC Adv. 2013;3(44):21697-705.
17. Kumar DV, Swetha P, Prasad GS, Kumar AA. Assay method development and validation for simultaneous quantitative estimation of diloxanide furoate and ornidazole in tablets by RP-HPLC. Int J Pharm Pharm Sci. 2015;7(10):357-62.
18. Mallick S, Pattnaik S, Swain K, De PK. Current perspectives of solubilization: Potential for improved bioavailability. Drug Dev Ind Pharm. 2007;33(8):865-73.
19. Mallick S, Pattnaik S, Swain K, De PK, Saha A, Mazumdar P, *et al*. Physicochemical characterization of interaction of ibuprofen by solid-state milling with aluminum hydroxide. Drug Dev Ind Pharm. 2008;34(7):726-34.
20. Mallick S, Sahu A, Pal K. Dissolution behaviour of nalidixic acid solid dispersions using water soluble dispersion carriers. Acta Pol Pharm. 2004;61(1):21-30.
21. Bhandari MS, Wairkar SM, Patil US, Jadhav NR. Co-amorphization of ibuprofen by paracetamol for improved processability, solubility and *in vitro* dissolution. Acta Chim Slov. 2018;65(3):492-501.
22. Mohapatra R, Mallick S, Nanda A, Sahoo RN, Pramanik A, Bose A, *et al*. Analysis of steady state and non-steady state corneal permeation of diclofenac. RSC Adv. 2016;6(38):31976-87.
23. Mallick S, Pradhan SK, Mohapatra R. Effects of microcrystalline cellulose based comilled powder on the compression and dissolution of ibuprofen. Int J Biol Macromol 2013;60:148-55.
24. Panda B, Parihar AS, Mallick S. Effect of plasticizer on drug crystallinity of hydroxypropyl methylcellulose matrix film. Int J Biol Macromol. 2014;67:295-302.
25. Mallick S, Pradhan SK, Chandran M, Acharya M, Digdarsini T, Mohapatra R. Study of particle rearrangement, compression behaviour and dissolution properties after melt dispersion of ibuprofen, avicel and aerosil. Results Pharm Sci. 2011;1(1):1-10.
26. Mallick S, Roy K, Chakraborty A, Saha S. Mechanism of *in vitro* release kinetics of flurbiprofen loaded ethylcellulose micropellets. Acta Pol Pharm. 2002;59:193-98.
27. Mallick S, Gupta BK, Ghosal SK. Development and characterization of release profile of nifedipine as an effective controlled release system. J Sci Ind Res. 1999;58(12):1010-16.
28. Dvockova K, Kaledaite R, Gajdziok J, Rabiskova M, Bajerova M, MuselikJ, *et al*. The development of Eudragit® NM-based controlled-release matrix tablets. Medicina. 2012;48(4):192-202.
29. Kumar L, Reddy MS, Shirodkar RK, Pai GK, Krishna VT, Verma R. Preparation and characterization of fluconazole vaginal films for the treatment of vaginal candidiasis. Indian J Pharm Sci. 2013;75(5):585-90.
30. Pramanik A, Sahoo RN, Nanda A, Mohapatra R, Singh R, Mallick S. Ocular Permeation and Sustained Antiinflammatory Activity of Dexamethasone from Kaolin Nanodispersion Hydrogel System. Curr Eye Res. 2018;43(6):828-38.

PICTORIAL ABSTRACT

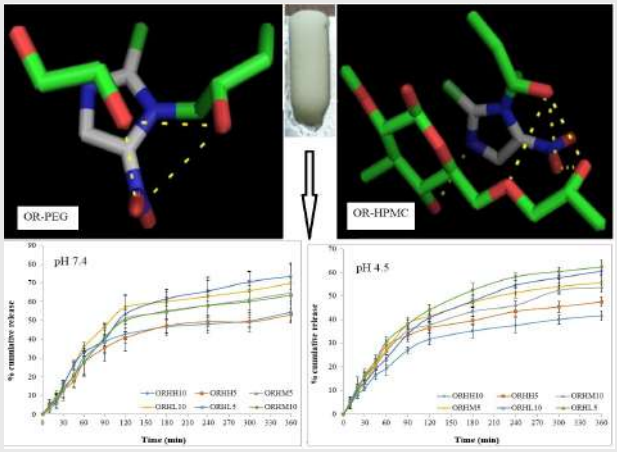

SUMMARY

- Sustained release ornidazole suppositories were prepared for systemic delivery to avoid abdominal disturbances and delayed onset of action after oral administration.
- *In silico* docking study revealed the affinity between ornidazole-HPMC and ornidazole-PEG of -2 and -0.9 k cal/mol respectively.
- Suppository (HPMC K100) showed the most sustained diffusion controlled release of ornidazole at pH 7.4 and 4.5.
- Bioadhesive suppositories could be conveniently utilized for sustained systemic delivery via rectal and vaginal route for more than 6 hr.

About Authors

Rasmita Dash, M.Pharm from School of Pharmaceutical Sciences, Siksha O Anusandhan (Deemed to be University), Bhubaneswar, Odisha, India.

Rudra Narayan Sahoo, M.Pharm, currently engaged as an INSPIRE Fellow under DST Government of India at School of Pharmaceutical Sciences, Siksha 'O' Anusandhan (Deemed to be University), Bhubaneswar, Odisha, India. His research area of interest is Formulation and Development, and Drug Delivery Systems.

Souvik Nandi, M.Pharm, currently engaged as a junior research fellow at School of Pharmaceutical Sciences, Siksha 'O' Anusandhan (Deemed to be University), Bhubaneswar, Odisha, India. His research area of interest is Formulation and Development, and Novel Drug Delivery Systems.

Rakesh Swain, M.Pharm, currently engaged as a junior research fellow at School of Pharmaceutical Sciences, Siksha 'O' Anusandhan (Deemed to be University), Bhubaneswar, Odisha, India

Subrata Mallick, (M.Pharm, PhD, PGDBM, FIC) is a life member of Association of Pharmaceutical Teachers of India, and Indian Pharmaceutical Association. At present he is the Professor and Heading the Department of Pharmaceutics, School of Pharmaceutical Sciences, Siksha'O' Anusandhan (Deemed to be University), Bhubaneswar, India. He is the reviewer of Elsevier, Wiley, Informa Healthcare, Taylor and Francis, Bentham Science, Springer, IEEE Xplore, Dovepressetc. and editorial board member of several International Journals of America, Canada, UK, Thailand, India etc. He is also aMember of doctoral committee of several universities. His current research areas of interest are: Ocular Drug Delivery Systems, Drug Stabilisation and Kinetics, Mucosal Delivey, Powder Compaction etc. More than 160 number of full research papers and conference proceedings are published in International and National levels under his guidance.

Cite this article: Dash R, Sahoo RN, Nandi S, Swain R, Mallick S. Sustained Release Bioadhesive Suppository Formulation for Systemic Delivery of Ornidazole: *In-silico* Docking Study. Indian J of Pharmaceutical Education and Research. 2019;53(4s):s580-s586.

Revista de Chimie
https://revistadechimie.ro
https://doi.org/10.37358/Rev. Chim.1949

Budesonide-Cyclodextrin in Hydrogel System: Impact of Quaternary Surfactant on *in vitro-in vivo* Assessment of Mucosal Drug Delivery

SUNIL PATTANAIK, SOUVIK NANDI, RUDRA NARAYANA SAHOO, ASHIRBAD NANDA, RAKESH SWAIN, SHUBHASHREE DAS, SUBRATA MALLICK*
School of Pharmaceutical Sciences, Siksha 'O' Anusandhan (Deemed to be University), Khandagiri, Bhubaneswar, Odisha, India, 751003

Abstract: *Budesonide, a glucocorticosteroid is generally used to treat chronic inflammation and asthma. Hepatic first-pass metabolism and poor solubility are the major causes of its limited oral bioavailability. Present work was undertaken for the preparation of hydrogel film formulation with cyclodextrin complexation of budesonide containing quaternary surfactant for possible enhancement of mucosal permeation. FTIR study confirmed drug-polymer hydrogen bonding. Almost complete amorphization of the drug was pronounced by SEM, DSC and XRD studies. The film containing benzalkonium and hydroxypropyl beta-cyclodextrin exhibited in vitro dissolution and mucosal permeation to the highest extent of 87.2 and 95.8 % respectively in contrast to the others. Film formed hydrogel in aqueous mucin and enhanced the mucosal tissue residence time due to the mucoadhesive nature of the polymer. Acute inflammation in the rabbit eye was controlled within 3 h by applying the film in the cul-de-sac. The presence of cyclodextrin and quaternary surfactant brought about significantly improved drug release and mucosal permeation compared to their absence in the HPMC film. Hydrogel formed in aqueous mucin enhanced the mucosal residence time and controlled acute inflammation in the rabbit eye within 3 h after topical application.*

Keywords: *Budesonide, cyclodextrin inclusion, mucosal delivery, ocular anti-inflammation.*

1. Introduction

Budesonide, a highly potent glucocorticosteroid is used to control asthma by decreasing swelling and irritation in air pathways for easier breathing. It is also used to treat inflammatory bowel disease (IBD), ulcerative colitis (UC), and Chron's disease (CD) [1]. It is available in the market as dry powder inhaler (DPI), tablet, and capsule formulations. According to the biopharmaceutical classification system (BCS) the drug is having high permeability and low solubility, with a log P of 3.2. The oral bioavailability of budesonide is highly affected due to its poor dissolution and high hepatic first-pass metabolism (11 %). Acid hydrolysis and enzymatic degradation in the GI tract affect the absorption process after oral administration. Budesonide also shows low inhalation bioavailability of 6 % with a very short elimination half-life of 2-3 h [2]. Fluidization and dispersion characteristics may be affected due to problems like upper airway deposition associated with budesonide DPI [3].

Transmucosal routes like ocular, buccal, nasal, rectal, vaginal give more discrete advantages for the administration of a drug over other non-parenteral routes. These mucosal routes also offer many times greater permeability rather than of skin [4]. Drug delivery through buccal route leads to absorption to the systemic circulation effectively bypassing the first-pass metabolism with minimal fluctuations in plasma concentration [5]. Buccal mucosal tissue is highly vascularised with blood vessels. Mucin concentration in the buccal mucosa is high for facilitating more effective mucoadhesion compared to inhalational therapy and many other mucosal deliveries [6]. Moreover, buccal tissue recovery is quicker than other delivery routes and could be appropriately explored for better drug delivery [7].

*email: profsmallick@gmail.com

Nowadays hydrophilic vehicles play a great role in incorporating various kinds of drugs in mucosal delivery. Hydrogels as the semisolid vehicle can also be adapted easily in sustained and controlled release and thus minimizing the side effect and toxicity [8-12]. Gaikwad et al have developed an enteric-coated self nano emulsifying capsule formulation for colonic delivery of budesonide [13,14]. The main limitations associated with these types of delivery systems are drug loading efficiency and bulkiness of the final volume of the formulation.

Inclusion agents are used to achieve better bioavailability and dissolution due to improved physicochemical stability and increased solubility [15-17]. Cyclodextrins, a non-toxic cyclic oligosaccharide has particularly drawn attention for improving the solubility and stability of drugs [18]. Cyclodextrin complexation increased the solubility and stability of lansoprazole [19]. The use of cetrimide and hydroxypropyl beta cyclodextrin independently improved the solubility of valdecoxib [20]. Oral pediatric formulation of budesonide was prepared by inclusion complexation using cyclodextrin for increased bioavailability [6]. Transbuccal diffusion of omeprazole was increased in the presence of cyclodextrins [21]. Presence of surfactants also in the delivery system is very much promising in improving mucosal permeation. Transmucosal permeation of fluorescein isothiocyanate dextran has been improved through cornea by incorporating benzalkonium chloride in the solution [22]. Another cationic surfactant, cetrimide was also found to increase the buccomucosal permeation of peptides and proteins [23].

The solubility of a surfactant can be increased by forming an inclusion complex with cyclodextrin [24]. Critical micelle concentration of surfactants increases markedly in the presence of cyclodextrin [25]. The impact of quaternary surfactants and cyclodextrin in combination on mucosal permeation of budesonide has probably not been reported yet and could be the potential for significant improvement of bioavailability of the drug. In our study, hydrogel film has been prepared with cyclodextrin complexation of budesonide containing quaternary surfactant for possible enhancement of mucosal permeation. Film formulation was chosen because of its better patient compliance, ease of application, and other advantages like transport and storage [26]. Solvent casting method was employed for the preparation of budesonide-in-HPMC films using β-cyclodextrin or HP-β-cyclodextrin as an inclusion agent. Benzalkonium chloride (BZK) or cetrimide (CET) was also used as quaternary surfactants in combination with inclusion agent for possible enhancement of transmucosal permeation of budesonide. Budesonide films were tested for *ex vivo* buccal mucosal tissue permeation. *In vivo* anti-inflammatory activity has also been examined after topical application of film on carrageenan induced rabbit eye model [27,28]. The utility of *ex vivo* permeation (using mucosal biomembrane) was demonstrated to predict the ability of budesonide *in vivo* (in life system) performance.

2. Materials and methods

2.1 Materials

Budesonide was obtained from Cipla Laboratories (Goa, India) as a gift sample. HPMC K 15M and Cetyl Trimethyl Ammonium (cetrimide) were procured from Burgoyne Burbidges & co. Laboratories (Mumbai, India). Triethanolamine and benzalkonium chloride (50 % solution) were purchased from SRL laboratories and MERCK laboratories India respectively. Beta cyclodextrin and hydroxypropyl beta-cyclodextrin were obtained from Dr. Reddy's Laboratories (Hyderabad, India) as gift samples. Carrageenan was purchased from TCI Laboratories Pvt. Ltd. Japan.

2.2 Preparation of budesonide film

HPMC K 15M was taken in a 100 mL beaker and 40 mL of distilled water was added and left for swelling at 2-8 °C for 24 h. β-cyclodextrin and HP-β-cyclodextrin, triethanolamine, and surfactants were incorporated into the viscous polymer solution with continuous stirring. Budesonide in 10mL of methanol solution was added to the mixture and stirring continued for 2-3 h until a fully transparent solution was obtained. The drug-polymer solution was then poured on Tarson Petri dish and left to dry at 40-50 °C for 36-48 h. Complete drying was assured when a constant weight was achieved of the

prepared film. Films were separated from the Petri dish and packed in the zip lock Tarson pouch and preserved in an airtight container until further studies [29] (Table 1). A standard calibration curve of Budesonide was prepared by recording the absorbance of various dilutions of the drug (1.44, 2.88, 4.32, 5.76, 7.20, 8.64, and 10.08 µg/mL) at 247 nm (JASCO V-630 spectrophotometer). Assay of the film formulations was estimated by placing a preweighed piece of film in a volumetric flask. Sufficient methanol was added and the flask was shaken for 24 h at laboratory ambient condition in an Orbital shaker (Remi Elektrotechnik Ltd, Vasai, India). Volume was made up to the 100 mL mark for the complete solubilization of film with methanol. The resulting solution was filtered (Whatman Uniflo 0.45µm, PVDF) and a serial dilution was made with aqueous phosphate buffer (*p*H 6.8) and checked spectrophotometrically at 247 nm [30,31]. Film thickness was measured 5-10 random portions by Mitutoyo Digimatic Micrometer (Japan) and the average values were recorded. Folding endurance of the film was observed by repeatedly folding a small strip of 2cm x 2cm till it breaks. The number of times the film folded was measured as the folding endurance value.

Table 1. HPMC hydrogel film formulation of budesonide-cyclodextrin containing quaternary surfactant[a]

Formulation code	HPMC k15M (mg)	Surfactant (0.1 %)	Inclusion agent (molar ratio 1:1)	Budesonide Assay mean ± sd (%)
BHT	900	-	-	3.78 ± 0.194
BHT_bC_1	900	BZK	β – cyclodextrin	2.48 ± 0.065
BHT_bC_2	900	BZK	HP-β–cyclodextrin	2.55 ± 0.03
BHT_cC_1	900	CET	β – cyclodextrin	2.66 ± 0.03
BHT_cC_2	900	CET	HP-β–cyclodextrin	2.49 ± 0.05

[a] Budesonide (40 mg) in HPMC matrix using triethanolamine (20 % of polymer) as a plasticizer

2.3 Moisture content and Moisture uptake

Prepared films were cut into small pieces and put into the desiccator containing activated silica gel at least for 24 h. The percentage of weight difference value of the films with respect to the initial was estimated as moisture content (%). For evaluation of moisture uptake film pieces were placed for equilibration in a closed desiccator containing the supersaturated solution of sodium chloride for maintaining 75 % RH up to a constant weight. The weight difference value between final weight and initial weight was used % of moisture uptake of the films [32].

$$\text{Moisture Content} = \frac{(Initial\ weight - dryweight\ after\ 24\ h)}{Initial\ weight} \times 100$$

$$\text{Moisture Uptake} = \frac{(Final\ weight - Initial\ weight\ before\ putting\ in\ dessicator)}{Initial\ weight} \times 100$$

2.4 Swelling and erosion study

Dynamic hydration of swelling and erosion of the film was determined from the percentage hydration and matrix erosion using the following equations. Randomly selected film sample (≈1 cm × 1 cm) was placed in Petri dishes containing 40 ml of simulated buccal fluid (phosphate buffer of pH 6.8) [33]. The weight gained by the films was noted at regular intervals after removing excess liquid by tissue paper swabbing [34].

$$\text{Dynamic hydration} = \frac{(\text{Hydrated weight} - \text{Initial dry weight of the film})}{\text{Weight after hydration}} \times 100$$

$$\text{Matrix erosion} = \frac{(\text{Initial dryweight} - \text{Dried final weight after swelling})}{\text{Initial dryweight}} \times 100$$

2.5 FTIR

FTIR study was done for the prepared films and pure budesonide to observe drug-excipient interactions. Samples were placed on the diamond ATR crystal (JASCO ATR PRO ONE) in the FTIR spectrometer (JASCO FT/IR 4600). All the scans were done between 4000-400 cm^{-1} and an average of 80 scan accumulations at a resolution of $4cm^{-1}$ were recorded.

2.6 DSC (thermal analysis)

Calorimetric study of budesonide and the formulations were performed by differential scanning calorimetry (Model: DSC-1, Mettler Toledo; Switzerland). The study was conducted at a temperature range of 30-300 °C under constant nitrogen flow (20.0 $mL.min^{-1}$) and a heating rate of +10 $°C.min^{-1}$.

2.7 X-ray diffractometry

X-ray diffraction pattern of pure budesonide and formulations were acquired by using X-ray diffractometry (Model: Rigaku Ultima IV). The voltage and current were 40 kV and 15 mA respectively. The X-ray source anode material used was CU. 1°/ min scan speed was maintained and X-axis values ranging between 5-70°C specifications test was carried out.

2.8 SEM analysis

Surface morphology of budesonide and the films were examined by scanning electron microscopy (Model: JEOL JSM-6510). Sputter coating with platinum was applied as a prior treatment before subjecting the samples in the SEM. Samples were scanned under an accelerated voltage of 30kv at room temperature. The film surfaces and crystal size of pure drug visualizing at 3,000-10,000X magnification.

2.9 In-vitro drug release study

Prepared budesonide films were attached on the surface of a glass slide with cyanoacrylate adhesive and fully merged it into the dissolution vessel containing 200 mL phosphate buffer (6.8 *p*H) in a USP Type-II dissolution apparatus (Dissolution Tester USP, Electrolab TDT06L, India). The paddle was adjusted to 50 rpm along with the temperature at 32±2 °C and the study was carried out for 6 h [35]. The release of the drug was estimated spectrophotometrically.

2.10 Mucosal permeation study

Fresh buccal skins were collected from local chicken meat shop within an hour of its sacrifice. Buccal mucosal membranes were made free from fat and then washed with distilled water and dipped into phosphate buffer *p*H 6.8 at room temperature. The dissected tissue was then attached to the diffusion tube in modified Franz diffusion cell. Buccal permeation was carried out for 6h using phosphate buffer 6.8, 200 mL as the diffusion media maintaining 34 ± 0.2°C. The samples were withdrawn at particular time intervals and assayed by UV Spectrophotometer to calculate the percentage of drug permeated [36].

2.11 Anti-inflammatory activity study

For in vivo anti-inflammatory study the ocular environment was much convenient because of its easy access and for the fact that mucin is present in both buccal and ocular environment [33]. New Zealand white rabbits of 1.5-2 Kg were used for the study. Animals were held for 24h in the laboratory before the experiment for environmental adaptation. This anti-inflammatory study was properly assessed and approved by the animal ethical committee of Siksha O Anusandhan (Deemed to be University) (IAEC no. IAEC/SPS/SOA/07/2019). Local ocular anesthesia was given with 0.5 % Proparacaine HCl (Ophthalmic Solution) USP. Carrageenan (200 μL, 3 % w/v) was injected in the upper palpebral region of the eye of the rabbit by BD U-40 syringe to induce acute inflammation. The film (BHT_bC_2) was sterilized under UV radiation by keeping it for 10 mins at a distance of 25 cm from

the UV source. The sterilized film then placed at the cul-de-sac and ocular anti-inflammatory activity was visualized and photographed.

3. Results and discussions

3.1 Physical characterization

The average thickness of the films was found in the range of 160-195 µm, well acceptable for mucosal application [37]. Films were showing good folding-endurance between 192-210 indicating sturdy and plasticized enough and not fragile due to the presence of triethanolamine [38]. The content of moisture in the films was found to be in the range of 1.25-2.41 % in laboratory conditions.

The main role of moisture content in a film is to deliver enough plasticity and keeping it from being brittle. But excess moisture content affects the properties of the films. Moisture uptake study of the films was carried out at 75% RH condition showed in the range of 5.59 - 5.69 % [39]. The physical properties of the films are illustrated in Table 2.

Table 2. Physical properties of polymeric film

Formulation Code	Moisture uptake Mean±sd, (n=4) (%)	Moisture content Mean±sd, (n=4) (%)	Thickness (µm) Mean±sd, (n=4)	Folding endurance
BHT	5.67 ± 0.26	2.41 ± 0.66	166.0 ± 3.3	192
BHT_bC_1	5.59 ± 0.40	1.25 ± 0.63	178.1 ± 7.5	203
BHT_bC_2	5.69 ± 0.30	1.70 ± 0.44	196.6 ± 7.7	209
BHT_cC_1	5.64 ± 0.36	1.67 ± 0.48	174.6 ± 4.9	196
BHT_cC_2	5.67 ± 0.377	2.12 ± 0.37	196.0 ± 8.0	201

3.2 Swelling and erosion study

The swelling profile of the films was depicted in Figure 1. Hydration of water in the polymeric matrix was seen followed by matrix erosion. Rate of swelling increased significantly in the presence of cyclodextrin compared to its absence in the films. BHT showed swelling rate up to 2.402 min^{-1} whereas the film containing inclusion agent (BHT_bC_1, BHT_bC_2, BHT_cC_1, and BHT_cC_2) showed 3.543, 3.656, 3.624, 3.134 min^{-1} (Table 3). Cyclodextrin in the polymeric film played a vital role in hydration to loosen the polymer network and increased water retention capacity [40,41].

Table 3. Swelling behaviour and permeability parameter of budesonide film

Formulation Code	Rate of swelling (K_s) (min^{-1}) (mean±sd; n=4)	Erosion (%), (mean±sd; n=4)	Flux (J_s) (µg/min) (mean±sd; n=4)	Permeability co-efficient (P_{ss}) (cm/min) *10^5 (mean±sd; n=4)
BHT	2.4 ± 0.4	72.16 ± 2.8	0.82 ± 0.15	1.6 ± 0.57
BHT_bC_1	3.5 ± 0.3	72.65 ± 12	1.41 ± 0.47	4.7 ± 1.4
BHT_bC_2	3.6 ± 0.1	72.39 ± 2.3	1.67 ± 0.74	8.3 ± 3.7
BHT_cC_1	3.6 ± 0.3	79.01 ± 3.5	2.12 ± 0.49	6.5 ± 2.0
BHT_cC_2	3.1 ± 0.1	77.80 ± 1.3	1.44 ± 0.21	4.8 ± 1.6

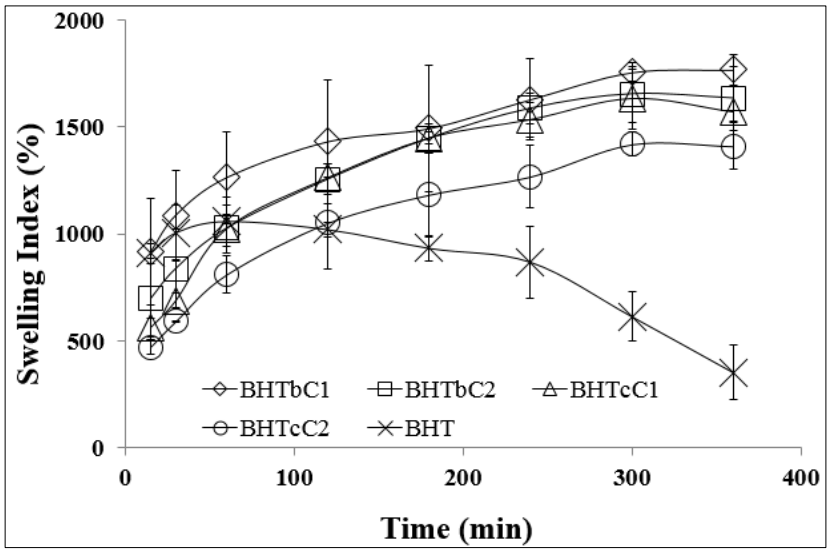

Figure 1. Swelling index profile of budesonide film

3.3 FTIR study

Polymer and drug intermolecular interactions were analyzed by the FTIR spectra (Figure 2A). Characteristic peaks of budesonide were showed at 3490, 2956, 1723, 1666, and 888 cm^{-1} due to the stretching of O-H, C-H, C=O, and C=C [42,43]. In the formulated films the peaks are masked, the characteristic C=O stretching peak at 1666 shifted to 1656 with a decreased intensity. Broadening of the peaks at 1200-1000 regions was found. Masking, shifting and broadening of the parent peak intensity are the clear evidence of interaction of drug with polymers and cyclodextrins due to H-bond formation [30].

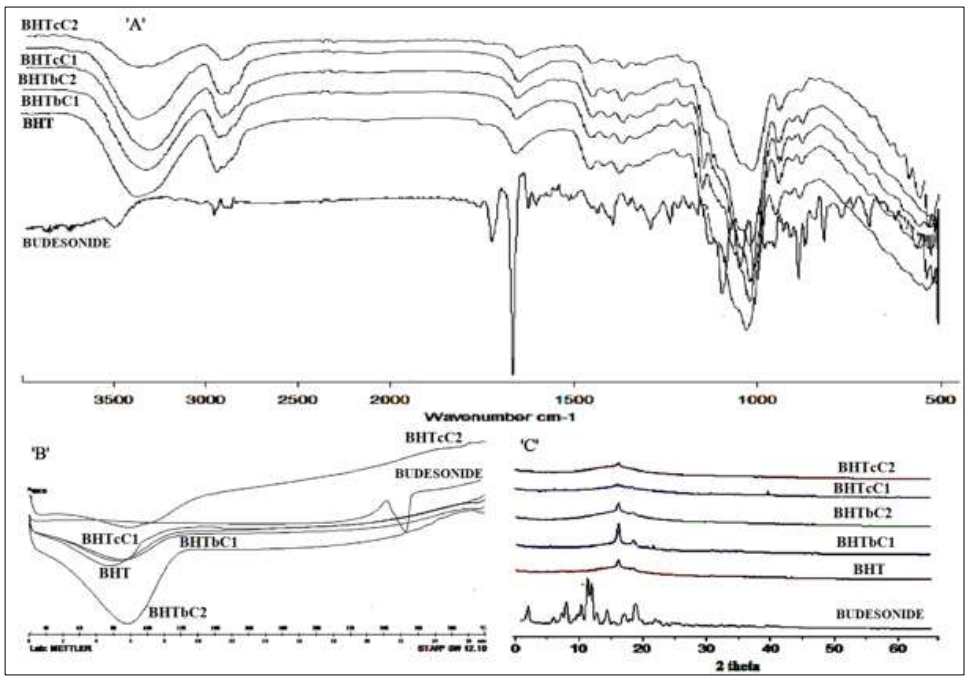

Figure 2. (A) FTIR study (B) DSC study (C) XRD study of pure drug and films

3.4 DSC study

DSC study was carried out to find the endothermic peak, crystalline behavior, and degradation of pure drug. Budesonide showed (Figure 2B) the sharp endothermic peak at 252.57°C due to the melting point of the drug. Polymeric films showed only a wide endothermic shouldering within 50-100°C

specifying water evaporation of water from the hydrogel matrix. Complete disappearance of the melting peak demonstrated complete dispersion of budesonide in the polymer matrix and almost complete amorphization [44].

3.5 XRD analysis

X-ray diffractogram of pure budesonide (Figure 2C) showed high-intensity peaks at 6.21, 10.18, 11.49, 12.17, 15.53, 16.10, 22.16 2θ which can only be observed if the drug is in crystalline form [42]. The disappearance of the diffraction peaks in the polymeric matrix indicated intermolecular complexation between drug and polymer and almost complete amorphization of the drug crystal.

3.6 SEM analysis

Figure 3 depicts the SEM images of pure budesonide as regular geometric crystal form [45] and loss of geometry were clearly observed in the formulated polymeric films. All the film formulations showed smooth and homogenous surfaces may be due to interpenetration and considerable solubility of budesonide into the matrix system. The crystal grains are not visible even after ×10000 magnification of the micrographs which confirms the lowering of crystalline intensity to a great extent. XRD and DSC report also confirmed the diminished crystallization of drug markedly in the polymeric film. Presence of HPMC arrested the crystal growth significantly in the film [38].

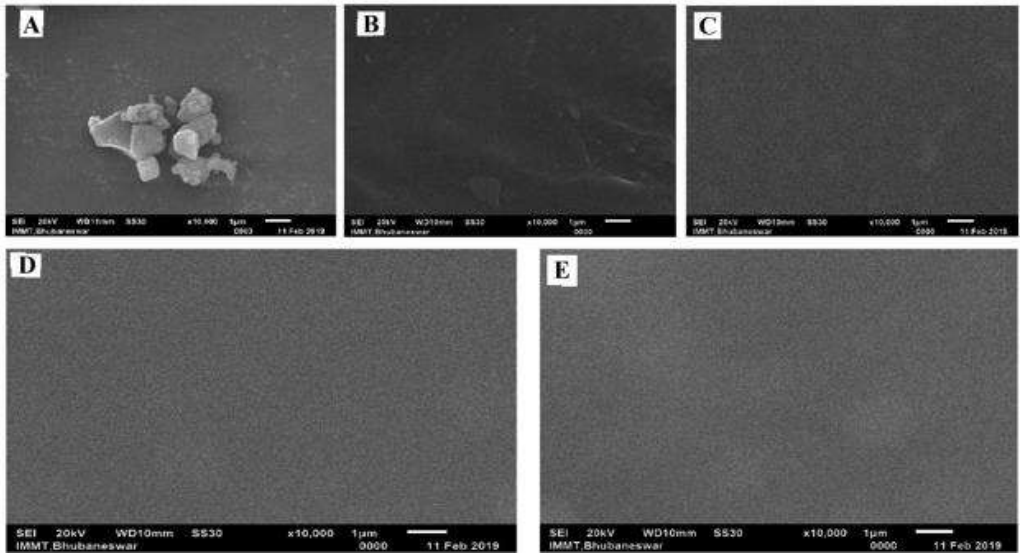

Figure 3. SEM images (A) Budesonide, (B) BHT_bC_1, (C) BHT_bC_2, (D) BHT_cC_1, (E) BHT_cC_2

3.7 *In-vitro* dissolution study

Improved in-vitro cumulative drug release profiles have been observed from all the film formulations for an extended period of 6 h in Figure 4A. Drug release has been more effective due to the presence of inclusion agents and quaternary surfactants [46]. BHT formulation showed a release up to 63 % whereas, the combination of cyclodextrin (β-cyclodextrin or, HP-β-cyclodextrin) as an inclusion agent and surfactant (cetrimide or, benzalkonium chloride) improved the dissolution of the drug (77.8 to 87.2 %). BHT_bC_2 formulation exhibited the in vitro release to the highest extent (87.2 %) due to the presence of benzalkonium chloride and HP-β-cyclodextrin compared to other formulations (BHT_bC_1: 84.12; BHT_cC_1: 77.8; and BHT_cC_2: 80.2 %). In a literature report, it was noticed that the rate and extent of budesonide dissolution have become significantly effective by the use of lung surfactant [47]. Akkari et al 2016 have claimed that the addition of HP-β-cyclodextrin in the hydrogel matrix has increased the solubility of budesonide [48]. Lansoprazole dissolution was increased by the addition of cyclodextrin [19]. In a study presence of cetrimide or cyclodextrin has improved the solubility of valdecoxib [20]. Sodium lauryl sulphate (0.5%) was used for maintaining sink condition in dissolution

testing of a hydrogel containing budesonide tablet at *p*H 6.8 [48]. Solubility of the budesonide-cyclodextrin complex has further been improved in the presence of quaternary surfactants during the *in vitro* release study of the present film formulation. The difference and similarity factor (f_1 and f_2) of the formulations (against BHT) has been tabulated (Table 4).

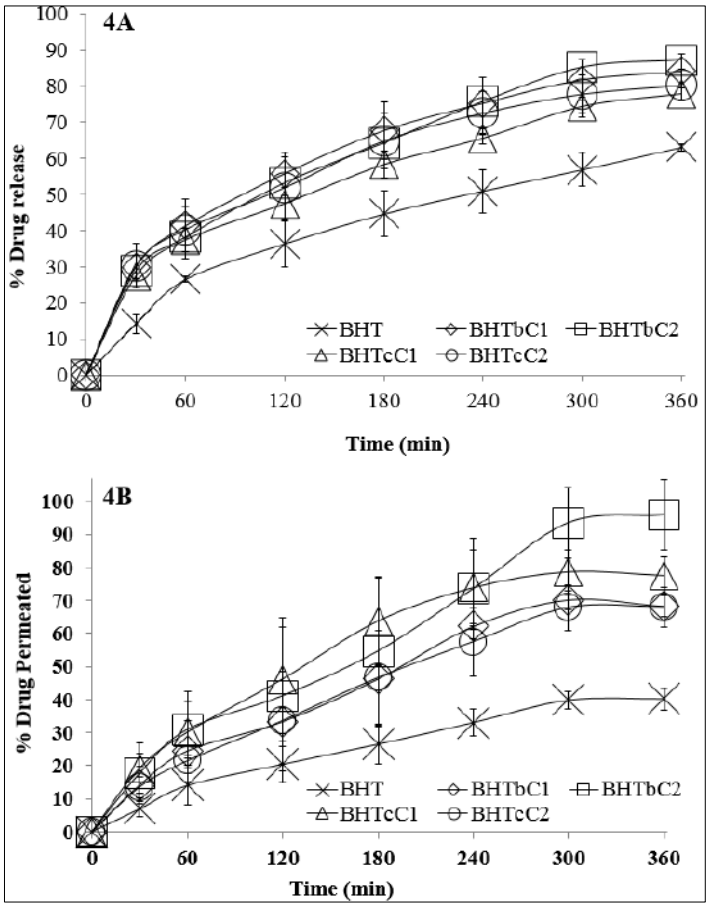

Figure 4. (A) In-vitro dissolution study (B) Buccal permeation study

Table 4. Comparison of *in-vitro* dissolution and mucosal permeation profiles

Comparison with BHT	*in-vitro* dissolution		mucosal permeation		Similarity or equivalence value
	Difference factor (f_1)	Similarity factor (f_2)	Difference factor (f_1)	Similarity factor (f_2)	
BHT vs. BHT_bC_1	49.054	34.024	76.176	33.234	$f_1 \leq 15$
BHT vs. BHT_bC_2	47.911	34.079	125.124	21.981	
BHT vs. BHT_cC_1	32.651	42.932	114.997	24.985	$f_2 \geq 50$
BHT vs. BHT_cC_2	42.847	37.046	70.520	34.805	

3.8 Mucosal permeation study

Mucosal permeation was carried out also for 6 h by using chicken buccal tissue as a mucosal membrane (Figure 4B). Presence of inclusion agent (β-cyclodextrin or, HP-β-cyclodextrin) and surfactant (cetrimide or, benzalkonium chloride) significantly improved also the permeation (BHT_bC_1: 70.1; BHT_bC_2: 95.8; BHT_cC_1: 78.5 and BHT_cC_2: 67.9 %) compared to its absence in the film (BHT: 40.2 %). Among all the formulations, the benzalkonium chloride-containing film along with HP-β-cyclodextrin showed the highest result (BHT_bC_2: 95.8 %). Benzalkonium chloride or cetrimide in the

film (BHT_bC_2 and BHT_cC_1 respectively) increased the release of drug on the mucosal surface because of its surfactant property and facilitated the better permeation via paracellular route compared to BHT [23]. Additionally, the cationic surfactants overcame the physiological and mucosal barrier for the increase of permeation and BZK exhibited better ability rather than CET [49]. Cyclodextrin exhibited increased transmucosal diffusion of omeprazole [21]. BZK was found to be facilitating the mucosal permeation of fluorescein isothiocyanate dextran [22]. f_1 and f_2 of the formulations with respect to BHT are tabulated in Table 4.

3.9 Kinetics of drug release and permeation

Korsmeyer-Peppas, Higuchi, and first-order model equations were used to describe the drug release and permeation kinetics of the drug [50,51]. The parameters were reported in Table 5.

Korsmeyer-Peppas:

$$\frac{W_t}{W_\infty} = K_k t^n$$

Higuchi Kinetics:

$$H = K_h\sqrt{t}$$

First-order:

$$logH = logH_0 + \frac{kt}{2.303}$$

Here, W_t is the fraction of drug released/permeated at time "t", and W_∞ maximum amount of drug available at the release/permeation site, K_k is the constant related to system structure and geometry and *n* is the drug release exponent. H and K_h signify the amount of drug released per unit area of the film and Higuchi rate constant for release/permeation respectively. The drug release of all the formulation could be described as a diffusion-controlled process (n = 0.40-0.56) [52].

$$P_{SS} = \frac{J_{SS}}{C}$$

C= drug concentration remaining in the formulation (X/V) [where X= cumulative drug amount in receiver compartment]

Jss= Flux of permeation at steady state calculated from the slope of X vs time plot.

The amount of drug permeated or permeability co-efficient 'P_{ss}' of BHT_bC_2 film ($8.311*10^{-5}$) was better than the other formulations demonstrated in Table 3 [53,54]. A low amount of drug was permeated from the BHT formulation ($1.675*10^{-5}$). According to the Korsmeyer-Peppas equation, the 'n' value lies in between 0.59 to 0.7 indicating majorly diffusion-controlled and partially erosion controlled release (Table 5) [50]. The erosion of the film (BHT) was higher relative to other formulations (BHT_bC_1, BHT_bC_2, BHT_cC_1, and BHT_cC_2). On the other hand, BHT_cC_1 has shown mostly diffusion-controlled compared to other films. The erosion of the films were in the order of: BHT > BHT_bC_2, BHT_cC_2 > BHT_bC_1 > BHT_cC_1.

Table 5. Kinetic parameter of in-vitro drug release and ex-vivo buccal permeation

Formulation code	Release					Permeation				
	First order	Higuchi		Peppas		First order	Higuchi		Peppas	
	r^2	k	r^2	n	r^2	r^2	k	r^2	n	r^2
BHT	0.978	3.372	0.995	0.569	0.981	0.976	2.295	0.980	0.71	0.986
BHT_bC_1	0.980	4.503	0.988	0.425	0.995	0.964	3.996	0.970	0.68	0.985
BHT_bC_2	0.988	4.699	0.996	0.463	0.996	0.966	5.307	0.960	0.69	0.984
BHT_cC_1	0.977	4.06	0.994	0.422	0.997	0.957	4.55	0.978	0.55	0.982
BHT_cC_2	0.970	4.262	0.986	0.406	0.995	0.984	3.919	0.978	0.69	0.995

3.10 Anti-inflammatory activity

Budesonide (1 mg equivalent) containing film formulation (26.4-40.3 mg) has been used for anti-inflammatory study after topical application. The probable methanol content in the film used for the anti-inflammatory study was well below the permissible daily exposure according to the European Medicines Agency – ICH guideline Q3C (R6) on impurities (30 mg/day). Carrageenan was found to be more convenient than the Freund's adjuvant for its chronic inflammation which can elongate up to 14 days but carrageenan causes an acute inflammation which gives effect up to 24 h [55]. After 30 minutes from the carrageenan injection (Figure 5A), frequent lacrimation, meibomian secretion, reddening, and swelling of the conjunctiva appeared in comparison to the normal eye (Figure 5B, 5C). But there were no signs and symptoms in the normal/control eye. (Figure 5E). The film, BHT_bC_2 has exhibited the highest extent of *in-vitro* dissolution and also *ex vivo* mucosal permeation and selected for *in vivo* anti-inflammatory activity study. After complete inflammation, the film (BHT_bC_2) was placed in the cul-de-sac region of the rabbit eye. The symptoms of inflammation like redness were decreased within 3 hours after the film was applied. But inflammation was not decreased in the positive controlled eye and redness not decreased within the 3 h (Figure 5F) [32,56].

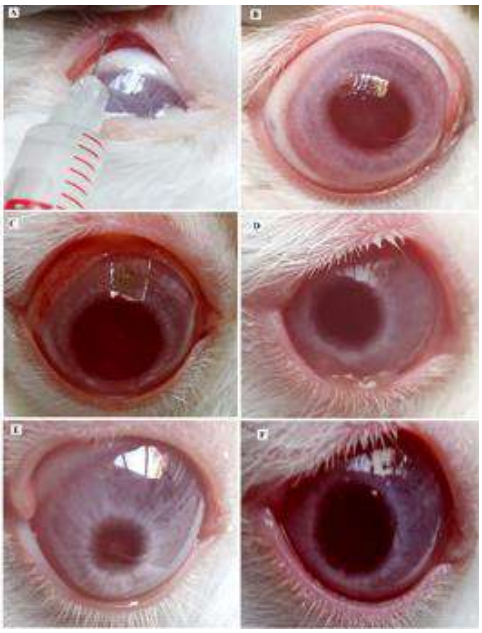

Figure 5. (A) Injecting carrageenan in the upper palpebral region; (B) Normal rabbit eye (right) before carrageenan injection; (C) Acute inflammation in the rabbit eye (right) 30 min after carrageenan injection; (D) Inflammation of the eye (right) significantly reduced after application of film formulation (BHT_bC_2) (E) Rabbit normal eye (left) without carrageenan injection and without application of film; (F) Acute inflammation in the rabbit eye (right) after 3 h of carrageenan injection without film application.

4. Conclusions

Hydrogel forming film formulation has been prepared with cyclodextrin complexation of budesonide containing quaternary surfactant and *in vitro-in vivo* assessment of mucosal drug delivery was carried out. Inclusion agents in the film increased the drug release and swelling rate. The erosion rate of the hydrogel film has been decreased in presence of inclusion agent. Enhanced mucosal permeation was also observed due to the increased release of drug on the mucosal surface and the surfactant property of the quaternary compounds which facilitated better permeation probably via paracellular route compared to others. A majorly diffusion-controlled mechanism was observed in the process of drug release and mucosal transport with minimal erosion. Budesonide hydrogel has finally shown ocular anti-inflammatory activity after topical application in vivo. Inflammatory conditions have believably been encountered after reaching of budesonide to the target site bypassing the first-pass metabolism and could be the cause of improved bioavailability.

Acknowledgement. The authors are thankful to Prof. Manoj Ranjan Nayak, President of Siksha 'O' Anusandhan (Deemed to be University) for providing the facilities required for successful completion of the work.

References

1.VARSHOSAZ, J., EMAMI, J., AHMADI, F., TAVAKOLI, N., MINAIYAN, M., FASSIHI, A., MAHZOUNI, P., DORKOOSH, F., Preparation of budesonide–dextran conjugates using glutarate spacer as a colon-targeted drug delivery system: in vitro/in vivo evaluation in induced ulcerative colitis. J Drug Target. 19(2), 2011, p. 140-53.
2.SZEFLER, S.J., Pharmacodynamics and pharmacokinetics of budesonide: a new nebulized corticosteroid. J. Allergy Clin. Immunol., 104(4), 1999, p. S175-83.
3.BEGAT, P., MORTON, D.A., STANIFORTH, J.N., PRICE, R., The cohesive-adhesive balances in dry powder inhaler formulations II: influence on fine particle delivery characteristics. Pharm. Res., 21(10) 2004, p. 1826-33.
4.HASSAN, N., AHAD, A., ALI, M., ALI, J., Chemical permeation enhancers for transbuccal drug delivery. Expert Opin Drug Deliv., 7(1), 2010, p. 97–112.
5.SMART, J.D., Buccal drug delivery. Expert Opin. Drug Deliv., 2(3), 2005, p. 507-17
6.LAQUINTANA, V., ASIM, M.H., LOPEDOTA, A., CUTRIGNELLI, A., LOPALCO, A., FRANCO, M., BERNKOP-SCHNÜRCH, A., DENORA, N., Thiolated hydroxypropyl-β-cyclodextrin as mucoadhesive excipient for oral delivery of budesonide in liquid paediatric formulation. Int J Pharm., 572, 2019, p. 118820.
7.NAKAMURA, K., MAITANI, Y., LOWMAN, A.M., TAKAYAMA, K., PEPPAS, N.A., NAGAI, T., Uptake and release of budesonide from mucoadhesive, pH-sensitive copolymers and their application to nasal delivery. J. Control. Release., 61(3), 1999, p. 329-35.
8.MUT, A.M., VLAIA, L., CONEAC, G., OLARIU, I.O., VLAIA, V.I., POPOIU, C.Ă., HÎRJĂU, M.I., LUPULIASA, D.U., Novel Topical Chitosan/Hydroxypropyl methylcellulose—Based Hydrogels Containing Fluconazole and Sucrose Esters. Formulation, Physicochemical Characterization. In vitro Drug Release and Permeation. Farmacia., 66, 2018, p. 59-69.
9.PANAINTE, A.D., POPA, G., PAMFIL, D., BUTNARU, E., VASILE, C., TARȚĂU, L.M., GAFIȚANU, C., In vitro characterization of polyvinyl alcohol/chitosan hydrogels as modified release systems for bisoprolol. Farmacia. 66(1), 2018, p. 144-8.
10.ESIM, O., SAVASER, A., OZKAN, C.K., BAYRAK, Z., TAS, C., OZKAN, Y., Effect of polymer type on characteristics of buccal tablets using factorial design. Saudi Pharm. J., 26(1), 2018, p. 53-63.
11.AL-DHUBIAB, B.E., NAIR, AB, KUMRIA, R, ATTIMARAD, M, HARSHA, S. Development and evaluation of nebivolol hydrochloride nanocrystals impregnated buccal film. Farmacia., 67, 2017, p. 282-289.
12.SALAMAT-MILLER, N., CHITTCHANG, M., JOHNSTON, T.P., The use of mucoadhesive polymers in buccal drug delivery. Adv. Drug Deliv. Rev., 57(11), 2005, p. 1666-91.
13.GAIKWAD, N.M., SHAIKH, K.S., CHAUDHARI, P.D., Development and Evaluation of a System for Colonic Delivery of Budesonide. Indian J Pharm Educ Res., 51(4), 2017, p. 551–61.
14.KUMAR, M., PATHAK, K., MISRA, A., Formulation and characterization of nanoemulsion-based drug delivery system of risperidone. Drug Dev Ind Pharm., 35(4), 2009, p. 387–95.
15.BANDI, N., WEI, W., ROBERTS, C.B., KOTRA, L.P., KOMPELLA, U.B., Preparation of budesonide and indomethacin hydroxypropyl-β-cyclodextrin (HPBCD) complexes using a single-step, organic-solvent-free supercritical fluid process. Eur. J. Pharm. Sci., 23(2), 2004, p. 159-68.
16.ANTAL, D.S., ARDELEAN, F., PINZARU, I., BORCAN, F., LEDEȚI, I., CORICOVAC, D., ZUPKÓ, I., BAGHDIKIAN, B., OLLIVIER, E., SOICA, C., BOLINITINEANU, S.L., Effects of cyclodextrin complexation on the anti-cancer effects of Cotinus coggygria extract and its constituents, butein and sulfuretin., *Rev. Chim.*, **67**(8), 2016, 1618-22.
17.MARIAN, E., JURCA, T., VICAȘ, L., KACSO, I., MICLĂUȘ, M., BRATU, I., Inclusion compounds of erythromycin with β-cyclodextrin., *Rev Chim.*, **62**(11), 2011, 1065-8.
18.POPA, G., DRAGOSTIN, O., BUZIA, O.D., TARTAU, L.M., PROFIRE, L., GAFITANU, C., Studies on Obtaining and Characterization a Pregabalin-cyclodextrin Complex for Taste Masking Purpose., *Rev Chim*., **68**, 2017, p. 337-80.

19.LU, Y., GUO, T., QI, J., ZHANG, J., WU, W., Enhanced dissolution and stability of lansoprazole by cyclodextrin inclusion complexation: Preparation, characterization, and molecular modeling. AAPS PharmSciTech., 13(4), 2012, p. 1222–9.
20.MODI, A., TAYADE, P., A comparative solubility enhancement profile of valdecoxib with different solubilization approaches. Indian J. of Pharm. Sci., 69(2), 2007, p. 274.
21.FIGUEIRAS, A., HOMBACH, J., VEIGA, F., BERNKOP-SCHNÜRCH, A., In vitro evaluation of natural and methylated cyclodextrins as buccal permeation enhancing system for omeprazole delivery. Eur J Pharm Biopharm., 71(2), 2009, p. 339–45
22.SASAKI, H., YAMAMURA, K., TEI, C., NISHIDA, K., NAKAMURA, J., Ocular permeability of FITC-dextran with absorption promoter for ocular delivery of peptide drug. J Drug Target., 3(2), 1995, p. 129-35.
23.JIN, L., BOYD, B.J., WHITE, P.J., PENNINGTON, M.W., NORTON. R.S., NICOLAZZO, J.A., Buccal mucosal delivery of a potent peptide leads to therapeutically-relevant plasma concentrations for the treatment of autoimmune diseases. J Control Release., 199, 2015, p. 37–44.
24.VALENTE, A.J.M., SÖDERMAN, O., The formation of host-guest complexes between surfactants and cyclodextrins. Adv Colloid Interface Sci., 205, 2014, p. 156–76
25.JIANG, B.Y., DU, J., CHENG, S.Q., PAN, J.W., ZENG, X.C., LIU, Y.J., SHUNZO, Y., YOSHIMI, S., Effects of cyclodextrins as additives on surfactant CMC. J Dispers Sci Technol., 24(1), 2003, p. 63–6.
26.ŞENEL, S., RATHBONE, M.J., CANSIZ, M., PATHER, I., Recent developments in buccal and sublingual delivery systems. Expert Opin. Drug Deliv., 9(6), 2012, p. 615-28.
27.GUSTAFSSON, B., MILLER-LARSSON, A., PERSSON, C.G., Topical and oral anti-inflammatory activity of budesonide compared with oral prednisolone in an animal model using allergen-induced gut mucosal exudation of plasma as a marker. Scand. J. Gastroenterol., 36(10), 2001, p. 1062-6.
28.MILLER-LARSSON, A., BRATTSAND, R., Topical anti-inflammatory activity of the glucocorticoid budesonide on airway mucosa. Evidence for a “hit and run” type of activity. Inflamm. Res., 29(1), 1990, p. 127-9.
29.MOHAPATRA, R., MALLICK, S., NANDA, A., SAHOO, R.N., PRAMANIK, A., BOSE, A., DAS, D., PATTNAIK, L., Analysis of steady state and non-steady state corneal permeation of diclofenac. RSC Adv., 6(38), 2016, p. 31976-87.
30.BHATT, H., NAIK, B., DHARAMSI, A., Solubility enhancement of budesonide and statistical optimization of coating variables for targeted drug delivery. J. Pharm., 2014, p. 1-13.
31.RAVAL, M.K., RAMANI, R.V., SHETH, N.R., Formulation and evaluation of sustained release enteric-coated pellets of budesonide for intestinal delivery. Int. J. Pharm Investigation., 3(4), 2013, p. 203-11.
32.NANDA, A., SAHOO, R.N., PRAMANIK, A., MOHAPATRA, R., PRADHAN, S.K., THIRUMURUGAN, A., DAS, D., MALLICK, S., Drug-in-mucoadhesive type film for ocular anti-inflammatory potential of amlodipine: effect of sulphobutyl-ether-beta-cyclodextrin on permeation and molecular docking characterization. Colloids Surf. B., 172, 2018, p. 555-64.
33.PANDA, B., SUBHADARSINI, R., MALLICK, S., Biointerfacial phenomena of amlodipine buccomucosal tablets of HPMC matrix system containing polyacrylate polymer/β-cyclodextrin: correlation of swelling and drug delivery performance. Expert Opin. Drug Deliv., 13(5), 2016, p. 633-43.
34.SUJJA-AREEVATH, J., MUNDAY, D.L., COX, P.J., KHAN, K.A., Relationship between swelling, erosion and drug release in hydrophillic natural gum mini-matrix formulations. Eur. J. Pharm. Sci., 6(3), 1998, p. 207-17.
35.PRAMANIK, A., SAHOO, R.N., NANDA, A., MOHAPATRA, R., SINGH, R., MALLICK, S., Ocular Permeation and Sustained Anti-inflammatory Activity of Dexamethasone from Kaolin Nanodispersion Hydrogel System. Curr. Eye Res., 43(6), 2018, p. 828-38.

36.ELKOMY, M.H., MENSHAWE, S.F., ABOU-TALEB, H.A., ELKARMALAWY, M.H., Loratadine bioavailability via buccal transferosomal gel: formulation, statistical optimization, in vitro/in vivo characterization, and pharmacokinetics in human volunteers. Drug Deliv., 24(1), 2017, p. 781-91.
37.SEMALTY, M., SEMALTY, A., KUMAR, G., Formulation and characterization of mucoadhesive buccal films of glipizide. Indian J. Pharm. Sci., 70(1), 2008, p. 43.
38.PANDA, B., PARIHAR, A.S., MALLICK, S., Effect of plasticizer on drug crystallinity of hydroxypropyl methylcellulose matrix film. International journal of biological macromolecules., 67, 2014, p. 295-302.
39.MOHAPATRA, R., SENAPATI, S., SAHOO C., MALLICK, S., Thermodynamic properties of ocular permeation of diclofenac: effect of triethanolamine. Farmacia., 64(1), 2016, p. 72-81.
40.FOLCH-CANO, C., YAZDANI-PEDRAM, M., OLEA-AZAR, C., Inclusion and functionalization of polymers with cyclodextrins: current applications and future prospects. Molecules., 19(9), 2014, p. 14066-79.
41.POSE-VILARNOVO, B., RODRÍGUEZ-TENREIRO, C., DOS SANTOS, J.F., VÁZQUEZ-DOVAL, J., CONCHEIRO, A., ALVAREZ-LORENZO, C., TORRES-LABANDEIRA, J.J., Modulating drug release with cyclodextrins in hydroxypropyl methylcellulose gels and tablets. J control release., 94(2-3), 2004, p. 351-63.
42.MALI, A.J., PAWAR, A.P., PUROHIT, R.N., Development of budesonide loaded biopolymer based dry powder inhaler: optimization, in vitro deposition, and cytotoxicity study. J. pharm., 2014, http://dx.doi.org/10.1155/2014/795371
43.CORTESI, R., RAVANI, L., MENEGATTI, E., ESPOSITO, E., RONCONI, F., Eudragit® microparticles for the release of budesonide: a comparative study. Indian J. pharm. sci., 74(5), 2012, p. 415-21.
44.VOZONE, C.M., MARQUES H.M., Complexation of budesonide in cyclodextrins and particle aerodynamic characterization of the complex solid form for dry powder inhalation. . J. Incl. Phenom. Macrocycl. Chem., 44(1-4), 2002, p. 111-6.
45.CARR, A.G., MAMMUCARI, R., FOSTER, N.R., Particle formation of budesonide from alcohol-modified subcritical water solutions. International journal of pharmaceutics., 405(1-2), 2011, p. 169-80.
46.LEUNER, C., DRESSMAN, J., Improving drug solubility for oral delivery using solid dispersions. Eur. J. Pharm. Biopharm., 50(1), 2000, p. 47-60.
47.PHAM, S., WIEDMANN, T.S., Note: Dissolution of aerosol particles of budesonide in Survanta™, a model lung surfactant. Journal of pharmaceutical sciences., 90(1), 2001, p. 98-104.
48.AKKARI, A.C., CAMPOS, E.V., KEPPLER, A.F., FRACETO, L.F., DE, PAULA, E., TOFOLI, G.R., DE ARAUJO D.R., Budesonide-hydroxypropyl-β-cyclodextrin inclusion complex in binary poloxamer 407/403 system for ulcerative colitis treatment: A physico-chemical study from micelles to hydrogels. Colloids and Surfaces B: Biointerfaces., 138, 2016, p. 138-47.
49.MOHAPATRA, R., SENAPATI, S., SAHOO, C., MALLICK, S., Transcorneal permeation of diclofenac as a function of temperature from film formulation in presence of triethanolamine and benzalkonium chloride. Colloids Surf. B., 123, 2014, p. 170-80.
50.RITGER, P.L., PEPPAS, N.A., A simple equation for description of solute release II. Fickian and anomalous release from swellable devices. J. Control. Release., 5(1), 1987, p. 37-42.
51.PATTNAIK, S., SWAIN, K., MALLICK, S., Influence of polymeric system and loading dose on drug release from alfuzosin hydrochloride transdermal films. Lat. Am. J. Pharm., 28(1), 2009, p. 62-9.
52.EL AFIF, A., GRMELA, M., Non-Fickian mass transport in polymers. J. Rheol., 46(3), 2002, p. 591-628.
53.UBAID, M., ILYAS, S., MIR, S., KHAN, A.K., RASHID, R., KHAN, M.Z., KANWAL, Z.G., NAWAZ, A., SHAH, A., MURTAZA, G., Formulation and in vitro evaluation of carbopol 934-based modified clotrimazole gel for topical application. An. Acad. Bras. Cienc., 88(4), 2016, p. 2303-17.

54.SWAIN, K., PATTNAIK, S., SAHU, S.C., MALLICK, S., Feasibility assessment of ondansetron hydrochloride transdermal systems: physicochemical characterization and in vitro permeation studies. Lat Am J Pharm., 28(5), 2009, p. 706-14.
55.FEHRENBACHER, J.C., VASKO, M.R., DUARTE, D.B., Models of inflammation: carrageenan or complete freund's adjuvant (CFA) induced edema and hypersensitivity in the rat. Curr Protoc Pharmacol., 56(1), 2012, p. 5.4.1-5.4.7.
56.LIN, N., POPOVICH, T., THOMPSON, H., PALACIOSPELAEZ, R., BAZAN, N.G., Prolonged anti-inflammatory effect of Budesonide Epimer R in experimental uveitis. Invest Ophth Vis Sci., 37(3), 1996, p. 180

Manuscript received: 5.03.2020

Scientific paper

Characterization of Hydration Behaviour and Modeling of Film Formulation

Arunima Pramanik,[1] Rudra Narayan Sahoo,[1,2] Souvik Nandi,[1] Ashirbad Nanda[1] and Subrata Mallick[1,*]

[1] *Department of Pharmaceutics, School of Pharmaceutical Sciences, Siksha 'O' Anusandhan (Deemed to be University), Bhubaneswar 751003, Odisha, India.*

[2] *Centurion University of Technology and Management, Odisha, India.*

* *Corresponding author: E-mail: profsmallick@gmail.com (Telephone: +91-674-2386209; fax: +91-674 2386271*

Received: 07-26-2020

Abstract

Hydration behavior of hydrogel-based polymeric film possesses great importance in mucosal drug delivery. Modified Lag phase sigmoid model was used for the investigation of hydration of the film. Kaolin incorporated HPMC K100LVCR (H_L) and K100M (H_H) films containing dexamethasone as a model drug have been prepared for studying swelling kinetics. Swelling of H_L and H_H films was decreased with the gradual increase of kaolin content and H_H of higher viscosity has shown higher value than H_L matrix. Kaolin also inhibited the film erosion process. Mathematically modified lag phase sigmoid model demonstrated similarity of the predicted swelling content with the observed value. High R^2 and small RMSE value confirmed the successful fitting of the modified lag phase sigmoid model to the experimental data of swelling content. τ value similar to the observed one was obtained. This modified model could be reliable enough for estimating hydration process in food grains, food packaging films etc.

Keywords: Hydration phenomenon; water diffusion; swelling kinetic model; modified lag phase.

1. Introduction

Swelling behavior of polymer films possesses a significant importance in hydrogel-based transmucosal drug delivery systems and diverse application in biomolecular electronics and sensors, wound dressings, adsorption of chemical materials and contact lenses.[1,2] Matrix film of hydrophilic polymer is susceptible to environmental moisture and water due to the presence of hydrophilic groups in the macromolecule chains.[3] Swelling of polymer network is affected by the cross-linking degree of polymer, solvent-polymer compatibility and polymer nature.[4] In the process of swelling, the solvent molecules get in contact with the polymer and diffuse into the polymer materials. Diffusion of solvent molecules into the polymer network, expansion of network, and relaxation of polymer chain are the three steps of dynamic hydration process. [5] Thus swelling is responsible for the polymer chain relaxation and facilitates the patterned release of drug. Swelling develops bioadhesion through the intimate contact between polymer and mucosal tissue due to the entanglement of polymer and mucin chains of mucosal membrane lining.[6] For transmucosal drug delivery amlodipine, budesonide, diclofenac film formulations were developed in our laboratory wherein dynamic hydration process has been described.[6–8] The mucoadhesion between the mucus layer and the natural and synthetic polymers covered the mucosal epithelial surface. Further, the controlled drug release is affected by the interaction capability of polymer with mucus layer.[9] Swelling gets much attention as an important mechanism of controlled drug delivery system.[10,11] For hydrogel film, the dynamic process of solvent penetration can be interpreted from swelling. Based on this knowledge, the drug release pattern can be adjusted by modifying the swelling of polymer matrix.[5]

The incorporation of clay minerals into the polymer matrix reduces the strain of polymer matrix due to their intercalation properties[12] and increments significant property.[13] Silicate clay, such as montmorrilonite, has been characterized for the improvement of the biodegradability and mechanical properties of polymeric film.[14,15] Kaolin, a

phyllosilicate (1:1) crystalline clay has the cation exchange capacity.[16] It consists of a tetrahedral silica sheet and an alumina octahedral sheet, and the layers are bonded together with hydrogen bonds.[17] Incorporation of kaolin in drug delivery design is promoted due to its characteristic features such as chemical inertness, rheological properties, high specific area, swelling capacity and sorption capacity. The effect of kaolin incorporation in the film on the quality and functionality of swelling of film could be investigated by applying the mathematical model. This type of utilization of mathematical models is almost unavailable in the literature. The water diffusion and swelling behaviour of the polymeric film was previously studied by several researchers.[18–21] In literature, the kinetic model for absorbent gels swelling was constructed by Tanaka and Filmore.[22] After that, Li and Tanaka[23] included some new approaches regarding swelling of gel and that was implemented by Chi Wu and Chui-Ying Yan[24] for the gelatin of film swelling. Hans Schott described the swelling kinetics of gelatin film using second order kinetics.[25] Peleg model has been utilized to describe the swelling kinetics of acrylamide-sodium acrylate hydrogel[26] and water sorption process of food packaging films as well.[27] The cellulose polymer contains hydroxyl group and it is used in different fields due to their hydrophilic and hygroscopic nature.[28] Hydroxypropyl methylcellulose (HPMC) contains many hydroxyl groups and is widely used in pharmaceutical industry and other fields.[29] Kinetics of food grain hydration process has already been studied by several researchers earlier using lag phase sigmoid model and other kinetic models.[30–32] In this study, lag phase sigmoid model and also the modified version of this model has been applied to investigate the swelling of the films. In our knowledge, no such modification of model was used to describe the swelling kinetics of any polymeric film. Mathematical modification of lag phase sigmoid model has been described as:

$$S_t = \frac{S_E}{1+\exp(-k(t-\tau))} \qquad (1)\text{(Lag phase model)}$$

Modification:

$$\frac{S_E}{S_t} = 1 + \exp(-k(t-\tau)$$

$$\frac{S_E}{S_t} - 1 = \exp(-k(t-\tau)$$

$$Ln\left(\frac{S_E - S_t}{S_t}\right) = k\tau - kt \qquad (2)$$

S_E is the equilibrium swelling, k (min^{-1}) is the swelling rate constant and τ is the time to obtain half of the swelling sat-ration (i. e. $S_t = S_E/2$ at $t = \tau$). The swelling rate constant (k) can be determined from the slope of $Ln\left(\frac{S_E - S_t}{S_t}\right)$ vs. t linear plot.

2. Experimental

2.1. Materials

Dexamethasone (DXM) was received as gift sample (Sigma Company). Kaolin, HPMC K100LVCR (H_L) and HPMC K100M (H_H), triethanolamine were purchased from Qualikems, Burgoyne, Burbidges & co., Merck specialities Pvt Ltd (Mumbai) respectively. Ethanol was bought from MERCK (Germany).

2. 2. Preparation of Hydrogel Film

The polymers (H_L and H_H) were swelled in distilled water overnight and stirred continuously for 24 hours at room temperature to prepare homogenous polymeric dispersion. Simultaneously, kaolin clay dispersion (10 wt. %) was prepared separately without any treatment by dispersing kaolin clay in distilled water and stirring for 24 h. This dispersion was centrifuged at 2500 rpm for 15 min and the thin nano-dispersion layer from the upper part was separated for film formulation. It was established that this process of dispersion in distilled water may be capable of reducing the average particle size to nano size clay particle.[33] Kaolin dispersion in different amount (25, 50, 75 or 100 mg content) was gradually added into the H_L or H_H polymer dispersion (800 mg) and stirred continuously for 1 h with a magnetic stirrer. Dexamethasone (model drug, 100 mg) and triethanolamine (15 % of polymer as plasticizer) were dissolved in 5 ml of ethanol and incorporated in each polymeric kaolin dispersion with continuous stirring for 3 h. According to solvent casting and solvent evaporation method, final dispersion into the petri dish was spread and dried in an incubator for 24 h at 60 °C until constant weight. The prepared films were subjected to the following characterizations. At least three repetitions of the following experiments were done and mean ± SD values were calculated.

2. 3. Water Sorption Studies

Films were accurately weighed (W_1) at room temperature (30 °C) and placed in desiccators containing activated silica gel. After 24 h films were discarded from desiccators and weighed (W_2) until constant weight achieved. Water content was estimated from the difference between initial and final weight with respect to final weight (W_2). For water sorption analysis each film was weighed (W_1) after removal from desiccators over silica gel and placed in the desiccators to maintain 65, 75, and 84 % relative humidity with 100 ml super saturated solution of sodium nitrite, sodium chloride and potassium chloride, respectively. After about 24 h or more films were weighed (W_2) till three resulted weights of each film were same. Moisture uptake was determined from the difference between final and initial weight with respect to initial weight (W_1) and expressed as percentage.

2. 4. FTIR Spectroscopy

The possible interaction between the components was interpreted from FTIR analysis. The FTIR characterization of pure drug and the film formulations (DH_HK_0, DH_HK_1, DH_HK_2, DH_HK_3, and DH_HK_4) was performed using JASCO FT/IR-4100 spectra. To prepare sample pellets, KBr pressed-disk method was used (ratio of sample to KBr is 1:20) and then sample pellet was placed in FTIR spectrometer. FTIR spectra were obtained in the range of 400–4000 cm^{-1} and at a resolution of 4 cm^{-1} as transmission mode by accumulating 80 scans.

2. 5. Scanning Electron Microscopy (SEM)

SEM images were utilized to visualize the morphology of pure drug, kaolin and film formulations (DH_LK_4, and DH_HK_4) of highest kaolin content. Samples were gold sputter-coated under argon atmosphere and placed in JEOL/EO $ CM_VERSION 1.0 Scanning Electron Microscope model no (JSM-6390) (operating at 5 kV) for imaging.

2. 6. Hydration and Swelling Studies

Films were cut into small pieces and weighed (W_0). Then the small pieces of film were immersed into each petri plate containing 25 ml of pH 7.4 phosphate buffer saline at room temperature. After predetermined time interval samples were taken out from the petri plate and excess buffer was soaked in filter paper. Then the final weight (W_t) was recorded and this process was continued up to 6 h. Swelling content was calculated by using the following equation,[34]

$$S = \frac{W_t - W_0}{W_0} \tag{3}$$

S is the swelling content (g water/ g dry film), W_t is the weight of film after time t, and W_0 is the weight of dry film.

Erosion of film can also be analyzed from swelling studies. After 6 h of swelling study, films were dried at 40 °C in hot air oven. Films were removed from the oven after 24 h and reweighed (W_e) and erosion (E) was calculated as follow,

$$E = \frac{W_0 - W_e}{W_0} \tag{4}$$

W_e is the weight of the eroded film after drying in oven.

Swelling of polymer involved diffusion of water and necessitated the understanding of mechanism of solvent diffusion. The swelling kinetics and diffusion of polymer structure can be explained by basic law of Peppas law.[24]

$$F = \frac{S_t}{S_{max}} = Kt^n \tag{5}$$

where, F is the fraction of swelling content, S_{max} i the maximum swelling content of the formulation, S_t the swelling content of the formulation at any time, K the gel network structure constant, and n the diffusion exponential of solvent. The 'n' value of Peppas equation was utilized to determine the diffusion type. Coefficient of diffusion, an important parameter, was also evaluated from the swelling kinetics. It can be calculated for the square shape film from the following equation which was derived by re-arranging the Fick's II law.

$$D = a^2\left(\frac{K}{4}\right)^{1/n} \tag{6}$$

where D is the diffusion coefficient expressed in cm^2s^{-1}, and "a" is the side of square film in cm.

In order to determine the swelling kinetics of films, lag phase sigmoid model was exploited in this study. The lag phase sigmoid equation has been modified to generalize the swelling kinetics study and also to compare it with the original lag phase sigmoid model.

Kaptso et al also proposed a sigmoid model and described the swelling of film.[36] The equation of this sigmoid model, comprised of an exponential rate of decay term, is accounted for an initial lag phase. The model is expressed as the following equation

$$S_t = \frac{S_E}{1 + \exp(-k(t - \tau))} \tag{7}$$

S_E is the equilibrium swelling, k (min^{-1}) is the swelling rate constant and τ is the time to obtain half of the swelling saturation (i. e. $S_t = S_E/2$ at $t = \tau$).

2. 7. Statistical Analysis

The model was statistically fitted with the experimental data and analyzed in Origin Pro 8.0 (OriginLab, Northampton, MA) software[37] by the nonlinear regression analysis. Model fitness to the experimental data has been assessed using R^2, χ^2, and root mean square error (RMSE) of statistical analysis data. χ^2 and RMSE can be calculated as

$$\chi^2 = \frac{\sum_{i=1}^{N}(S_{exp,i} - S_{pre,i})^2}{N - z} \tag{8}$$

$$RMSE = \left[\frac{1}{N}\sum_{i=1}^{N}\left(SR_{pre,i} - SR_{exp,i}\right)^2\right]^{1/2} \tag{9}$$

3. Results and Discussion

3. 1. Water Sorption Properties

The moisture content and moisture uptake of DXM film composed of HPMC and kaolin were measured at

Table 1. Water sorption properties of the film formulations.

Formulation	DXM : kaolin	% Water uptake at RH (mean ± SD, n = 3) 65 %	75 %	85 %	Water content (%) (mean ± SD, n=3)
DH_LK_0	–	4.50 ± 0.02	12.61 ± 0.03	21.62 ± 0.03	2.80 ± 0.01
DH_LK_1	1 : 0.25	4.31 ± 0.03	12.06 ± 0.03	19.82 ± 0.03	2.58 ± 0.01
DH_LK_2	1 : 0.5	3.81 ± 0.02	11.45 ± 0.03	19.08 ± 0.02	2.34 ± 0.01
DH_LK_3	1 : 0.75	3.42 ± 0.02	10.28 ± 0.03	17.00 ± 0.03	2.06 ± 0.01
DH_LK_4	1 : 1	3.40 ± 0.03	10.20 ± 0.04	16.57 ± 0.03	1.14 ± 0.02
DH_HK_0	–	6.76 ± 0.04	14.28 ± 0.08	24.81 ± 0.11	3.87 ± 0.02
DH_HK_1	1 : 0.25	5.81 ± 0.05	13.95 ± 0.09	22.09 ± 0.10	3.52 ± 0.02
DH_HK_2	1 : 0.5	5.22 ± 0.05	13.43 ± 0.08	19.40 ± 0.10	3.22 ± 0.01
DH_HK_3	1 : 0.75	4.65 ± 0.05	12.79 ± 0.06	19.76 ± 0.06	2.68 ± 0.02
DH_HK_4	1 : 1	4.57 ± 0.06	11.76 ± 0.07	18.30 ± 0.03	2.40 ± 0.02

25 °C, and at 65, 75, and 85 % relative humidity. Table 1 displays the gradual depletion of both water content and water uptake while kaolin content increases in the film. It is also seen that moisture uptake of all respective formulations is progressively increasing with increasing RH from 65 to 85 %. The highest kaolin content in the film resulted in the decreased percent moisture uptake from 4.50 ± 0.02 to 3.40 ± 0.03 and 6.76 ± 0.04 to 4.57 ± 0.06 at 65 % RH for H_L and H_H matrices respectively in comparison with the absence of kaolin film. Percent moisture content of film has also been reduced from 2.80 ± 0.004 to 1.14 ± 0.02 and from 3.87 ± 0.02 to 2.40 ± 0.02 for H_L and H_H matrices respectively in the presence of kaolin (1:1) compared to the kaolin free films. The observed result indicated that the water resistance of both the matrix formulations was increased when kaolin was present in the film. In presence of triethanolamine as plasticizer, fine kaolin particles in the HPMC matrix enhanced the HPMC-kaolin interactions and left less free hydroxyl groups available for water binding. Thus, increased kaolin content gradually enhanced the barrier effect for the water uptake.[38,39]

3. 2. FTIR

The analysis of the chemical constituent of pharmaceutical solids has been carried out by the FTIR spectroscopy. The drug-excipient interaction nature was also confirmed from the changes in the IR spectra. The changes in drug-excipient interactions are displayed as the disappearance of existing bands and appearance of new bands in the IR spectra, and also as intensity alteration and absorption band broadening. Figure 1 shows the IR spectra of kaolin, pure DXM and formulations. The characteristic absorption peaks of DXM in IR spectra that appear at 3000–2800 cm^{-1}, 885 cm^{-1}, 1718 cm^{-1}, 1665 cm^{-1} and 1621 cm^{-1}, are assigned to CH_2 group, axial deformation of C-F group,

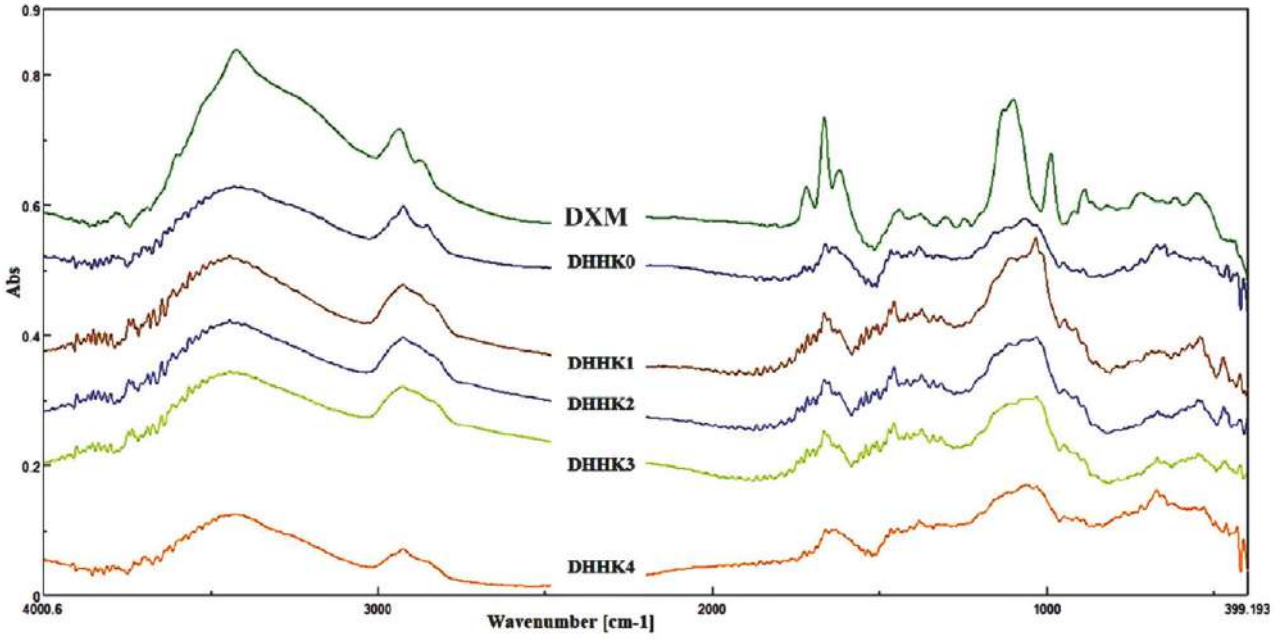

Figure 1. FTIR spectra of pure DXM and of the prepared film formulations (DH_HK_0, DH_HK_1, DH_HK_2, DH_HK_3, and DH_HK_4).

carbonyl group (C=O) of aliphatic ester and ketone,[40] and C=C group, respectively.[41] IR spectrum of pure kaolin demonstrated absorption peak at 1032 cm^{-1} with high intensity due to Si-O stretching in kaolin.[42] Kaolin contains hydroxyl groups at different position, i.e. outer hydroxyl groups (OuOH, positioned in the upper unshared plan) and inner hydroxyl groups (InOH, positioned in the lower unshared plan of octahedral sheet). Kaolin spectra showed peaks at 3693, 3669, 3649 cm^{-1} and at 3619 cm^{-1} due to the stretching of OuOH and stretching of InOH in Al-OH.[43] The broadening of absorption band at 3000–2800 cm^{-1} appeared due to the presence of polymer in the film. The successful incorporation of DXM in films has been confirmed by the presence of the main characteristic absorption peak

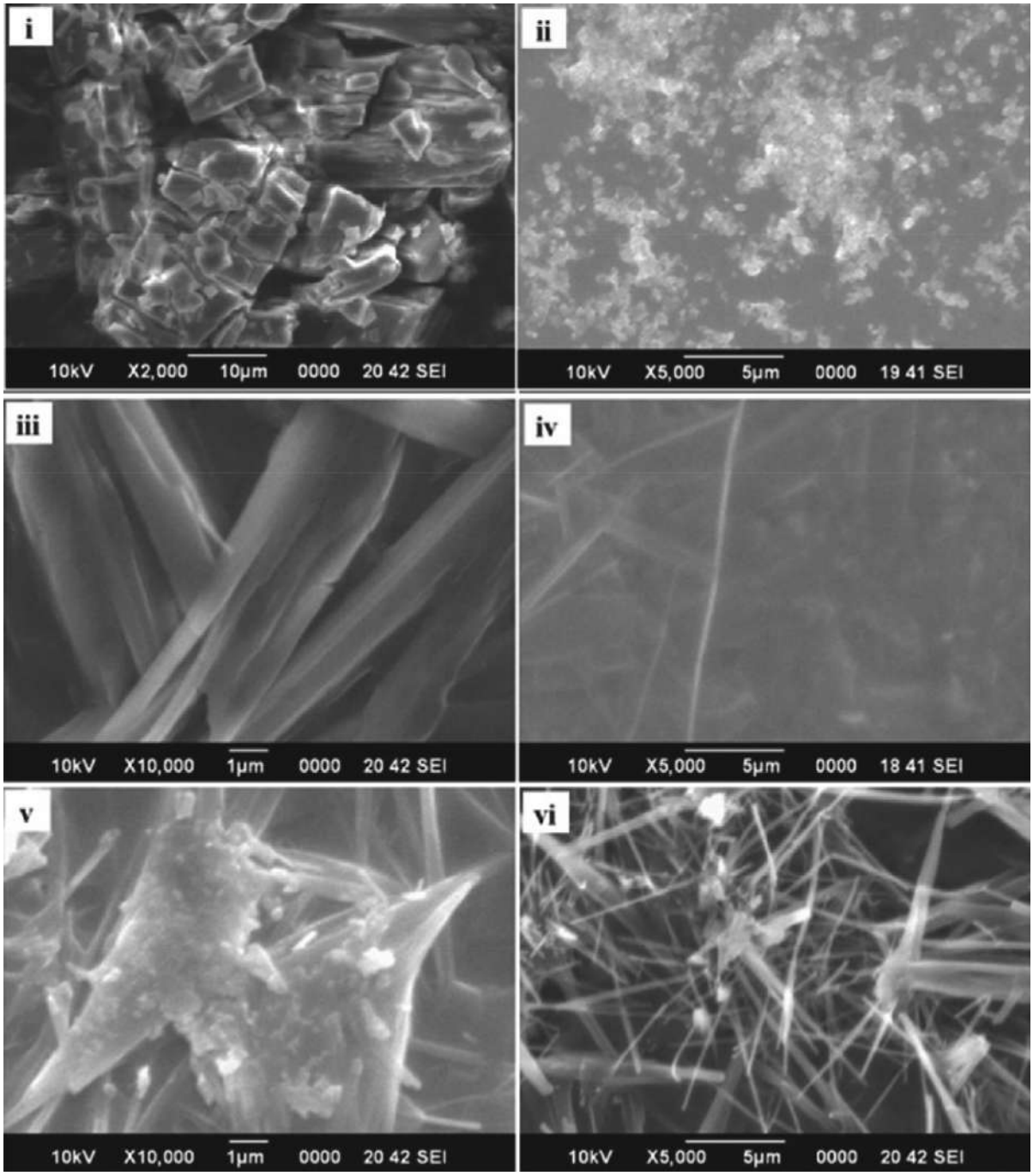

Figure 2. Scanning electron micrograph of pure DXM (magnification 2,000) (i); kaolin (magnification 5,000) (ii); films with kaolin (magnification 10,000) (iii), (magnification 5,000) (iv) of HPMC K100 LVCR; and films with kaolin (magnification 10,000) (v), (magnification 5,000) (vi) of HPMC K100 M matrices.

at 1665 cm^{-1}. This result suggested that the chemical properties of DXM have remained the same in the films. Interaction between DXM and kaolin in the film formulations has been confirmed by the shifting of the peak at 1032 cm^{-1}. The formation of hydrogen bond can be concluded as a result of this band shifting. The broadening of the characteristic peak at 1032 cm^{-1} was observed in the wide range in IR spectra of films containing higher kaolin content. This result indicates stronger binding between DXM and kaolin with the corresponding increase of kaolin content in the films.

3. 3. Scanning Electron Microscopy

The surface morphology of pure DXM, kaolin, and films of both HPMC K100 LVCR and HPMC K100 M matrices is demonstrated in Figure 2 by the scanning electron micrographs. The SEM images of Figure 2(i) demonstrate the geometric plate shaped microstructure of pure DXM and Figure 2(ii) that of nanosized kaolin. Figure 2(iii & iv) and (v & vi) represent the SEM images of films with higher kaolin content of both H_L and H_H matrices, respectively. The SEM images of films with added kaolin demonstrate the distinct distribution of nano-sized kaolin particles in the film. It can also be observed that the crystalline shape of DXM has almost disappeared in the films. In the presence of triethanolamine, the growth of drug crystal in HPMC film was not adequately noticed in the SEM micrographs due to the interfacial adhesion between the polymer phases and drug.[44] The crystal growth is also inhibited by HPMC in the matrix.[45]

3. 4. Hydration Behavior

The biological characteristic of hydrogel-based transmucosal drug delivery system significantly depended on the swelling of polymer present. Swelling capacity and swelling content of the film formulations were investigated in phosphate buffer saline (pH 7.4) at the laboratory ambient conditions. Swelling process included water uptake followed by the process of erosion of polymer matrix. The change of swelling content of film of both H_L and H_H matrix with varied kaolin content is depicted in Figure 3 and Figure 4 respectively. Graphs display that film of H_L and H_H matrices exhibited maximum swelling at 60 min and 6 h respectively. Decreased swelling content was observed while kaolin content increased in the film. The water resistance ability of kaolin resulted in sustaining swelling of polymer-based film matrix. Water resistance ability has been improved by increasing the kaolin content and gradually sustained the swelling of the film. Water uptake, the main basis for swelling, depends on the hydrophilicity and other parameter such as morphology (macro voids), free volume, and crystal size. Hence, swelling may also be dependent on these parameters. Kaolin produced a tortuous pathway and also formed a denser cross-linking network due to its certain level of hydrophilicity.[46,47] Thus kaolin had the capability of reducing the length of free pathway for water uptake into matrix, which led to sustained swelling of the film matrix.

In film formulations (H_L and H_H) swelling content was increased with the time of swelling. Higher swelling was found in the initial stage followed by a slower swelling at the later stages, known as hyperbolic form.[25] The form of difference in swelling content in the graphs (between H_L and H_H) is related probably to the polymer viscosity and molecular weight, because high molecular weight polymers exhibit high viscosity in the swelling stage.[48] The result of swelling content demonstrated higher value for the film of HPMC K100 M matrix compared with the film of HPMC K100LVCR matrix. This result suggests that the polymer viscosity and molecular weight play a role in the process of film swelling. The water uptake process did not easily empower through higher viscosity polymer of HPMC K100 M matrix. High molecular weight polymer increased the impact resistance due to higher degree of entanglement for rupturing more polymer bonds. In a fully hydrated state polymer chain disentanglement occured when there was no polymer-polymer interactions and higher viscosity induced greater chain entanglement than lower viscosity. Praveen et al.[49] also described in their report that the polymer chain disentanglement is affected by the polymer viscosity. Film of H_H matrix with maximum kaolin content showed higher swelling index, which suggests decreased movement of DXM molecules from the film matrix to the medium.

Erosion of film matrix is the process that follows after swelling and proceeds slowly. In this process, drug molecules diffuse through the micropores of polymer after

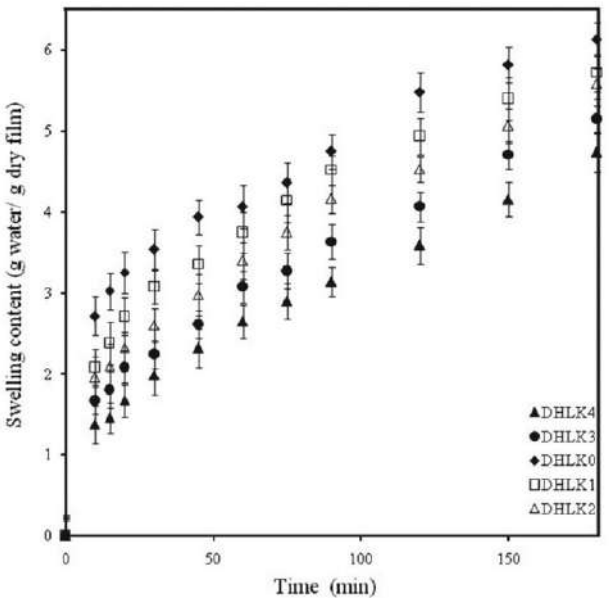

Figure 3. Swelling content of film of HPMC K100 LVCR (H_L) matrix with varied kaolin content.

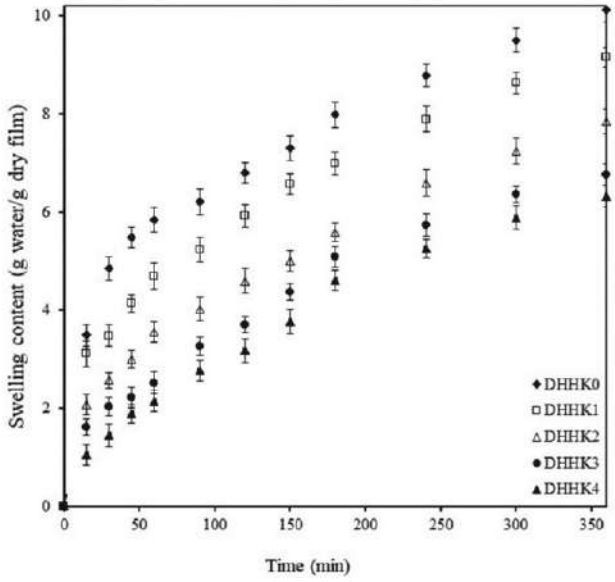

Figure 4. Swelling content of film of HPMC K100 M (H_H) matrix with varied kaolin content.

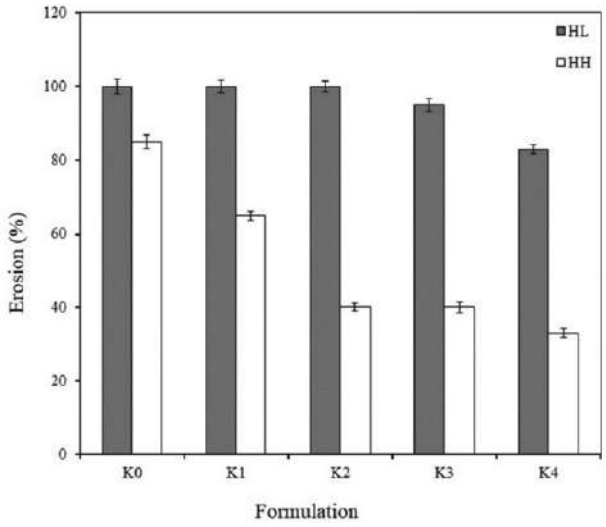

Figure 5. Erosion of film of HPMC K100 LVCR (H_L) and HPMC K100 M (H_H) matrix with varied kaolin content.

water uptake of the matrix.[6] After 6 h of the swelling study, erosion of films has been measured in pH 7.4 phosphate buffer saline. Figure 5 shows the progressive decrease in erosion with gradually increased kaolin content in the film. Presence of kaolin in the film hinders the process of erosion of film due to the entrapment of kaolin in the HPMC matrix networks. Higher kaolin content in the film has developed relatively stronger affinity between kaolin and polymer. Thus, the film with higher kaolin content shows more resistance for erosion. More resistance to the film erosion was also seen due to greater viscosity of H_H compared to H_L.

3. 5. Diffusion of Water

The predicted swelling value is similar with the experimental swelling value, when the swelling kinetics of films has been described by the Peppas model (RMSE = 0.016–0.02 for H_L matrix film and 0.016–0.02 for H_H matrix film). The diffusion exponential (n), k, R^2, reduced chi-square (χ^2) and RMSE values of all matrix films are demonstrated in Table 2. In order to investigate the water diffusion mechanism into hydrogel DXM film, Peppas equation was utilized. On the basis of the n value, the diffusion type of swelling was determined.[50] Fickian and non-Fickian diffusion are identified by the n values of 0.5 and 1.0, respectively. The ranges of swelling exponent values of films of H_L and H_H matrix are 0.28–0.43 and 0.31–0.59 respectively. According to the calculated n value, the diffusion mechanism of swelling of films of H_L and H_H matrix was Fickian and anomalous diffusion, respectively. Diffusion coefficient (D) is an important factor that describes how quickly water can diffuse through the polymeric matrix film. The results revealed that the D value increased with the increased kaolin content in the film

Table 2. Estimated swelling parameters of the film as per Peppas model and the diffusion coefficient of water.

Formulation	Parameter of Peppas model					
	k	n	R^2	χ^2	*RMSE*	D (cm^2s^{-1})
DH_LK_0	0.23	0.28	0.98	3.17E-04	0.016	$1.32*10^{-4}$
DH_LK_1	0.16	0.35	0.99	8.81E-05	0.008	$4.04*10^{-4}$
DH_LK_2	0.14	0.37	0.99	3.61E-04	0.017	$4.59*10^{-4}$
DH_LK_3	0.12	0.39	0.98	4.93E-04	0.020	$5.54*10^{-4}$
DH_LK_4	0.10	0.43	0.99	4.44E-04	0.019	$7.31*10^{-4}$
DH_HK_0	0.16	0.31	0.98	3.19E-04	0.016	$1.23*10^{-4}$
DH_HK_1	0.12	0.36	0.99	2.98E-04	0.016	$2.24*10^{-4}$
DH_HK_2	0.08	0.43	0.99	2.76E-04	0.015	$4.12*10^{-4}$
DH_HK_3	0.06	0.49	0.98	0.00101	0.029	$6.30*10^{-4}$
DH_HK_4	0.03	0.59	0.99	4.04E-04	0.018	$10.89*10^{-4}$

(Table 2). With the gradual increase in the kaolin content, water penetration becomes faster in both the polymers (H_L and H_H). The calculated diffusion coefficient increases from 1.32 *10^{-4} cm^2s^{-1} to 7.31 *10^{-4} cm^2s^{-1} for H_L matrix and 1.23 *10^{-4} to 10.89 *10^{-4} for H_H matrix.

3. 6. Evaluation of Lag Phase Model and Modified Lag Phase Model

The fitting of lag phase sigmoid model on the swelling data of film of both matrices (H_L and H_H) is shown in Figure 6 & Figure 7, respectively. The swelling data fitting with modified lag phase sigmoid model is depicted in Figure 8 & Figure 9 of H_L and H_H, respectively. The parameters (R^2, k, τ, $S_{obs.eq}$, RMSE, χ^2) of this model are presented in Table 3 for all films. These parameters describe the kinetics of all films with lower RMSE and χ^2 value and high correlation coefficient indicating appropriate fitting of model on swelling data. The time to obtain half of the swelling saturation (τ) is increased by higher kaolin content in the film. The predicted equilibrium swelling content and τ show higher value for H_H compared to H_L matrix film. Predicted equilibrium swelling content is similar to the experimentally obtained equilibrium moisture content. Modified lag phase sigmoid model demonstrates the increasing order of observed τ (17.6 to 105.7 and 38.4 to 283.1) and decreasing or almost similar order of k (20.3 to 12.4 and 9.4 to 6.3) with increased kaolin content in the film of both matrices (H_L and H_H matrix). Lag phase sigmoid model rate constant (k) decreases with increasing kaolin content in the film of both matrices supporting the effect of kaolin on prolonged swelling of the film. Kaptso et al [25] also described that the increased sigmoid model rate constant is due to increased mass transfer rate. However,

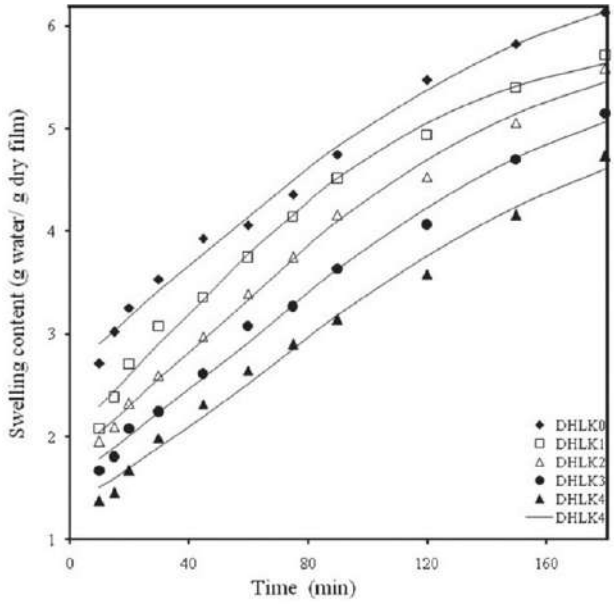

Figure 6. Fitting of the Lag phase sigmoid model of films of HPMC K100LVCR (H_L) matrix with varied kaolin content.

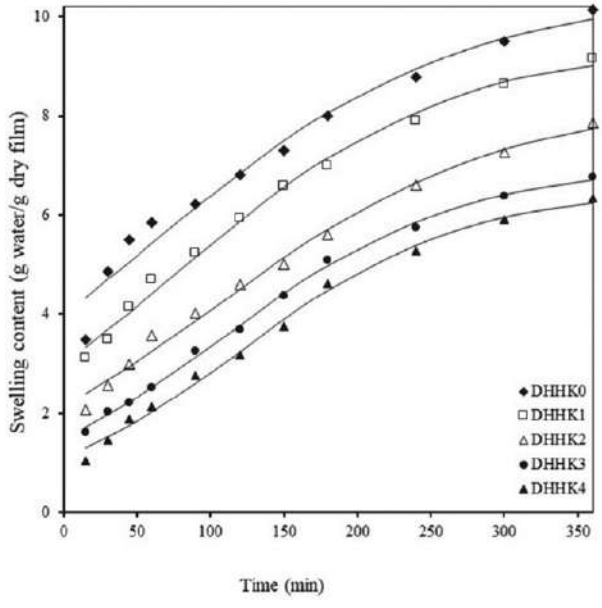

Figure 7. Fitting of the Lag phase sigmoid model of films of HPMC K100 M (H_H) matrix with varied kaolin swelling content.

Table 3. Estimated parameters of the modified Lag phase model.

Formulation	Parameter of the modified lag phase model						
	$S_{obs.eq}$	Obs τ (min)	Predicted τ (min)	$k \times 10^3$ (min^{-1})	R^2	RMSE	χ^2
DH_LK_0	6.32	17.6	24.3	20.3	0.951	0.174	0.03
DH_LK_1	6.38	37.2	41.6	16.1	0.984	0.138	0.01
DH_LK_2	6.70	55.2	64.3	14.1	0.996	0.119	0.01
DH_LK_3	6.75	80.6	84.5	13.0	0.999	0.121	0.01
DH_LK_4	6.77	105.7	107.1	12.4	0.998	0.145	0.01
DH_HK_0	10.62	38.4	57.7	9.4	0.964	0.338	0.03
DH_HK_1	11.02	103.6	115.4	7.1	0.994	0.290	0.02
DH_HK_2	11.14	173.3	196.2	6.5	0.999	0.321	0.02
DH_HK_3	11.33	219.7	253.1	6.3	0.995	0.412	0.04
DH_HK_4	11.70	283.1	287.3	6.9	0.989	0.485	0.06

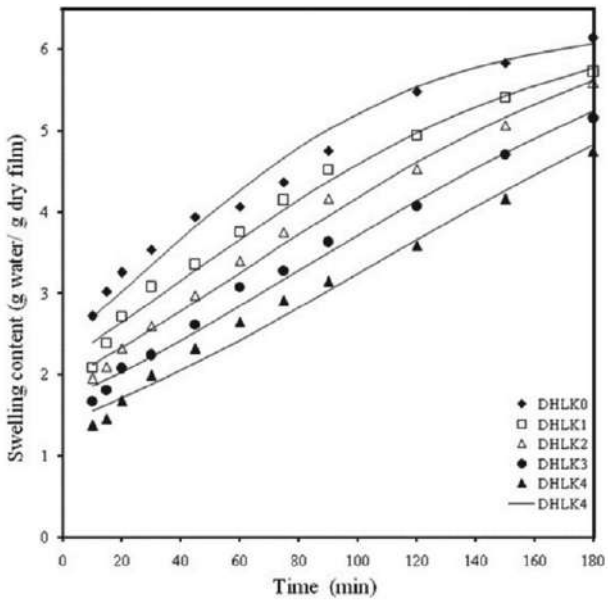

Figure 8. Fitting of the modified Lag phase sigmoid model of films of HPMC K100LVCR matrix with varied kaolin content.

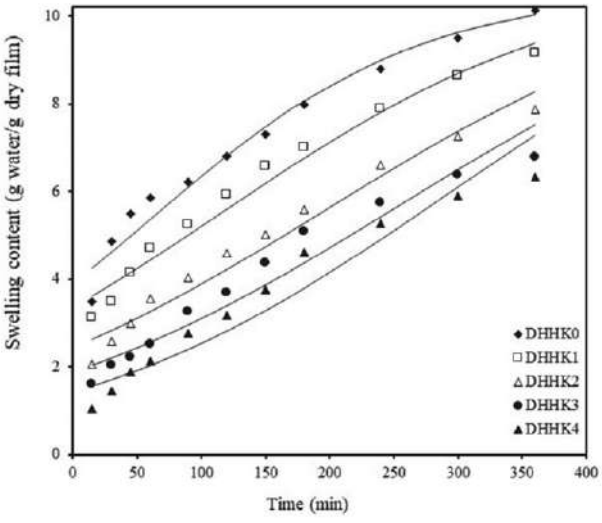

Figure 9. Fitting of the modified Lag phase sigmoid model of films of HPMC K100 M (H_H) matrix with varied kaolin swelling content.

the predicted value of τ increased from 24.26 to 107.10 and from 57.75 to 287.29 min for H_L and H_H, respectively. Correspondingly, *k* value decreased from 0.02 to 0.012 and from 0.009 to 0.006 min^{-1} for H_L and H_H, respectively. The fitting of this model is justified by the small RMSE and high R^2 value. Hence, the proposed modified Lag phase sigmoid model may be acceptable in the hydration study.

4. Conclusion

Kaolin incorporated HPMC films containing dexamethasone as a model drug have been prepared for characterization of hydration behaviour utilizing modified lag phase model. In this study, the effect of kaolin on swelling of H_L and H_H hydrogel films was investigated. Gradually decreased water content and water uptake were observed with increased kaolin content in the film. Distribution of nano-sized kaolin particles in the films was noticed in the SEM images. Swelling of both the matrices (H_L and H_H) has been decreased with increasing the kaolin content in the film, while H_H has shown higher value because of higher viscosity compared to the H_L matrix. Presence of kaolin in the film inhibited the erosion process of the film due to the entrapment of kaolin in the HPMC matrix networks. Greater viscosity of H_H also resulted in more resistance to the film erosion compared to H_L. Increasing diffusion coefficient value indicated that water penetration became faster in presence of kaolin in the film. The calculated value of diffusion coefficient increased with increasing kaolin content in both the matrices. Swelling kinetics of the films with varied kaolin content was investigated by the lag phase sigmoid mathematical model. The predicted swelling content value from the modified lag phase sigmoid model was similar to the observed value. This modified lag phase sigmoid model was successfully fitted to the experimental data, as confirmed by R^2 and lower RMSE value. The modified Lag phase sigmoid model resulted in τ values almost equal to the observed τ. Hence, we suggest that the modified version of the lag phase sigmoid model is also reliable enough to calculate kinetics in different food products.

Acknowledgements

We are very much grateful to the president, Siksha 'O' Anusandhan (Deemed to be University) Prof. (Dr) Manoj Ranjan Nayak for financial support and laboratory facility. Authors are also expressing our gratitude to the Pharmacia and Upjohn Company and Birla Institute of Technology, Mesra, Ranchi, for their gift sample and instrumental facility respectively.

5. References

1. A. S. Hoffman, *Adv. Drug Deliv. Rev.* **2002**, *54*, 3–12. **DOI:**10.1016/S0169-409X(01)00239-3
2. N. A. Peppas, K. B. Keys, M. Torres-Lugo, A. M. Lowman, *J. Control. Release.***1999**, *62*, 81–87. **DOI:**10.1016/S0168-3659(99)00027-9
3. K. Xu, J. Wang, Q. Chen, Y. Yue, W. Zhang, P. Wang, *J. Colloid Interf. Sci.* **2008**, *321*, 272–278. **DOI:**10.1016/j.jcis.2008.02.024
4. A. Martinez-Ruvalcaba, J. C. Sanchez-Diaz, F. Becerra, L. E. Cruz-Barba, A. Gonzalez-Alvarez, *Express Polym. Lett.* **2009**, *3*, 25–32. **DOI:**10.3144/expresspolymlett.2009.5
5. Y. Tang, J. R. Lu, A. L. Lewis, T. A.Vick, P. W. Stratford, *Macromolecules.* **2001**, *34*, 8768–8776. **DOI:**10.1021/ma010476i

6. B. Panda, R. Subhadarsini, S. Mallick, *Expert Opin. Drug* Del. **2016**, *13*, 633–643. **DOI:**10.1517/17425247.2016.1154038
7. S. Pattanaik, S. Nandi, R. N. Sahoo, A. Nanda, R. Swain, S. Das, S. Mallick, *Rev. Chim.* **2020**, *71*, 332–345. **DOI:**10.37358/RC.20.6.8200
8. R. Mohapatra, S. Senapati, C. Sahoo, S. Mallick, *Colloids Surf. B: Biointerfaces,* **2014**, *123*, 170–180. **DOI:**10.1016/j.colsurfb.2014.09.012
9. M. Birsan, I. C. Cojocaru, M. I. Stamate, V. Teodor, C. Tuchilus, *Rev. Chim.* **2016**, *67*, 1385–1388.
10. N. A. Peppas, A. R. Khare, *Adv. Drug Deliv. Rev.* **1993**, *11*, 1–35. **DOI:**10.1016/0169-409X(93)90025-Y
11. P. Colombo, *Adv. Drug Deliv. Rev*. **1993**, *11*, 37–57. **DOI:**10.1016/0169-409X(93)90026-Z
12. H. Hosseinzadeh, M. Sadeghi, *Asian J. Chem*. **2012**, *24*, 85–88.
13. M. Pannirselvam, A. Genovese, M. C. Jollands, S. N. Bhattacharya, R. A. Shanks, *Express Polym. Lett.* **2008**, *2*, 429–439. **DOI:**10.3144/expresspolymlett.2008.52
14. M. Alexandre, P. Dubois, *Mat. Sci. Eng.* R. **2000**, *28*, 1–63. **DOI:**10.1016/S0927-796X(00)00012-7
15. S. S. Ray, M. Bousmina, *Prog. Mater. Sci.* **2005**, *50*, 962–1079. **DOI:**10.1016/j.pmatsci.2005.05.002
16. M. I. Carretero, *App. Clay Sci*. **2002**, *21*, 155–163. **DOI:**10.1016/S0169-1317(01)00085-0
17. E. Cortes-Trivino, I. Martinez, *Express Polym. Lett.* **2018**, *12*, 616–627. **DOI:**10.3144/expresspolymlett.2018.52
18. W. Thakhiew, P. Waisayawan, S. Devahastin, *Dry. Technol.* **2011**, *29*, 1396–403. **DOI:**10.1080/07373937.2011.588816
19. D. Moreau, C. Chauvet, F. Etienne, F. P. Rannou, L. Corté, *Proc Natl Acad Sci.* **2016**, *113*, 13295–13300. **DOI:**10.1073/pnas.1609603113
20. M. Gagliardi, *Macromol Theor Simul.* **2019**, *28*, 1800063. **DOI:**10.1002/mats.201800063
21. H. R. Lee, Y. D. Lee, *Chem. Eng. Sci*. **1991**, *46*, 1771–1779. **DOI:**10.1016/0009-2509(91)87023-6
22. T. Tanaka, D. J. Filmore, *J. Chem. Phys*. **1979**, *70*, 1214–1218. **DOI:**10.1063/1.437602
23. Y. Li, T. Tanaka, *J. Chem. Phys.* **1990**, *92*, 1365–1371. **DOI:**10.1063/1.458148
24. C. Wu, C. Yan, *Macromol.* **1994**, *27*, 4516–4520. **DOI:**10.1021/ma00094a013
25. H. J. Schott, *Macromol. Sci.* B. **1992**, *31*, 1–9. **DOI:**10.1080/00222349208215453
26. A. S. Kipcak, O. Ismail, I. Doymaz, S. Piskin, *J. Chem.* **2014**, *2014*, 1–9. **DOI:**10.1155/2014/281063
27. S. H. Othman, N. R. A. Kechik, R. A. Shapi'i, R. A. Talib, I. S. M. A. Tawakkal, J Nanomater, vol. 2019, Article ID 3843949, 12 pages, 2019. **DOI:**10.1155/2019/3843949
28. Y. Cao, *Express Polym. Lett.* **2018**, *12*, 768–780. **DOI:**10.3144/expresspolymlett.2018.66
29. M. Grassi, G. Grassi, *Curr. Drug Deliv.* **2005**, *2*, 97–116. **DOI:**10.2174/1567201052772906
30. P. V. Pramiu, R. L. Rizzi, N. V. Do Prado, S. R. Coelho, P. Z. Bassinello, *J. Food Eng.* **2015**, *165*,112–23. **DOI:**10.1016/j.jfoodeng.2015.05.020
31. K. G. Kaptso, Y. N. Njintang, A. E. Komnek, J. Hounhouigan, J. Scher, C. M. F. Mbofung, *J. Food Eng*. **2008**, *86*, 91–99. **DOI:**10.1016/j.jfoodeng.2007.09.014
32. B. C. Marques, L. M. de Matos Jorge, R. M. Jorge, *J. Cereal Sci.* **2016**, *71*, 93–98. **DOI:**10.1016/j.jcs.2016.08.005
33. Lagaly, G., Olphen, H. Van, An Introduction to Clay Colloid Chemistry. Second ed. John Wiley and Sons, New York London, Sydney, Toronto (**1977**).
34. F. C. H. Pinto, A. Silva-Cunha, G. A. Pianetti, E. Ayres, R. L. Orefice, G. R. Da Silva, *J Nanomater*. **2011**, *2011*, Article ID 528628. **DOI:**10.1155/2011/528628
35. N. A. Peppas, P. Bures, W. Leobandung, H. Ichikawa, *Eur. J. Pharm. Biopharm*. **2000**, *50*, 27–46. **DOI:**10.1016/S0939-6411(00)00090-4
36. K. G. Kaptso, Y. N. Njintang, A. E. Komnek, J. Hounhouigan, J. Scher, C. M. F. Mbofung, *J. Food Eng*. 2008, **86**, 91–99. **DOI:**10.1016/j.jfoodeng.2007.09.014
37. http://www.originlab.com/OriginProLearning.aspx
38. S. Mallick, S. Pattnaik, K. Swain, P. K. De, A. Saha, G. Ghosal, A. Mondal, *Eur. J. Pharm. Biopharm*. **2008**, *68*, 346–351. **DOI:**10.1016/j.ejpb.2007.06.003
39. J. A. Mbey, S. Hoppe, F. Thomas, *Carbohyde. Polym.* **2012**, *88,* 213–222. **DOI:**10.1016/j.carbpol.2011.11.091
40. G. R. Silva, A. Silva-Cunha, F. Behar-Cohen, E. Ayres, R. L. Orefice, *Mater. Sci. Eng. C*. **2011**, *31*, 414–422. **DOI:**10.1016/j.msec.2010.10.019
41. M. M. Doile, A. K. Fortunato, I. C. Schhücker, S. K. Schucko, M. A. Silva, P. O. Rodrigues, *AAPS Pharm. Sci. Tech*. **2008**, *9*, 314–321. **DOI:**10.1208/s12249-008-9042-z
42. B. J. Saikia, G. J. Parthasarathy, *Mod. Phys*. **2010**, *1*, 206–210. **DOI:**10.4236/jmp.2010.14031
43. J. Kristo, R. L. Frost, A. Felinger, J. Mink, *J. Mol. Struct*. **1997**, *410–411*, 119–122. **DOI:**10.1016/S0022-2860(96)09488-4
44. F. S. Aleanizy, F. Alqahtani, A. O. Gohary, E. E. Tahir, R. A. Shalabi, *Saudi Pharm. J*. **2015**, *23*, 167–176. **DOI:**10.1016/j.jsps.2014.06.006
45. R. Mohapatra, S. Mallick, A. Nanda, R. N. Sahoo, A. Pramanik, A. Bose, D. Das, L. Pattnaik, *RSC Adv.* **2016**, *6*, 31976–31987. **DOI:**10.1039/C6RA03604J
46. A. Saada, B. Siffert, E. Papirer, *J Colloid Interf. Sci.***1995**, *174*, 185–190. **DOI:**10.1006/jcis.1995.1381
47. A.Ghebaur, S. A. Garea, S.Cecoltan, H. Iovu, *Mater. Plast*. **2017**, *54*, 8–13. **DOI:**10.37358/MP.17.1.4774
48. https://polymerdatabase.com/polymer%20physics/Solution_Viscosity.html
49. S. P. Hiremath, N. R. Saha, *AAPS Pharm. Sci. Tech*. **2008**, *9*, 1171–1178. **DOI:**10.1208/s12249-008-9159-0
50. N. A. Peppas, L. Brannon-Peppas, *J. Food Eng.***1994**, *22*, 189–210. **DOI:**10.1016/B978-1-85861-037-5.50015-1

Povzetek

Hidracijsko obnašanje polimernega filma na osnovi hidrogela ima velik pomen pri dostavi zdravil v sluznico. Za raziskovanje hidracije filma je bil uporabljen modificirani sigmoidni model na osnovi faznega zamika. Za preučevanje kinetike nabrekanja so bili pripravljeni filmi s kaolinom z vgrajenim HPMC K100LVCR (H_L) in K100M (H_H), ki so vsebovali deksametazon kot modelno zdravilo. Nabrekanje H_L in H_H filmov se je s postopnim povečevanjem vsebnosti kaolina zmanjšalo, H_H z višjo viskoznostjo pa je kazal večjo vrednost kot H_L. Kaolin je zaviral tudi postopek erozije filma. Spremenjen matematični sigmoidni model faznega zamika je pokazal podobnost med predvideno in opaženo vsebnostjo nabrekanja. Visoka vrednost R^2 in majhna vrednost RMSE sta potrdili uspešno prilagajanje modela eksperimentalnim podatkom za obseg nabrekanja. Tudi dobljena vrednost τ je bila podobna opaženi. Ta spremenjeni model bi lahko bil dovolj zanesljiv za oceno postopka hidracije v zrnih živil, filmih za pakiranje hrane itd.

Online version at http://www.minervamedica.it

Minerva Biotechnology and Biomolecular Research 2021 March;33(1):43-50
DOI: 10.23736/S2724-542X.20.02730-5

REVIEW

3D printing in managing supply disruptions related to COVID-19 pandemic: Food and Drug Administration's current thinking on regulation

Soumya R. SATAPATHY [1], Rudra N. SAHOO [1, 2], Souvik NANDI [1], Biswaranjan SATAPATHY [3], Lalatendu PANIGRAHI [4], Subrata MALLICK [1] *

[1]School of Pharmaceutical Sciences, Siksha 'O' Anusandhan (Deemed to be University), Bhubaneswar, India; [2]Centurion University of Technology and Management, Odisha, India; [3]Orbicular Pharmaceutical Technologies Pvt. Ltd, Hyderabad, India; [4]Encube Ethicals Pvt. Ltd, Mumbai, India

*Corresponding author: Subrata Mallick, School of Pharmaceutical Sciences, Siksha 'O' Anusandhan (Deemed to be University), Bhubaneswar, India. E-mail: profsmallick@gmail.com

ABSTRACT

Recent developments and collaborations of pharmaceutical manufacturers, hospitals, and government funded research bodies using 3D printing technology have been highlighted for the management of the healthcare crisis. 3D printing is a process of converting virtual 3D models developed by computer aided design into physical forms upon addition of material layer-by-layer (also known as additive manufacturing). This 3D printing is supposed to revolutionize significantly the healthcare system in the coming years. This process involves a tailored deposition of biomaterials layer by layer such as polylactic acid (PLA), polyvinyl alcohol (PVA), or other suitable pharma-grade polymers, copolymers, and their combinations to formulate three-dimensional custom designs with controlled architecture and composition. Food and Drug Administration (FDA) is currently thinking on regulation to ease the import restrictions for products intended for the detection and diagnosis of COVID-19 to ensure the timely availability of test kits.

(*Cite this article as:* Satapathy SR, Sahoo RN, Nandi S, Satapathy B, Panigrahi L, Mallick S. 3D printing in managing supply disruptions related to COVID-19 pandemic: Food and Drug Administration's current thinking on regulation. Minerva Biotechnol Biomol Res 2021;33:43-50. DOI: 10.23736/S2724-542X.20.02730-5)

KEY WORDS: COVID-19; Pandemics; Ventilators, mechanical; Printing, three-dimensional; Personal protective equipment.

Towards the end of the first quarter of 2020, there is a sharp escalation of COVID-19 related infection rate as well as numbers and it becomes apparent that the deadly virus, originated in the Wuhan city of China, spread its tentacles to all parts of the globe. In March 2020, this has been declared as a global pandemic by the WHO (World Health Organization). Despite all kinds of precautionary and counteractive measures, the disease is continuously spreading at a high pace throughout the globe.[1, 2] The world was yet to witness another unprecedented increase in the number of patients, probably the second time in more than a century, after the outbreak of Spanish Flu in 1918. Firstly, a worldwide surge in demand for assisted breathing devices and accessories, secondly global lockdown resulted in a limited supply of medicated masks, hand gloves, facial shields, spare parts of ventilators, diagnostic kits, and many personal protective equipment (PPE) meant for frontline workers. The infectious disease is not going to be under control until the availability of a successful vaccine or until 60-70% of the population develop herd immunity; and both are not going to be achieved before a year.[3] This will probably pave the way to a blueprint of how 3D printing is going to revolutionize the healthcare system in the years to come.[4, 5]

There is no specific medication identified until date for

the treatment to cure this infection, and we are at least one year away from developing the commercial vaccine meant for prevention. Thus, too many patients are being infected to get accommodation to the hospitals. As a result of social distancing and traveling restrictions, air carriers have drastically reduced their available flight connections. It is estimated that approximately 60-70% of the fleet of the leading air service providers responsible for connecting the world are not in the air presently. In the management of crises related to this pandemic, 3D printing has captured imaginations worldwide. Three-dimensional (3D) printing is a manufacturing method for producing objects by fusion or depositing materials like metal, plastic, ceramics, powders, liquids, or even living cells – in layers to produce a 3D object.[6-8] Disruption of healthcare supplies as a result of global lockdown and the inherent desire to find a solution for the quick management of the crises resulted in increased activity for 3D printing applications and witnessing its potential of commercial viability. The primary advantage of innovative ideas of 3D printing can be transformed into a product within a very short period. Once the 3D designs are made available, the digital file can be shared with any healthcare systems anywhere in the globe. The moment it is downloaded and shared with a 3D printer; it will start printing the products. Thus, no need to wait for products to be shipped from one corner of the world to another; rather it can be printed on time at the place of need. For example, the essential spare parts of hospitals can be printed in a nearby 3D printing facility and shipped in the next few hours. Speed is very much important to tackle such deadly infectious diseases like COVID-19 where every minute counts. Apart from rapid prototyping, other advantages of 3D printing technology include lower CapEx required for manufacturing machinery, the ability to create the most complex structures, and the ability of personalization with the single equipment. There exist certain limitations such as difficulty to scale up, lack of pharmaceutical-grade raw materials, and evolving regulation are the major challenges. One important point we need to acknowledge that at the time of writing this review (June 2020), few of the following mentioned 3D printed medical devices and accessories, described below are not approved and in the process of review with the regulatory bodies. The term 3D printing, also known as additive manufacturing technology uses data of computer aided design (CAD) and direct hardware for depositing material layer-by-layer in a precise manner to create an object of geometric shape.[9-14]

Ventilator and respiratory support accessories

The infection related to COVID-19 causes severe acute respiratory distress in many of these infected patients, thus supportive care such as providing oxygen to the patients is critical. Regional hospitals are facing acute depletion of critical medical supplies and in dire need of important respiratory support pieces of equipment such as mechanical ventilators, non-invasive ventilation hoods, ventilator valves, valve splitters, and other ventilator spare parts such as adjustable flow control valves.[4, 15] This untimely supply chain disruption of the crucial devices from the original manufacturers has been addressed by the 3D printing community of doctors and scientists.[16, 17] For example, an Italian start-up firm Isinnova was quick enough to design and develop the right valve, manufactured in a local 3D printing firm, and supplied it to the Italian hospitals within 24 hours, when they ran out of stock.[18] Similarly, 3D printed no2covid-ONE valves by Materialize, is an auto adjustable flow control valve. When fitted to the ventilator, it can direct the desired oxygen flow to multiple patients concerning the patient's requirements. Similarly, other 3D printed products from the same organization such as no2covid-two pressure port and no2covid-three ventilator are the milestones in COVID-19 management.[19] 3D printed H connectors (Figure 1) when fitted with ventilators are another such example, where we can make the single ventilator made available at a time for four COVID-19 patients suffering from respiratory failure. But one thing should always be kept in mind that, this is an off-label use because the ventilators are meant to be used in one patient. But in rare circumstances like the COVID-19 disaster, healthcare professionals came across situations when the number of patients lying at the hospital beds with the same respiratory infections is very high compared to the number of ventilators available at that particular time; *e.g.* in March

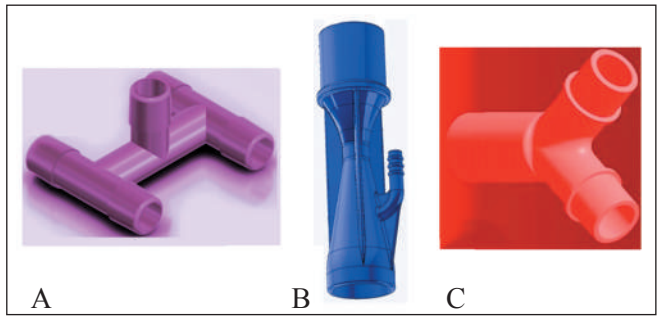

Figure 1.—A) H connector for ventilators; B) ventilator valve; C) Y connector for ventilators.

2020, there was a tsunami of patients in Italy and doctors had to decide who will get the ventilator based on survival chances. In such circumstances, the risk of cross-contamination is rare, as all the patients are suffering from the same infectious disease and admitted to a dedicated ward. H connector plays a critical role to save the life of the patients. For example, copper 3D developed an additive manufactured "H" connector for ventilators, made up of a proprietary material known as PLActive™ which is biocompatible as well as has antimicrobial and viral inactivation properties.[20] Another such example is the 3D Printed VESper™ device produced by Prisma Health (Richland, SC, USA), a Y shaped connector splitting the airflow to the ventilator, enabling a single ventilator to be made available for two patients. Prisma Health received emergency use authorization for VESper™ from USFDA. Emergency use authorization (EAU) enables healthcare professionals to use a medical device or an accessory that has not gone through the complete FDA approval process during acute equipment shortages like the current COVID-19 crisis.[21-23]

Door handles

Infestation through door handles is one of the biggest concerns as they are amongst the most contagious places in hospitals, public areas, houses, factories, and offices. There are large numbers of doors in the hospital for ward management, departmental segregation, or patient privacy. The virus can easily enter the body if anyone after opening and closing the doors touches his face. Thus, timely and periodic surface cleaning is of paramount importance to restrict infectious disease. In the current scenario of COVID-19, there is a huge shortage of healthcare workers due to roaster or shift duties making the cleaning process even more challenging. 3D printed hands-free door opener is providing a readymade solution to manage this issue by modifying and printing the door handles in such a way that it can be used by putting one's sleeved forearms or elbow on the surface of the handle closest and pushing it down (Figure 2). So, in this way the door can be opened without exposing bare hand to the surface thereby preventing the spread of viruses *via* shared door handles.[24]

Noninvasive ventilator

This assembly consists of a non-invasive PEEP (positive end respiratory pressure) mask, valve and filters. The noninvasive ventilation system is regarded as complementary to the mechanical ventilators in the sense it will keep the critical patient alive for an extended period until the mechanical ventilator is made available in the hospitals. Noninvasive PEEP masks can be fitted to the standard oxygen lines of the hospitals and keep patients safe for an extended period before lifting to mechanical ventilators. Both the masks and its valves can be 3D printed locally to address the under-supply issue of the mechanical ventilators. Belgium based company Materialize is developing 3D printed connectors, to be fitted with scuba masks to allow for air filtration and regulated controlled oxygen supply.

Figure 2.—A, B) 3D printed door handles of different type.

Specimen collection kit

Timely testing and quarantine are the most important measures to control the rate of infection. In order to tackle the growing demand for testing kit, 3D printed test swabs are made available quickly, which increased the COVID-19 testing capacity significantly. There are two components for the 3D printed sample collection kit, the shaft and the micro-fine swab bud lattice. The shaft should be long enough to collect the nasopharyngeal and oropharyngeal swabs. The shaft is made up of polystyrene and the tip containing swab bud lattice is 3D printed from fibers made up of calcium alginate (Figure 3). Formalabs are using 250 3D printers in full swing to manufacture a hundred thousand nasal swabs for COVID-19 per day and supply to various hospitals in the USA.

Figure 3.—Nose swab for specimen collection.

Personal protective equipment

Social distancing and steps like quarantine created psychological stress and fear on the minds of the general public resulting in panic buying of products in bulk and some cases buying those products such as N95 mask, meant for frontline healthcare workers resulting in shortage.[25] In a time of need, 3D printing technologies produced a plethora of PPEs like splash resistant facial shields, medical masks, mask fitters, antimicrobial masks, and safety goggles.

Face shield and fitters

These face shield holders come with a 3D-printed visor band, two re-usable 500 µ transparent polymeric sheets, and an adjustable elastic strap to fit on all. The bands and the shields are adjustable, meant for one-size-fits-all. The ideal property of the face shields is it should be transparent and provide high levels of optical clarity (Figure 4). The polymers used in 3D printing are polyvinyl chloride, polycarbonate, and polyesters along with some synthetic biopolymers.

Mask fitters

The purpose of a mask fitter is to ensure a practical face fit eliminating the risk of any leaks which usually takes place at the boundary region of the mask and face. The breathing becomes heavier to a certain extent by using it, but that is an indication that it becomes leak-proof and offers better protection. Thus, by wearing mask fitters, the performance of the masks increases significantly. The mask fitters are

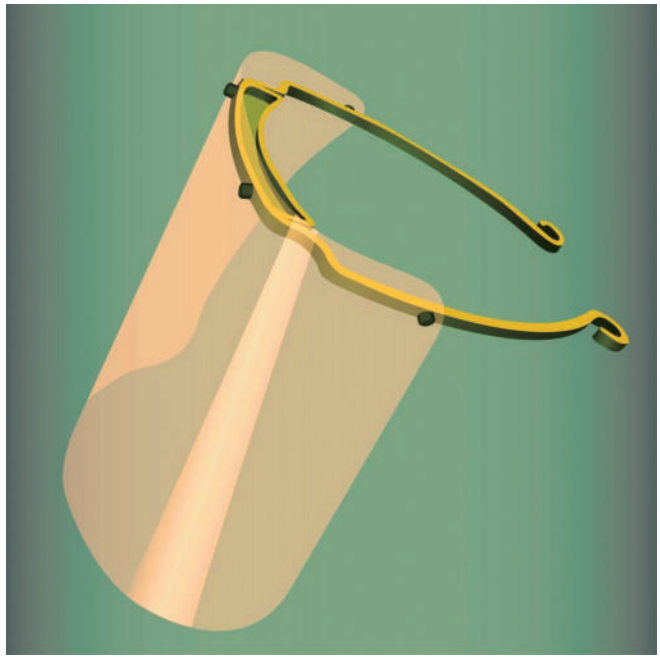

Figure 4.—Transparent face shield.

available in standard sizes or it can also be personalized to enhance the airflow and comfort. One such example of the personalized 3D printed mask fitter service provider is Bellus3D, Inc in the USA.

Face mask

The N95 masks have been recommended for healthcare workers for COVID-19 as well as patients for they are capable of filtering >95% airborne particles of size 0.3 µm. The seal is fit tested for each user so that air and small droplets do not enter around the edges. 3D printing technology not only addresses the supply disruptions but also improves the mask comfort and fit by tailor-made seal design. Firstly the facial parameters such as face and nose lengths and dimensions, jawline and chin arc, etc. are collected using 3D laser scanning technology, and then a 3D design (Figure 5) is prepared in alignment with the N95 template or any other suitable template.[26] Although there is no provision of incorporation of a valve in 3D printed masks, it has been observed that the valve respirator N95 masks are precarious to the measures adopted for the prevention of spreading the COVID-19 according to Indian health authorities, "the Director-General of Health Services" (DGHS).[27] Additionally, as the COVID-19 virus size range is 65 to 125 nm which is much lower than the effective filtration range (~300 nm) for the N95 mask, thus a re-

Figure 5.—3D printed face mask.

placeable nanoporous membrane with a narrower range of pore size can be incorporated into the reusable 3D printed valves to increase the efficacy and prevent infection.[28]

The seal is 3D printed using (fused deposition modeling) FDM technology using a polymer named acrylonitrile butadiene styrene (ABS), showed an improved contact pressure compared to marketed respirator masks 3M© 8210 N95 FFR.[4] Although polypropylene (PP) fiber is used to prepare standard N95 masks, significant distortion is observed with the FDM 3D printer. Hence a combination of PP and styrene-(ethylene butylene)-styrene (SEBS) is used which not only enables to print at low processing temperature but also manages the distortion. Again, by rightly manipulating the copolymer ratio the flexibility and elasticity of the 3D printed mask can be optimized as per the requirements. Maker Nexus is operating with its full capacity with thirteen 3D printers and laser cutters using the open-source 3D printed shield designed by Prusa.

Face masks with an exhalation valve is now being advised against in India. According to the Health Ministry of Government of India, these valved masks are to be used when there is a necessity to protect your respiration from the environment *e.g.* pollution. These masks do provide an advantage for and easy respiration but fail to keep the contamination inside the mask due to the lack of filter placement in the exhalation valve.[29] California Government has also said that the valved N95 masks do not stop the corona virus from escaping, hence spreading would not be stopped from an infected person.[30]

Safety Goggles

For prevention from infection safety Goggles are as important as masks for frontline medical workers. The mucous membrane located below the eyelid known as conjunctiva is an easy access point for viruses. Safety goggles protect the eye from flying particles and liquid droplets (Figure 6). In a collaboration of Farsoon, Huaxiang and Lehvoss group manufactured 3D printed goggles and supplied to hospitals in China and Italy, the first two epicenters of Asia and Europe respectively. Scientists at Huaxiang were able to design, optimize, and validate these safety goggles in less than two weeks. The optimized design also decreases weight while improving comfort for extended periods of use. The frames of the goggle are produced from Farsoon FS3300PA material, which offers good strength and durability. The sealing rings are made of Luvosint TPU material from Lehvoss with excellent elongation and flexibility, which ensure a better fit and improved sealing protection compared to traditional PC material. The lens is prepared from transparent acrylic and coated with an antifogging coating. The 3D printed individual components assembled, then disinfected under UV light, temperature, and pressure. The design and production of these safety goggles have been registered for Category One Medical Tools in China. The file is freely available for downloading and use.

Medications

No drugs or vaccines have yet been received FDA approval for potential COVID-19 treatment. USFDA has

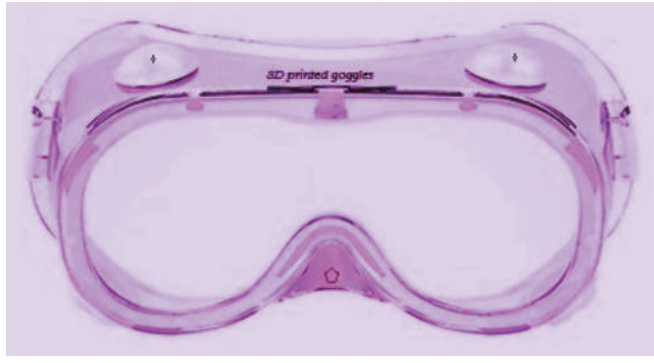

Figure 6.—3D printed safety goggles.

issued emergency-use authorizations (EUA) for antiviral Remdesivir to be used in adults and children with severe cases, such as patients on a mechanical ventilator or with low blood oxygen level requiring supplemental oxygen therapy. Similarly, EUA provided for Propoven (2%) for sedation of patients under mechanical ventilators in ICU. There was EUA for antimalarial hydroxychloroquine sulfate (HCQ) and chloroquine phosphate (CP) for a temporary period, which was later revoked by mid of June 2020 despite its potential benefits due to its association with severe cardiac adverse events. Due to the shortage and emergency EUA, many pharmaceutical companies are exploring the possibilities of additive manufacturing technology to rapidly print these medications.[31]

Apart from antivirals, steroids, and combination therapies, other medications are immunomodulators, neutralizing antibodies, cell and gene therapies, etc. Other medications are being evaluated by the flagship emergency program of FDA known as the Coronavirus Treatment Acceleration Program (CTAP).

3D printed quarantine booths

WinSun, a Chinese company has deployed its 3D printing technology for the construction of 15 isolation rooms of 10 square meters surface area and a height of 2.8 meters, for Chinese hospitals, located in the epicenter of Hubei province. It was an extrusion process and took 24 hours that means less than 2 hours for each quarantine room. These quarantine booths (Figure 7) reduced the burden on hospitals by accommodating quarantined people and the necessary medical staff members.[32, 33]

Regulations

The 3D printed product may be considered as a medical device or an accessory. As 3D printing is still an emerging technology in healthcare systems, there are no harmonized guidelines available for 3D printed medical devices and its parts. Although accessories, spare parts, and components of medical devices, are not by themselves considered as medical devices, rather are intended to be used as a critical component of a medical device for its functionality. Hence, they must fulfill the medical device legislation and Directive 93/42/EEC.[34] For example, 3D printed ventilated valves which are not a medical device, but an accessory of mechanical ventilators must comply with the requirements of medical devices legislation. The manufacturers of medical devices can also refer to the current harmonized quality management systems (QMS).[35] The production process must be validated as per the section 7.5.6 EN ISO 13485:2016. The raw material used for 3D printing should be of appropriate grade *i.e.* the 3D printed product must be resistant to cleaning and compatible with sterilization and suitable for biologics evaluation tests. Regulatory bodies are taking quick actions to ease the import restrictions and expedite registration processes, for products intended for the detection and diagnosis of COVID-19 infection to ensure the timely availability of good quality test kits. The medical device working group enacted key relevant guidelines received from regulatory bodies in various countries such as Korea, Japan, Taiwan, Australia, and Singapore to allow emergency use for medical devices and *in-vitro* diagnostic devices (IVDs) during this pandemic.[36-41] FDA published a draft guidance titled "Technical Considerations for Additive Manufactured Devices" outlines FDA's current thinking and considerations on the use of 3D printing for medical devices and accessories.[42] FDA has released FAQs and technical considerations for 3D printed medical devices, accessories, and PPEs to support patients infected with COVID-19. FDA also launched a website COVID-Manufacturing@fda.hhs.gov to actively discuss very specifics on the development and queries related to 3D printing with the manufacturers.[43, 44] USFDA and European Medicines Evaluation Agencies (EMEAs) are working on a war front basis in evaluating the safety and efficacy and providing approval on fast track.[45, 46] USFDA and many other regulatory bodies facilitated the import of products intended for the detection and diagnosis of COVID-19 infection to ensure the timely availability of quality test kits. The 3D printed mask can be fitted with a filter that satisfies the filtration efficiency level as per 42 CFR 84.181.[47]

In the context of medication, many leading pharmaceutical companies are evaluating the possibilities of 3D printing tablets in such a critical time. However, the regulatory challenge is one of the important hurdles. There are several FDA driven initiatives such as position papers

Figure 7.—3D printed quarantine booth.

illustrating the benefits of 3D printing in pharmaceutical applications. First FDA approved 3D printed drug Spritam based on binder jetting powder-liquid technology has provided the foundation for future developments. Although the overall market for 3D printing is very large compared to the 3D printed drugs which are estimated to be $ 278 million in 2020 and would probably land a little over $ 500 million by 2030. This decade witnessed the beginning of 3D printing for pharmaceutical applications and the landing numbers can be significantly higher with timely favorable regulations and acceptance of additional suitable technology platforms such as fused deposition modeling, selective laser sintering, and Ink Jet 3D printing technology.

Conclusions

3D printing may be a support in fighting against the COVID-19 pandemic by addressing the medical shortages and making them available on time at the site of requirement. Regulatory agencies are working on an emergency basis to evaluate the safety and efficacy of providing fast track approval. Manufacturing products by 3D printing can fulfill the urgent need for medical supplies. It will save the lives of patients by better care healthcare providers by better safety equipment. The world has witnessed that 3D printing has got the innovative power of creating a practical product at the time of need. 3D printing can develop real-time solutions in improving healthcare systems. The regulatory bodies need to lay down harmonized guidelines to nourish this technology to the full extent, making it ready to tackle not only the COVID-19 but also the possibility of any future pandemic condition. To summarize, 3D printing can be a potentially disruptive technology that may change the entire supply chain and the way pharmaceutical products are manufactured.

References

1. Bellan M, Sainaghi PP, Gavelli F, Patrucco F, Avanzi GC, Pirisi M, *et al.* Lessons from the Italian COVID-19 frontline. Minerva Med 2020;111:303–5.

2. Patrucco F, Gavelli F, Shi R, De Vita N, Pavot A, Castello LM, *et al.* Coronavirus disease 2019 outbreak. Panminerva Med 2020;62:73–4.

3. Fagoonee I, Pellicano R. COVID-19 brings the world economy to its knees. Minerva Med 2020;111:297–9.

4. Cai M, Li H, Shen S, Wang Y, Yang Q. Customized design and 3D printing of face seal for an N95 filtering facepiece respirator. J Occup Environ Hyg 2018;15:226–34.

5. Banerjee SS, Burbine S. KodihalliShivaprakash N, Mead J. 3D-printable PP/SEBS thermoplastic elastomeric blends: preparation and properties. Polymers (Basel) 2019;11:347.

6. Schubert C, van Langeveld MC, Donoso LA. Innovations in 3D printing: a 3D overview from optics to organs. Br J Ophthalmol 2014;98:159–61.

7. Klein GT, Lu Y, Wang MY. 3D printing and neurosurgery—ready for prime time? World Neurosurg 2013;80:233–5.

8. Wren K. Science and society. Experts warn against bans on 3D printing. Science 2013;342:439.

9. Norman J, Madurawe RD, Moore CM, Khan MA, Khairuzzaman A. A new chapter in pharmaceutical manufacturing: 3D-printed drug products. Adv Drug Deliv Rev 2017;108:39–50.

10. Palekar S, Nukala PK, Mishra SM, Kipping T, Patel K. Application of 3D printing technology and quality by design approach for development of age-appropriate pediatric formulation of baclofen. Int J Pharm 2019;556:106–16.

11. Cerda JR, Arifi T, Ayyoubi S, Knief P, Ballesteros MP, Keeble W, *et al.* Personalised 3D printed medicines: optimising material properties for successful passive diffusion loading of filaments for fused deposition modelling of solid dosage forms. Pharmaceutics 2020;12:345.

12. Araújo MR, Sa-Barreto LL, Gratieri T, Gelfuso GM, Cunha-Filho M. The digital pharmacies era: How 3D printing technology using fused deposition modeling can become a reality. Pharmaceutics 2019;11:128.

13. Korte C, Quodbach J. Formulation development and process analysis of drug-loaded filaments manufactured via hot-melt extrusion for 3D-printing of medicines. Pharm Dev Technol 2018;23:1117–27.

14. Jamróz W, Szafraniec J, Kurek M, Jachowicz R. 3D Printing in Pharmaceutical and Medical Applications - Recent Achievements and Challenges. Pharm Res 2018;35:176.

15. Gavelli F, Castello LM, Patrucco F, Bellan M, Sainaghi PP, Avanzi GC. Insights from Italy: the Novara-COVID Score for rapid destination of COVID-19 patients at Emergency Department presentation. Minerva Med 2020;111:300–2.

16. Bateman NT, Leach RM. ABC of oxygen. Acute oxygen therapy. BMJ 1998;317:798–801.

17. Tino R, Moore R, Antoline S, Ravi P, Wake N, Ionita CN, *et al.* COVID-19 and the role of 3D printing in medicine. 3D Print Med 2020;6:11.

18. Italian hospital saves COVID-19 patients' lives by 3D printing valves for reanimation devices. 3D Printing Media; 2020 [Internet]. Available from: https://www.3dprintingmedia.network/covid-19-3dprinted-valve-for-reanimation-device/ [cited 2020, Nov 21].

19. The no2covid-ONE. No 2 Covid; 2020 [Internet]. Available from: https://no2covid.com/ [cited 2020, Nov 21]. The "H" Connector for Ventilators. Copper 3D; [Internet]. Available from: https://copper3d.com/hconnector/ [cited 2020, Nov 21].

20. Prisma Health Introduces VESper™. Prisma Health; [Internet]. Available from: https://www.prismahealth.org/VESper/ [cited 2020, Nov 21].

21. Neyman G, Irvin CB. A single ventilator for multiple simulated patients to meet disaster surge. Acad Emerg Med 2006;13:1246–9.

22. Lai BK, Erian JL, Pew SH, Eckmann MS. Emergency open-source three-dimensional printable ventilator circuit splitter and flow regulator during the COVID-19 pandemic. Anesthesiology 2020;133:246–8.

23. Hands-Free Door Openers. Materialise; [Internet]. Available from: https://www.materialise.com/en/hands-free-door-opener/technical-information [cited 2020, Nov 21].

24. Ranney ML, Griffeth V, Jha AK. Critical Supply Shortages - The Need for Ventilators and Personal Protective Equipment during the Covid-19 Pandemic. N Engl J Med 2020;382:e41.

25. Zuniga JM, Cortes A. The role of additive manufacturing and antimicrobial polymers in the COVID-19 pandemic. Expert Rev Med Devices 2020;17:477–81.

26. Explained: Why you should not wear N95 masks with valved respirators. Indian Express; [Internet]. Available from: https://indianexpress.com/article/explained/coronavirus-covid-19-health-ministry-n95-masks-with-valved-respirators-6518118/ [cited 2020, Nov 21].

27. El-Atab N, Qaiser N, Badghaish H, Shaikh SF, Hussain MM. Flexible Nanoporous Template for the Design and Development of Reusable Anti-COVID-19 Hydrophobic Face Masks. ACS Nano 2020;14:7659–65.

28. Health Ministry warns against use of N95 masks with valves. CNBCTV; [Internet]. Available from: https://www.cnbctv18.com/healthcare/health-ministry-warns-against-usage-of-N95-masks-with-valves-6392141.htm [cited 2020, May 28].

29. Face mask rules for the Bay Area: When and how to use them. SFChronicle; [Internet]. Available from: https://www.sfchronicle.com/news/article/Coronavirus-FAQ-Should-you-wear-a-face-mask-15147298.php [cited 2020, Nov 21].

30. Ishack S, Lipner SR. Applications of 3D Printing Technology to Address COVID-19-Related Supply Shortages. Am J Med 2020;133:771–3.

31. 3D printed quarantine wards. 3D Natives; [Internet]. Available from: https://www.3dnatives.com/en/winsun-coronavirus-260220205/ [cited 2020, Nov 21].

32. Shanghai Company donates 3D printed quarantine wards to Hubei Hospital. Global China Daily; [Internet]. Available from: https://global.chinadaily.com.cn/a/202002/13/WS5e450172a31012821727758a.html [cited 2020, Nov 21].

33. Directive 93/42/EEC. Eurlex; [Internet]. Available from: https://eur-lex.europa.eu/LexUriServ/LexUriServ.do?uri=CONSLEG:1993L0042:20071011:en:PDF [cited 2020, Nov 21].

34. EN ISO 13485:2016 Medical devices - Quality management systems - Requirements for regulatory purposes (ISO 13485:2016) EN ISO 13485:2016/AC:2018. Geneva, Switzerland: International Organization for Standardization; 2016.

35. Ministry of Food and Drug Safety. MFDS; [Internet]. Available From: https://www.mfds.go.kr/eng/index.do [cited 2020, Nov 21].

36. Basic Policies for Novel Coronavirus Disease Control by the Government of Japan (summary). MHLW; [Internet]. Available from: https://www.mhlw.go.jp/content/10900000/000617686.pdf [cited 2020, Nov 21].

37. Taiwan Food and Drug Administration. FDA; [Internet]. Available from: https://www.fda.gov.tw/eng/siteContent.aspx?sid=11195 [cited 2020, Nov 21].

38. Legal supply of COVID-19 test kits. TGA; 2020 [Internet]. Available from: https://www.tga.gov.au/legal-supply-covid-19-test-kits [cited 2020, Nov 21].

39. HSA expedites approval of COVID-19 diagnostic tests in Singapore via provisional authorization. HSA; 2020 [Internet]. Available from: https://www.hsa.gov.sg/announcements/regulatory-updates/hsa-expedites-approval-of-covid-19-diagnostic-tests-in-singapore-via-provisional-authorisation [cited 2020, Nov 21].

40. NOTICE. X-11026/07/2020-PRO, Government of India, Directorate General of Health Services, Central Drugs Standard Control Organization. CDSCO; [Internet]. Available From: https://cdsco.gov.in/opencms/opencms/system/modules/CDSCO.WEB/elements/download_file_division.jsp?num_id=NTc3MA [cited 2020, Nov 21].

41. FDA. Technical considerations for additive manufactured devices 2016. FDA; [Internet]. Available from: http://www.fda.gov/downloads/medicaldevices/deviceregulationandguidance/guidancedocu ments/ucm499809.pdf [cited 2020, Nov 21].

42. FAQs on 3D printing of medical devices, accessories, components and parts during COVID-19 pandemic. FDA; 2020 [Internet]. Available from: https://www.fda.gov/medical-devices/3d-printing-medical-devices/faqs-3d-printing-medical-devices-accessories-components-and-parts-during-covid-19-pandemic [cited 2020, Nov 21].

43. Technical considerations for additive manufactured medical devices Guidance for Industry and Food and Drug Administration Staff. FDA; 2020 [Internet]. Available from: https://www.fda.gov/media/97633/download [cited 2020, Nov 21].

44. Conformity assessment procedures for 3D printing and 3D printed products to be used in a medical context for COVID-19. EC Europa; 2020 [Internet]. Available from: https://ec.europa.eu/health/sites/health/files/md_sector/docs/md_mdcg_qa_3d_ppp_covid-19_en.pdf [cited 2020, Nov 21].

45. Coronavirus FD. (COVID-19) supply chain update. FDA; 2020 [Internet]. Available from: https://www.fda.gov/news-events/press-announcements/coronavirus-covid-19-supply-chain-update [cited 2020, Nov 21].

46. Enforcement Policy for face masks and respirators during the Coronavirus disease (COVID-19) Public Health Emergency (Revised). FDA; 2020 [Internet]. Available from: https://www.fda.gov/regulatory-information/search-fda-guidance-documents/enforcement-policy-face-masks-and-respirators-during-coronavirus-disease-covid-19-public-health [cited 2020, Nov 21].

47. 42 CFR Ch. I (10–1–09 Edition). Gov Info; 2020 [Internet]. Available from: https://www.govinfo.gov/content/pkg/CFR-2009-title42-vol1/pdf/CFR-2009-title42-vol1-sec84-181.pdf [cited 2020, Nov 21].

Conflicts of interest.—The authors certify that there is no conflict of interest with any financial organization regarding the material discussed in the manuscript.

Authors' contributions.—Soumya R. Satapathy has given substantial contributions to manuscript writing, Rudra N. Sahoo to manuscript writing and data curation, Souvik Nandi to formal analysis and software, Biswaranjan Satapathy to manuscript revision and editing and software, Lalatendu Panigrahi to manuscript validation and visualization, Subrata Mallick to manuscript supervision. All authors read and approved the final version of the manuscript.

Acknowledgements.—The authors acknowledge Prof. Manoj Ranjan Nayak, President, Siksha O Anusandhan (Deemed to be University) for providing other facilities and encouragement.

History.—Manuscript accepted: November 19, 2020. - Manuscript revised: November 18, 2020. - Manuscript received: October 16, 2020.

Gmail

Souvik Nandi <arghanandi@gmail.com>

Fwd: Decision on submission to Journal of Drug Delivery Science and Technology

2 messages

Subrata Mallick <profsmallick@gmail.com> Fri, Oct 29, 2021 at 11:27 PM
To: Rakesh Swain <rakeshswainofficial@gmail.com>, Souvik Nandi <arghanandi@gmail.com>, rudra narayan Sahoo <rx.rudra@gmail.com>

---------- Forwarded message ---------
From: **Journal of Drug Delivery Science and Technology** <em@editorialmanager.com>
Date: Fri, 29 Oct 2021, 22:50
Subject: Decision on submission to Journal of Drug Delivery Science and Technology
To: Subrata Mallick <profsmallick@gmail.com>

Manuscript Number: JDDST-D-21-01357R1

Bentonite clay incorporated topical film formulation for delivery of trimetazidine: Control of ocular pressure and in vitro-in vivo correlation

Dear Professor Mallick,

Thank you for submitting your manuscript to Journal of Drug Delivery Science and Technology.

I am pleased to inform you that your manuscript has been accepted for publication.

My comments, and any reviewer comments, are below.
Your accepted manuscript will now be transferred to our production department. We will create a proof which you will be asked to check, and you will also be asked to complete a number of online forms required for publication. If we need additional information from you during the production process, we will contact you directly.

We appreciate you submitting your manuscript to Journal of Drug Delivery Science and Technology and hope you will consider us again for future submissions.

Kind regards,
feng zhang
Associate Editor

Journal of Drug Delivery Science and Technology

Editor and Reviewer comments:

More information and support

FAQ: When and how will I receive the proofs of my article?
https://service.elsevier.com/app/answers/detail/a_id/6007/p/10592/supporthub/publishing/related/

You will find information relevant for you as an author on Elsevier's Author Hub: https://www.elsevier.com/authors

FAQ: How can I reset a forgotten password?